INL/MIS-24-78485-Revision-0

ECAR-7210 Steady-state Thermo-mechanical Analysis of the MARVEL Fuel Bundle

October 2023

Brandon L Moon

Changing the World's Energy Future

INL is a U.S. Department of Energy National Laboratory operated by Battelle Energy Alliance, LLC

INL/MIS-24-78485-Revision-0

ECAR-7210 Steady-state Thermo-mechanical Analysis of the MARVEL Fuel Bundle

Brandon L Moon

October 2023

Idaho National Laboratory
Idaho Falls, Idaho 83415

http://www.inl.gov

Prepared for the
U.S. Department of Energy
Under DOE Idaho Operations Office
Contract DE-AC07-05ID14517

Steady-state Thermo-mechanical Analysis of the MARVEL Fuel Bundle

1. Effective Date	10/02/23	**Professional Engineer's Stamp** Not required per LWP-10010, Sec. 4.1, par. cc
2. Does this ECAR involve a Safety SSC (see def. LWP-10200)?	YES	
3. Safety SSC Determination Document ID	TBD	
4. SSC ID	TBD	
5. Project No.	33526	
6. Engineering Change (EC) No.	1759	
7. Building	MFC-720	
8. Site Area	MFC	

9. Objective / Purpose

This document reports the steady-state thermal-hydraulic and static mechanical analyses of the MARVEL micro-reactor core. The objective of this work is to investigate whether fuel-to-fuel contact could occur due to the thermal deformation of the fuel cladding during the normal operation and to assess the resulting impact on the peak cladding temperatures (PCT) if contact occurs.

The scope of the work consists of three computational tasks. First, a conjugate heat transfer analysis using computational fluid dynamics (CFD) model was performed to evaluate the PCTs during normal operating conditions. Second, a finite element analysis (FEA) using the cladding temperature field obtained from the CFD analysis was performed to evaluate the thermal deformation of cladding and determine the occurrence of fuel-to-fuel contact. Finally, a CFD analysis of FEA-informed fuel-to-fuel gap (represented by a conservative 0.05 mm uniform gap) was performed to evaluate whether the PCT exceeds the safety criteria.

10. If revision, please state the reason and list sections and/or page being affected.

Initial Release

11. Conclusion / Recommendations

The peak temperatures of fuel cladding with the nominal fuel-to-fuel gap of 2.0 mm were calculated to be 545.9 °C. The ABAQUS code calculated the axial expansion of 7.51 mm for the fuel rods. It was found that the maximum change in the rod-to-rod gap was 0.642 mm. In the worst-case scenario, the maximum displacement of fuel rod considering a straightness tolerance of the fuel rod could be 2.279 mm, which is greater than a nominal gap and can cause the fuel rods to come into contact at some length or points. The CFD model, assuming 0.05 mm uniform fuel-to-fuel gap, calculated that the peak temperature of fuel cladding were 586.66 °C. It can be concluded that the changes in the fuel-to-fuel gap considering the straightness tolerance and thermal deformation would not cause the fuel and cladding temperature to exceed the safety criteria for the normal operation, which is 764 °C for cladding. For a conservative safety assessment during reactor transients, the hot channel factor in the system safety analysis should consider the temperature increase caused by the changes in the fuel-to-fuel gap.

CONTENTS

1. PROJECT ROLES AND RESPONSIBILITIES 5

2. SCOPE AND BRIEF DESCRIPTION 6

3. DESIGN OR TECHNICAL PARAMETER INPUT AND SOURCES 6

4. RESULTS OF LITERATURE SEARCHES AND OTHER BACKGROUND DATA 6

5. ASSUMPTIONS 6

6. COMPUTER CODE VALIDATION 8

7. DISCUSSION/ANALYSIS 9

8. REFERENCES 48

APPENDIXES

- Appendix A – Abaqus Validation Test Report (Thermal)
- Appendix B – Abaqus Validation Test Report (Standard)
- Appendix C – Thermo-physical Properties of MARVEL Reactor Core Internal Structures and Working Fluid
- Appendix D – Boundary Condition Inputs for CFD model
- Appendix E – Pressure Load for ABAQUS Finite Element Analysis
- Appendix F – Mesh Sensitivity Test Results of MARVEL Reactor Core CFD Model
- Appendix G – Azimuthal Temperature Profiles of Cladding
- Appendix H – Python Script to Calculate Coordinates of Deformed Claddings and Minimum Fuel-to-fuel Gap Distance
- Appendix I – Straightness Tolerance of MARVEL Fuel Element

FIGURES

Figure 1. The overview of modeling and simulation process. 10
Figure 2. CFD model of MARVEL reactor core internal structures 11
Figure 3. Dimensions of fuel rod in the CFD model 12
Figure 4. MARVEL reactor thermal power inputs [11]. 13
Figure 5. Volumetric heat generation rate distribution in the MARVEL reactor core [Unit: W/m^3] 14
Figure 6. Mesh structure of MARVEL reactor core CFD model 15
Figure 7. The statistics of wall Y+ value on the cladding wall (Base size: 10 mm) 16
Figure 8. Axial pressure distribution in the MARVEL reactor core 17
Figure 9. Plane sections to visualize the CFD simulation result. 17
Figure 10. Flow velocity distributions at different elevations in the MARVEL reactor core 19
Figure 11. Temperature distributions at different elevations in the MARVEL reactor core 21
Figure 12. Azimuthal temperature profiles of fuel rod 1-1 at three elevations P1, P2 and P3. 23
Figure 13. Azimuthal temperature profiles of fuel rod 2-1 at three elevations P1, P2 and P3. 24
Figure 14. Azimuthal temperature profiles of fuel rod 3-1 at three elevations P1, P2 and P3. 26
Figure 15. Isometric view of fuel and cladding temperature distributions. 26
Figure 16. Model Keywords Function in Abaqus to defined Predefined Fields with mapped data. 28
Figure 17. Mapped temperature field of fuel cladding imported into Abaqus [unit: Kelvin]. 29
Figure 18. Tetrahedral mesh structure of claddings generated for STAR-CCM+ solid stress analysis . 30
Figure 19. Boundary conditions for finite element analysis 31
Figure 20. Mesh structure of ABAQUS cladding model. 32
Figure 21. Displacement components of claddings calculated by STAR-CCM+ (free thermal bowing). 34
Figure 22. Displacement magnitude of claddings (free thermal bowing condition) [unit: m] 35
Figure 23. Spatial displacement component U1 of the claddings in each ring (free thermal bowing condition) [unit: m] 37
Figure 24. Spatial displacement component U3 of the claddings in each ring (free thermal bowing condition) [unit: m] 38
Figure 25. Isometric view of thermal deformation (displacement magnitude) of claddings [unit: m]. 39
Figure 26. Spatial displacement component U1 of the claddings in each ring [unit: m] 41
Figure 27. Spatial displacement component U3 of the claddings in each ring [unit: m] 42
Figure 28. Exporting the field output from Abaqus (“Report” >> “Field Output…”). 43
Figure 29. Tolerance definitions given in the GD&T Y14.5 Standard [13]. 44
Figure 30. Cross-sectional view of MARVEL reactor core with 0.05 mm gap between fuel rod 2-1 and the fuel rods adjacent to it (1-1, 2-2, 2-12, 3-1, 3-2, and 3-18). 45
Figure 31. The temperature distribution on the cladding surface of fuel rod 2-1 and the cross-sectional temperature distribution of the reactor core at three elevations by modifying the positions of fuel rods adjacent to the fuel rod 2-1. 46
Figure 32. Mesh sensitivity test result for the PCT 62
Figure 33. Reference angle of azimuthal temperature profile. 63
Figure 34. Azimuthal temperature profiles of the claddings in the first ring (Elevation: P3) 64
Figure 35. Azimuthal temperature profiles of the claddings in the second ring (Elevation: P3) 66
Figure 36. Azimuthal temperature profiles of the claddings in the third ring. (Elevation: P3) 69

TABLES

Table 1. Model Properties of Data Mappers for STAR-CCM+ Solid Stress Analysis 30
Table 2. Thermo-physical Properties of liquid NaK (Fluid) [11]..... 54
Table 3. Thermo-physical Properties of Air (Fuel Plenum)..... 55
Table 4. Thermo-physical Properties of Uranium-Zirconium Hydride (Fuel) [18] [19]..... 56
Table 5. Thermo-physical Properties of Stainless Steel 304 (Cladding) [20] 56
Table 6. Thermo-physical Properties of Graphite H-451 (Top and Bottom Reflectors) [2] 56
Table 7. Thermo-physical Properties of Beryllium (internal reflector) [22]..... 57
Table 8. Thermo-physical Properties of Zirconium (Zirconium rod) [22] 58
Table 9. Young's Modulus (Modulus of Elasticity) and Poisson's Ratio of SS-304 (Cladding)..... 58
Table 10. Thermal Expansion Coefficient of SS-304(Cladding) [25]..... 59
Table 11. The weight of the component above the MARVEL reactor 61
Table 12. Maximum and minimum azimuthal temperature of fuel cladding at elevation P1(-1.80693m), P2 (-1.48943m) and P3 (-1.17193m). 70
Table 13. Change in Fuel-to-Fuel Gap Distance (Top constrained condition) 77

1. PROJECT ROLES AND RESPONSIBILITIES

Project Role	Name	Organization	Pages Covered (if applicable)
Performer	SuJong Yoon	C130	See DCR 705230
Checker[a]	Austen D. Fradeneck	C140	See DCR 705230
Independent Reviewer[b]	Changhu Xing	C140	See DCR 705230
CUI Reviewer[c]	Mike Patterson	C120	See DCR 705230
Manager[d]	George L. Mesina	C130	See DCR 705230
Requestor[ef]	Yasir Arafat	C120	See DCR 705230
Nuclear Safety[f]	Doug Gerstner	H374	See DCR 705230
Document Owner[f]	Yasir Arafat	C120	See DCR 705230
Reviewer[f]	Carlo Parisi	C130	See DCR 705230

Responsibilities:

a. Confirmation of completeness, mathematical accuracy, and correctness of data and appropriateness of assumptions.

b. Concurrence of method or approach. See definition, LWP-10106.

c. Concurrence with the document's markings in accordance with LWP-11202.

d. Concurrence of procedure compliance. Concurrence with method/approach and conclusion.

e. Authorizes the commencement of work of the engineering deliverable.

f. Concurrence with the document's assumptions and input information. See definition of Acceptance, LWP-10200.

NOTE: *Delete or mark "N/A" for project roles not engaged. Include ALL personnel and their roles listed above in the eCR system. The list of the roles above is not all inclusive. If needed, the list can be extended or reduced.*

2. SCOPE AND BRIEF DESCRIPTION

This document reports the steady-state thermal-hydraulic and static mechanical analyses of the MARVEL micro-reactor core. The MARVEL micro-reactor is designed to remove thermal energy from nuclear fuel by the natural circulation of the primary coolant. An increase in pressure drop across the reactor core could potentially disrupt the natural circulation of primary coolant. Consequently, no fuel spacer has been introduced to avoid additional pressure drop caused by these spacers, while the upper and lower grid plates ensure a proper fuel alignment. However, this design may have a drawback, specifically the possibility of fuel-to-fuel contact due to thermal deformation and the straightness tolerance of the fuel rods, which can elevate the peak cladding temperature, ultimately reducing the reactor's thermal margin. Therefore, it is necessary to investigate whether fuel-to-fuel contact could occur due to the thermal deformation of the fuel cladding during the normal operation and to assess the resulting impact on the peak cladding temperature (PCT). The scope of the work consists of three computational tasks. First, a conjugate heat transfer analysis using computational fluid dynamics (CFD) model was performed to evaluate the PCTs during normal operating conditions. Second, a finite element analysis (FEA) using the cladding temperature field obtained from the CFD analysis was performed to evaluate the thermal deformation of cladding and determine the occurrence of fuel-to-fuel contact. Finally, a CFD analysis of FEA-informed fuel-to-fuel gap was performed to evaluate whether the PCT exceeds the safety criteria.

3. DESIGN OR TECHNICAL PARAMETER INPUT AND SOURCES

1. Fuel Rod Assembly: DWG No.1011202 Rev.0
2. Fuel Rod and Adapter Assembly: DWG No.1014587 Rev.0
3. Lower Fuel Grid Plate: DWG No. 1014588 Rev.0
4. Core Reflector: DWG No.1014603 Rev.0
5. Lower Grid Adapter Assembly: DWG No.1014590 Rev.0
6. Upper Fuel Grid Plate: DWG No.1014679 Rev.0
7. Upper Grid Adapter: DWG No.1014593 Rev.0
8. Alignment Pin: DWG No.1014594 Rev.0
9. Top Screw Pin: DWG No. 1014595 Rev.0

4. RESULTS OF LITERATURE SEARCHES AND OTHER BACKGROUND DATA

N/A

5. ASSUMPTIONS

1. The MARVEL reactor core internal structure design shall allow the axial expansion of the fuel rods. (See DWG-1014587).
2. Assembled upper core internal structures shall constrain the transversal displacement of the fuel rods at the top end of the rod: fuel rod and adapter assembly (DWG-1014587), upper fuel grid plate (DWG-1014679), upper grid adapter (DWG-1014593), alignment Pin (DWG-1014594), and top screw pin (DWG-1014595).

3. Assembled lower core internal structures shall constrain the transverse displacement of the fuel rods at the bottom ends of the rod. The structures also shall constrain the axial displacement of the fuel rods toward the bottom of the rods: The lower grid adapter assembly (DWG-1014590) and lower fuel grid plate (DWG-1014588).
4. The thermal resistance of Molybdenum disk between the fuel meat and graphite reflector is negligible due to its high thermal conductivity.
5. Unirradiated properties of H-451 graphite was used in this work because total neutron fluences for the design lifetime of the reactor [1] was much smaller than irradiated conditions reported in Reference [2].
6. The CFD model assumes no fuel-to-cladding gap. The direct contact of fuel and cladding shall result in the conservative prediction of cladding peak temperature.
7. There are 36 fuel rods in the reactor core, each of which has five fuel meats that have been simplified as a single volume in the CFD model. The impact of contact resistance between the fuel meats was assumed to be negligible.
8. The reactor components irrelevant to the scope of this ECAR could be removed from the CFD model because those are not directly involved with the heat and mass transfer in the reactor core region.
9. An adiabatic condition was imposed on the outer surface of the Beryllium internal reflector. This assumes no heat loss to the environment and will increase the temperature of internal structures. Hence, this boundary condition will also lead to a conservative prediction of the cladding temperature.
10. Differences in dimensions in the order of 1.0E-4 mm may arise due to truncation errors in the built-in measurement tools of the CAD software or computational tools such as STAR-CCM+ and ABAQUS. However, these discrepancies are not expected to significantly impact the computational results.
11. The difference in dimension within the fabrication tolerance of each component is not expected to significantly impact the computational result.
12. It is assumed that the pressure load due to the weight of the components and NaK volume above the reactor core is uniformly distributed to the fuel pins. The components considered in the pressure load calculation are the upper alignment grid plate, fuel pin to upper grid adapter, top adaptor, locating pin, and top screw pin.
13. It is assumed that no heat loss to the environment through the outer surface of the Beryllium internal reflector.
14. It is assumed that the total heat generation of fuel rods in the reactor core is 85 kW_{th} while it was approximately 83.16 kW_{th} in the MCNP calculation. This assumption will provide a conservative prediction of PCTs.

6. COMPUTER CODE VALIDATION

Computational Fluid Dynamics Analysis (STAR-CCM+)

A. Computer type: Nodes on INL High Performance Computing cluster “SAWTOOTH” (each node: 1 intel Xeon 8268 CPUs Cascade Lake Platinum chipset 24 cores per CPU 2.9 GHz, 192 GB of RAM), LINPACK: 5600.00 TFlops

B. Operating System and Version: CentOS Linux version 7

C. Computer program name and revision: STAR-CCM+ 2206.0001 Build 17.06.008 [3].

D. Inputs (may refer to an appendix): N/A

E. Outputs (may refer to an appendix): N/A

F. Evidence of, or reference to, computer program validation: Siemens’s STAR-CCM+, the commercial multi-physics CFD software, has achieved ASME Nuclear Quality Assurance (NQA)-1 compliance [4]. The addition of NQA-1 compliance in rigorous ASME QA certification program ensures the code meets industry-standard requirements for nuclear industry customers in support of safety-related applications. Furthermore, Siemens provides the “Verification Suite” document to provide cases that come from the Siemens Digital Industries Software quality-assurance process [5]. Acceptance testing result of STAR-CCM+ is documented in ECAR-3020 [6].

G. Bases supporting application of the computer program to the specific physical problem: Solving governing equations for the mass, momentum and energy conservations performed herein are common analysis types for which the identified program, STARCCM+ is designed to be used and has been acceptably demonstrated through commercial use and application. The identified software package is well suited for the calculations documented by this report to the quality level indicated on the title page.

Finite Element Analysis (Abaqus)

A. Computer type: Nodes on INL High Performance Computing cluster “SAWTOOTH” (each node: 1 intel Xeon 8268 CPUs Cascade Lake Platinum chipset 24 cores per CPU 2.9 GHz, 192 GB of RAM), LINPACK: 5600.00 TFlops

B. Operating System and Version: CentOS Linux version 7

C. Computer program name and revision: Abaqus Version 2018.HF3 [7]

D. Inputs (may refer to an appendix): N/A

E. Outputs (may refer to an appendix): N/A

F. Evidence of, or reference to, computer program validation: Abaqus is listed in the INL Enterprise Architecture (EA) repository of qualified scientific and engineering analysis software (EA Identifier 336418). Abaqus/Standard is validated for the INL High Performance Computing (HPC) cluster per ECAR-3845 [8]. Additional validation tests for Abaqus/Thermal and

Abaqus/Standard were conducted in the SAWTOOTH cluster and the test reports are attached in **Appendix A** and **Appendix B**, respectively.

G. Bases supporting application of the computer program to the specific physical problem: Abaqus is a software suite to solve the finite element analysis, including static, dynamics, and thermal analyses.

7. DISCUSSION/ANALYSIS

An overview of the modeling and simulation process is illustrated in Figure 1. To assess the cladding deformation in the reactor core due to thermal expansion, a three-dimensional temperature field of the cladding is required for a finite element structural analysis. The cladding temperature field can be obtained by solving the conjugate heat transfer in the reactor core using the CFD code STAR-CCM+ (v.17.06.008).

The individual fuel power peaking factors and the axial power profile obtained from the MCNP calculation [1] were employed to define the fuel power distribution in the CFD analysis. Since this work focuses on the core region, the computational domain only includes the reactor core region between the lower and upper grid plates. The uniform inlet velocity distribution and constant inlet temperature are imposed on the inlet boundary of the model. The details of the CFD modeling for the conjugate heat transfer analysis are discussed in Section 7.1.

The temperature fields of claddings obtained from the finite volume method (FVM)-based CFD analysis must be converted for the finite element method (FEM)-based solid stress/deformation analysis. The Data Mapper in STAR-CCM+ was employed to interpolate and map the data from FVM-based cells to FEM-based vertices. The external data mapping in Figure 1 was performed using the Volume Data Mapper function of STAR-CCM+ code. The details of the data mapping process are discussed in Section 7.2.

The Abaqus simulations were performed to assess the thermal deformation of claddings and the change in the fuel-to-fuel gap distance. Two scenarios were assumed for the boundary condition of the Abaqus analysis. The first scenario assumed the free thermal bowing of the claddings. This means there is no constraint at the upper end of the cladding. This is a hypothetical case because the reactor core components such as the upper alignment grid plates and fuel pin to upper grid adapter will restrain the transverse displacement of the fuel rods. The second scenario assumed the constraints in transverse direction but allowed the axial expansion of claddings. This is considered a more realistic scenario. In both scenarios, the bottom of the claddings assumed to be fully fixed, i.e. there are no displacements in X-, Y- and Z-directions. The details of the Abaqus models are discussed in Section 7.3.

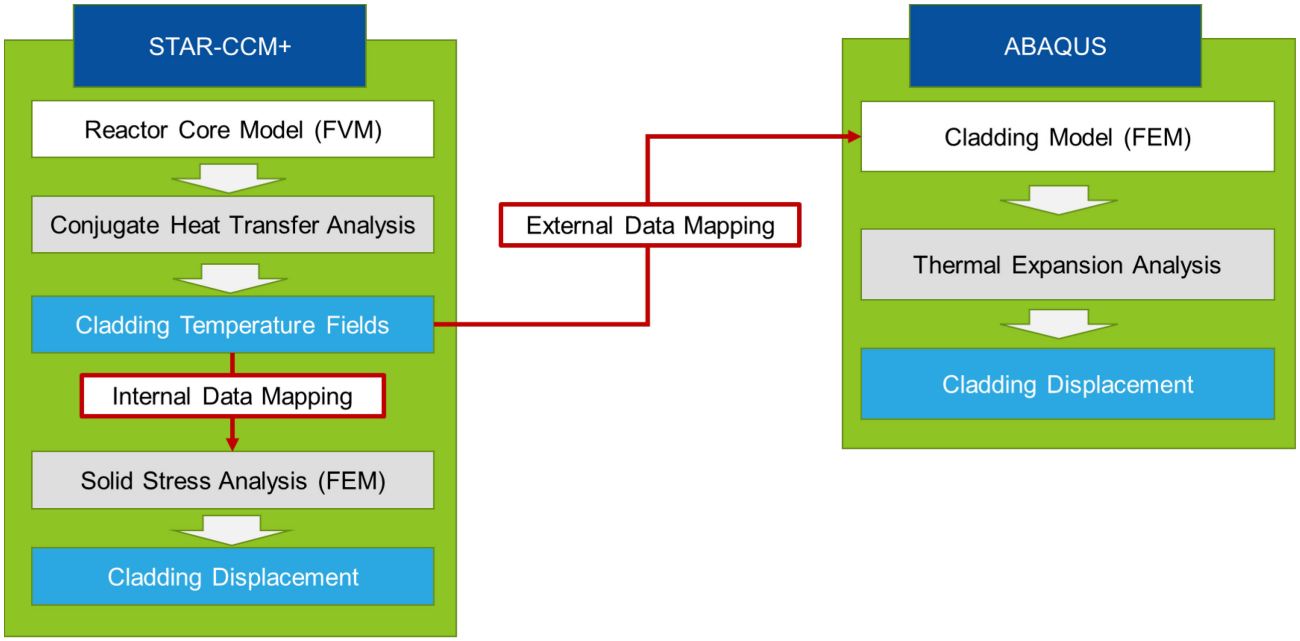

Figure 1. The overview of modeling and simulation process.

7.1. Conjugate Heat Transfer Analysis of MARVEL Reactor Core

7.1.1 Overview of CFD model

The CFD model of MARVEL reactor core internal structures is illustrated in Figure 2. The working fluid is NaK (sodium-potassium). The dimensions of the fuel rod are shown in Figure 3. The CFD model was generated based on the CAD geometry which is stored in the HPC storage "/projects/MARVEL_CFD/MARVEL/ECAR7210/Final/CAD." The total length of cladding in the CAD model is 32.332" (0.8213 m) which is slightly longer than the nominal design length of cladding (32.222" = 0.8184 m). Although this discrepancy in the length of the fuel rod is originated from the simplified CAD geometry provided for this work, its impact was expected to be negligible. The reactor components irrelevant to the scope of this ECAR were removed from the CFD model.

The solid parts of fuel rod internals were modeled based on the CAD drawings. The fuel rod model (DWG-1011202) consists of the fuel plenum, zirconium rod, top and bottom graphite reflectors, fuel meat, and cladding. The key dimensions of the fuel rod model are illustrated in Figure 3. The Molybdenum disks between the fuel meat and reflector were simplified, since it is expected the Molybdenum disk will not have a significant impact on the heat transfer between the graphite reflector and fuel meat due to its very thin the thickness (0.031") and the very high thermal conductivity of molybdenum [9]. The 0.002"-thick gap between the fuel meat and cladding inner wall was also simplified by assuming the diameter of cladding inner wall is same to the outer diameter of fuel meat. The volumetric changes of fuel and cladding could be different, and the fuel-to-cladding gap can decrease if the radius of fuel increases faster than that of cladding per [10]. The fuel-to-cladding gap plays a role in the thermal resistance between the fuel and the cladding material so that an increase in gap size leads to an increase in the maximum temperature of the fuel. On the other hand, the maximum temperature of the cladding material decreases as the fuel-to-cladding gap size increases. Because

thermal expansion is directly proportional to temperature, assuming no fuel-to-cladding gap between the fuel and cladding will result in a conservative estimate of cladding deformation. In the same manner, 0.0425”-thick gap between the graphite reflector and the cladding is also removed by assuming the outer diameter of graphite reflector is same to the outer diameter of fuel meat.

The material properties of the modeled core internal structures and the working fluid are summarized in **Appendix C**.

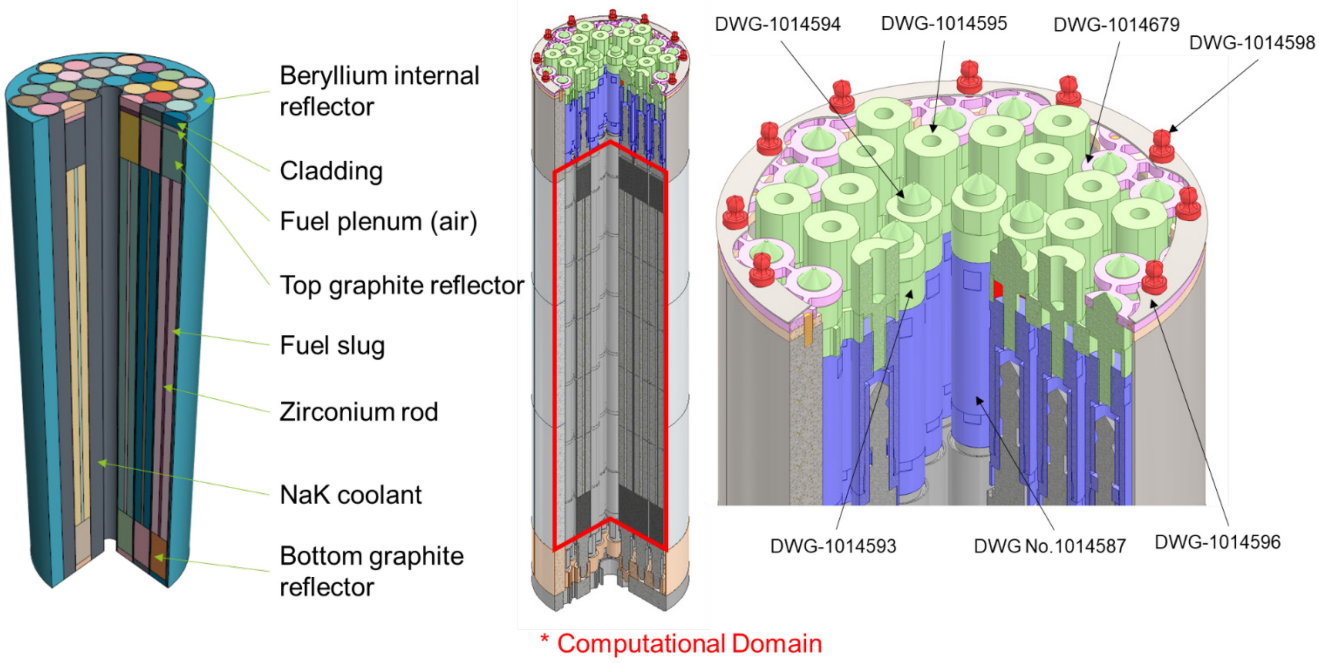

Figure 2. CFD model of MARVEL reactor core internal structures

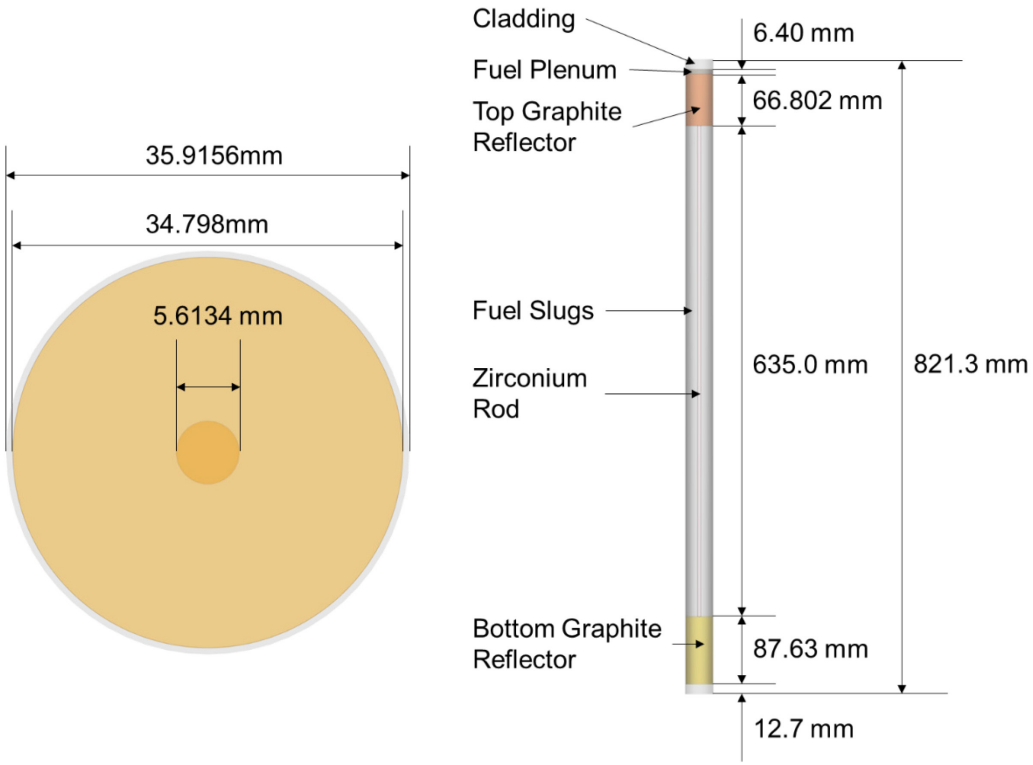

Figure 3. Dimensions of fuel rod in the CFD model

7.1.2. Boundary conditions

There are 36 fuel rods in the reactor core, each of which has five fuel meats that have been simplified as a single volume in the CFD model. Figure 4 shows the fuel pin peaking factor distribution and axial power profile which were used to define the power distribution in the reactor core. Figure 4-(a) shows the numbering of the fuel rod IDs. The fuel rods are divided into three zones. A 4th-order polynomial function implemented in the field function “Axial power profile” to calculate the volumetric heat generation rate of modeled fuel volume based on the axial power factor profile is given by:

$$APF=1.4080\cdot x^4 + 8.4258\cdot x^3 + 17.9597\cdot x^2 + 16.0240\cdot x + 5.0625 \quad (-1.8069\ m \leq x \leq -1.1719\ m) \qquad \text{Eqn. (1)}$$

where x in Eqn.(1) represents the axial position, and the values -1.8069 and -1.1719 represent the bottom and top elevations of the fuel volume in the CFD model, respectively.

The volumetric heat generation rate of the fuel meat was determined by multiplying the thermal power density of individual fuel rods by the radial power factor in Figure 4-(b) and the axial power factor in Eqn. (1) or Figure 4-(c). In this work, the thermal power density of the individual fuel rods was calculated by dividing the total reactor power by the number of fuel rods and the volume of fuel meat.

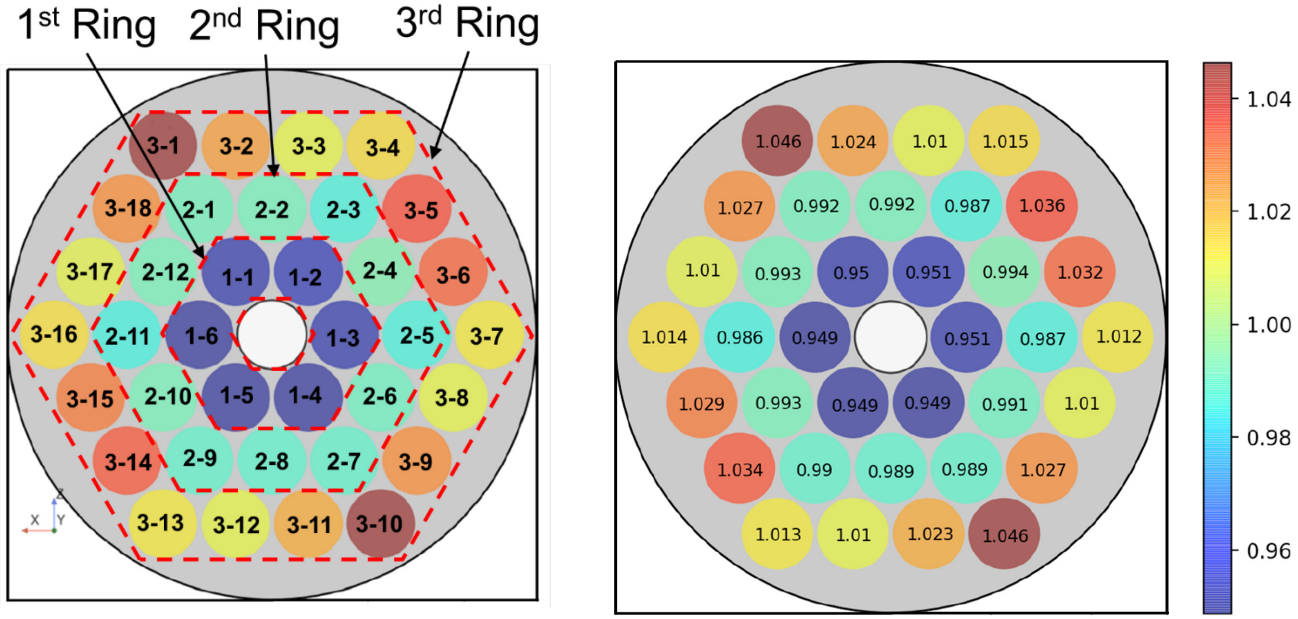

(a) Fuel pin numbering / zoning

(b) Fuel pin peaking factors

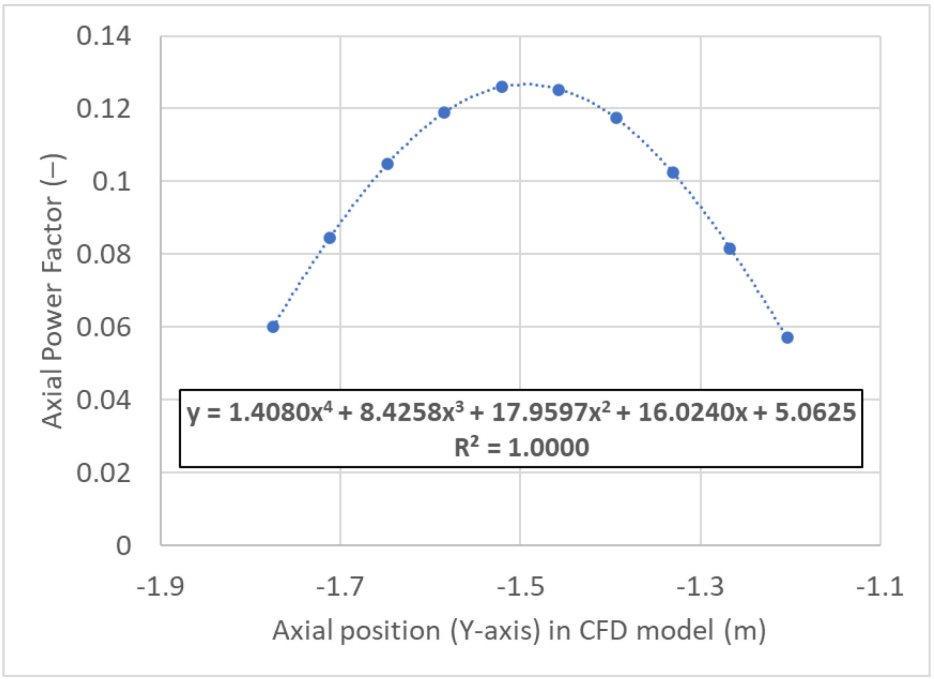

(c) Fuel axial power factor profile

Figure 4. MARVEL reactor thermal power inputs [11].

The reactor core power distribution in the CFD model is shown in Figure 5. Note that the power distributions in the fuel and side reflector derived from the Monte Carlo neutron transport code, MCNP [1], were 83.161 kW_{th} and 1.839 kW_{th}, respectively. This ECAR assumed 85 kW_{th} of reactor power in the fuel to provide a conservative assessment of cladding deformation. The adiabatic condition was imposed on the outer surface of the Beryllium internal reflector. This assumes no heat loss to the environment and will increase the temperature of internal structures. Hence, this boundary condition will also lead to a conservative prediction of the cladding temperature.

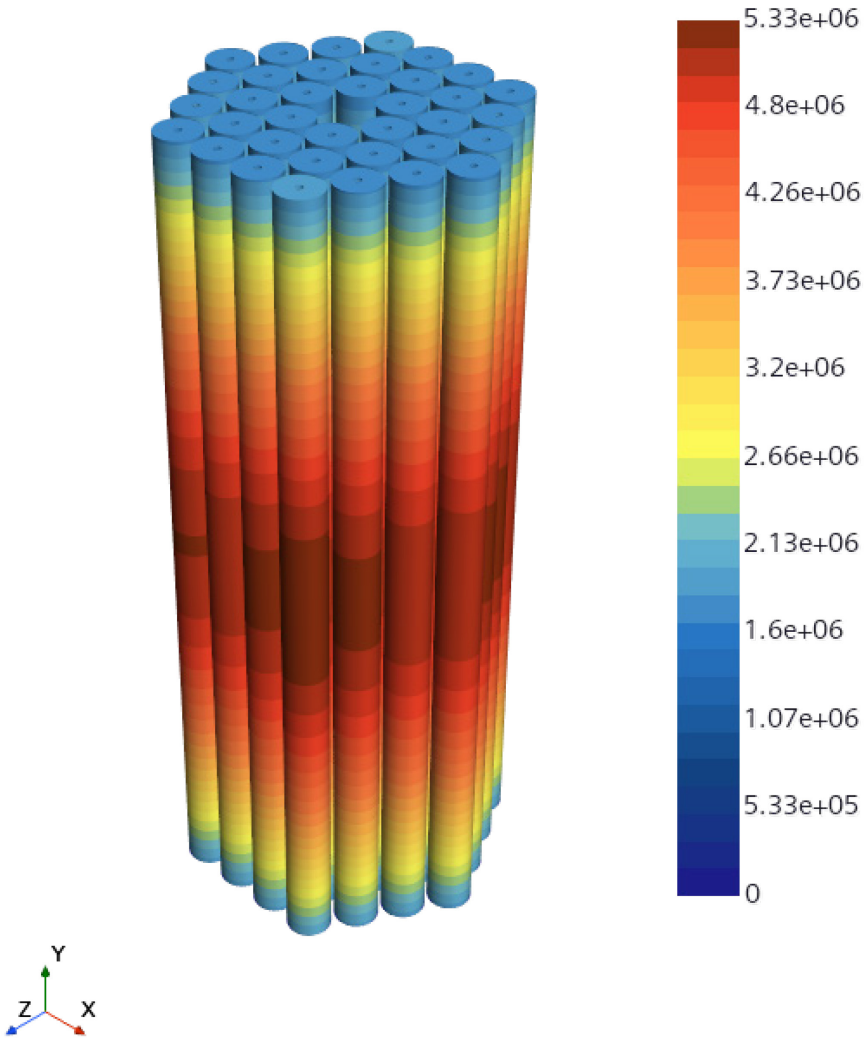

Figure 5. Volumetric heat generation rate distribution in the MARVEL reactor core [Unit: W/m^3]

The velocity inlet and pressure outlet conditions were imposed on the inlet and outlet boundaries of the model, respectively. At the pressure outlet boundary, the reference pressure of 0 Pa was specified. The total inlet mass flow rate and inlet temperature are specified to be 1.49 kg/s and 471.0°C (744.15 K), respectively, based on PCS mass flow rate and core inlet temperature reported in ECAR-6332 [11].

7.1.3. Numerical solver configuration

The CFD software, STAR-CCM+ ver. 2206.0001 Build 17.06.008, was adopted to solve the conjugate heat transfer in the MARVEL reactor core. A three-dimensional and Reynolds-averaged Navier-Stokes (RANS) equation-based CFD simulation was performed to calculate the cladding temperatures. The segregated flow and the segregated fluid temperature solvers were adopted to compute the heat and mass transfers in the fluid domain. The segregated solid energy solver was adopted to compute the heat transfer through the solid domains. Shear Stress Transport (SST) k-ω turbulence model with all y+ wall treatment method was adopted to solve the turbulence transport equations. The second-order convection scheme was adopted for segregated flow, segregated fluid temperature and turbulence model solvers. The simulation was iterated until the residuals of governing equations became smaller than 1E-4 and the monitored variables such as PCTs, NaK temperatures showed minimal change with successive iterations.

7.1.4. Computational mesh generation

The computational cells of the CFD model were generated by utilizing the polyhedral mesh for the conjugate heat transfer analysis, and the tetrahedral mesh was used for the STAR-CCM+ solid stress analysis. Figure 6 illustrates the mesh structure of MARVEL reactor core internal structures. To improve the accuracy of the temperature gradient calculation across the cladding wall, the built-in “Thin Mesher” scheme in STAR-CCM+ was utilized. This meshing scheme generated 3 mesh layers across the wall. The near-wall mesh was refined using the “Prism Layers Mesher”. The total thickness of the prism cell layers was set to be 16.665% of the base size mesh with a total of four prism boundary layers being generated. To investigate the sensitivity of the solution to mesh size, three different mesh structures were generated using the base sizes of 10.0mm, 20.0mm and 40.0mm.

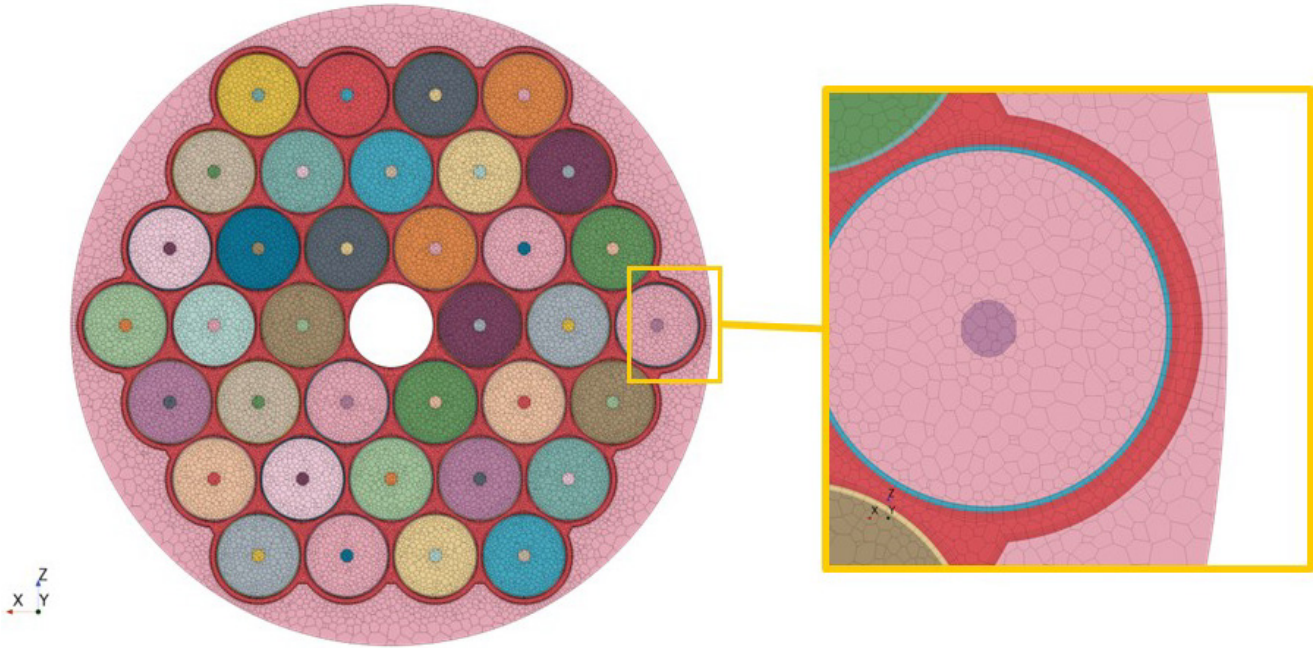

Figure 6. Mesh structure of MARVEL reactor core CFD model

The mesh sensitivity test results are presented in **Appendix F**. While the mesh sensitivity for the PCT was insignificant (less than 0.4%), the finest mesh with base size of 10.0 mm resulted in the highest PCT. Therefore, the calculation results discussed in this ECAR were obtained from the CFD model that was meshed using a base size of 10.0mm. The total number of computational cells generated using the base size of 10.0 mm was 44.74 million. Most of the near wall meshes fall in the viscous sublayers (y^+<5) as shown in as shown in Figure 7. Therefore, the velocity field near the wall could be well-resolved.

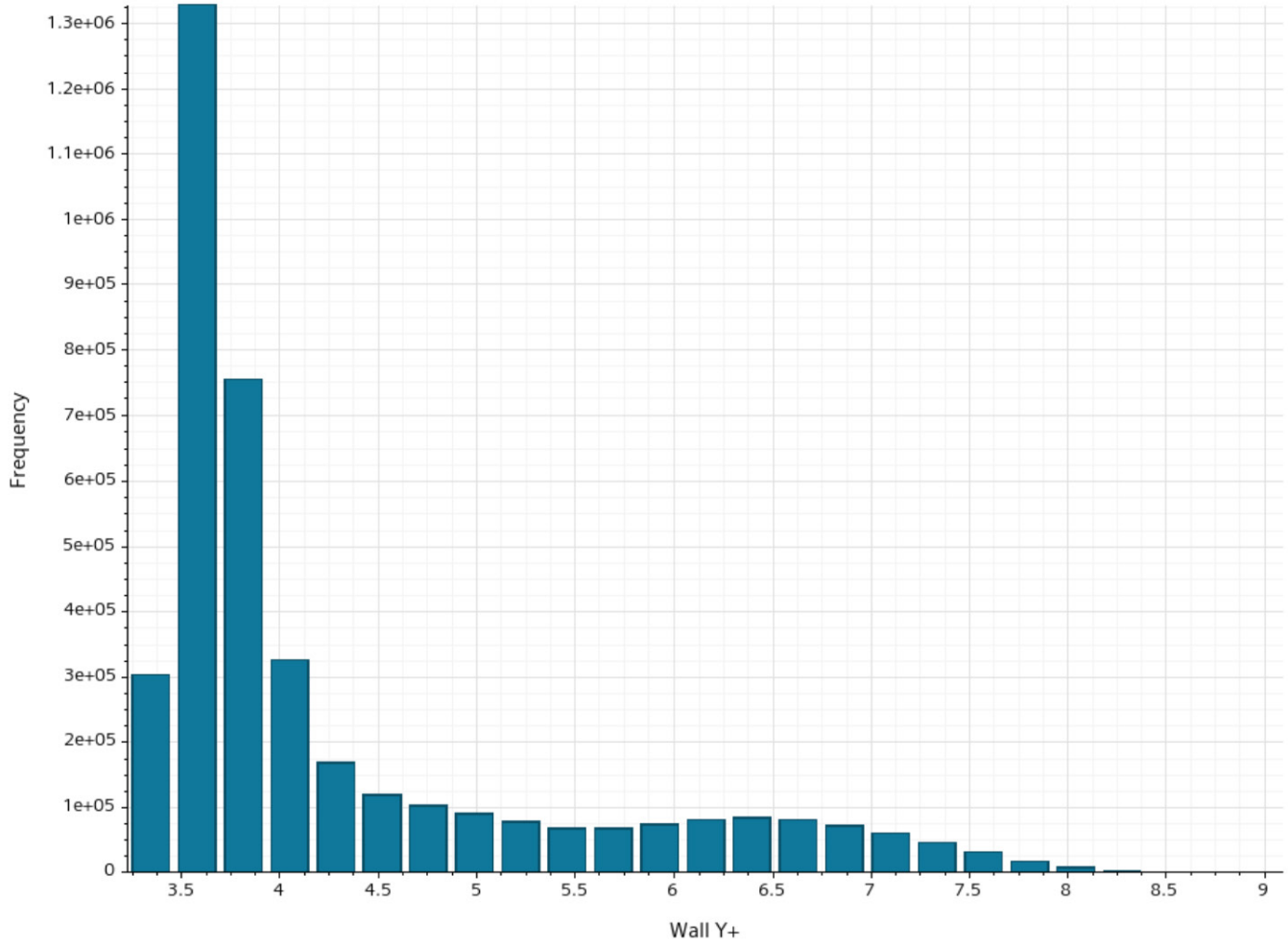

Figure 7. The statistics of wall Y+ value on the cladding wall (Base size: 10 mm)

7.1.5. CFD results

A total of five line probes were generated to evaluate the pressure drop across the reactor core. Figure 8 shows that the axial pressure profiles at different radial positions in the reactor core. The pressure drop across the reactor core was calculated to be 71.17 Pa for the given inlet flow rate of 1.49 kg/s. Although ECAR-6581 [12] reports the pressure drop of the bare-rod bundle, the pressure drop of this

work is not directly comparable to ECAR-6581 due to the differences in the total mass flow rate and thermal conditions.

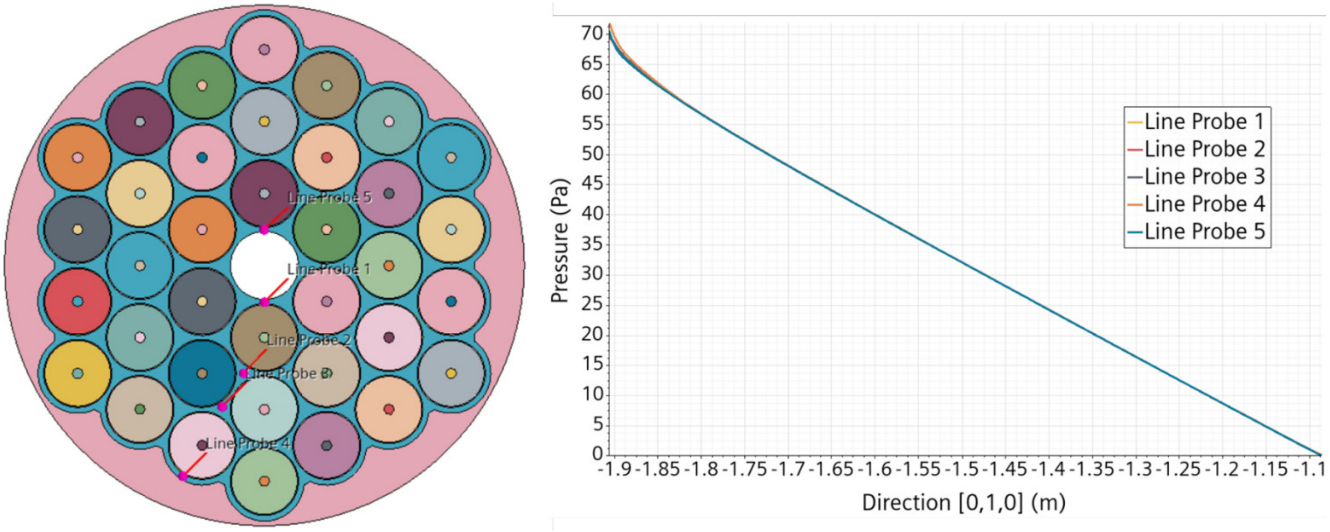

Figure 8. Axial pressure distribution in the MARVEL reactor core

Figure 9 shows three horizontal planes to investigate the local temperature and flow distributions in the reactor core. Three planes are located at the bottom (y=-1.807 m), midpoint (y=-1.489 m) and the top (y=-1.172m) elevations of the fuel meat volume.

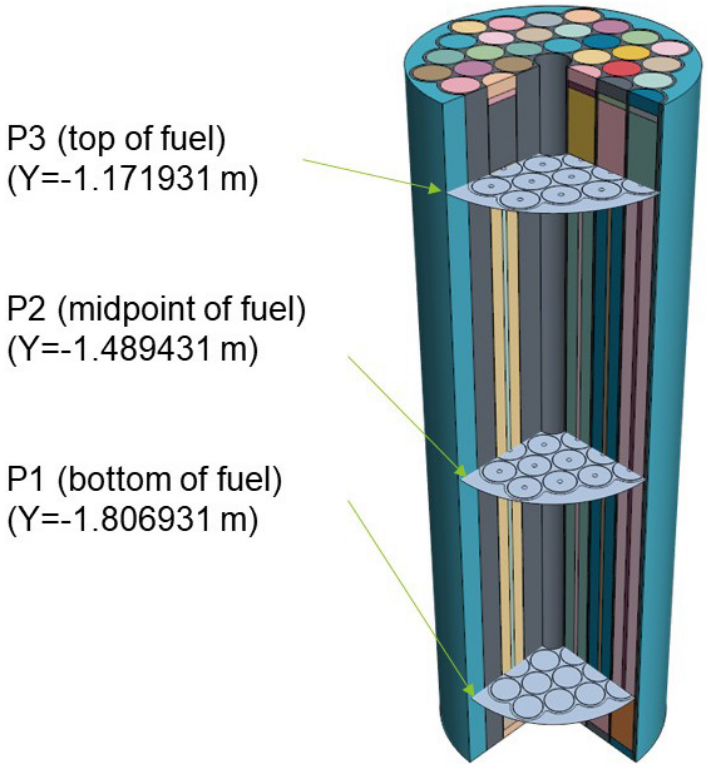

Figure 9. Plane sections to visualize the CFD simulation result.

Figure 10 shows the flow velocity distributions at different elevations in the core. As the coolant flows up and heated, the surface averaged flow velocity increases due to the changes in density and viscosity. The maximum velocity of the fluid increased as the flow along the subchannel was developed. The maximum velocity of the subchannel at the top elevation of the fuel (P3) was approximately 0.31 m/s.

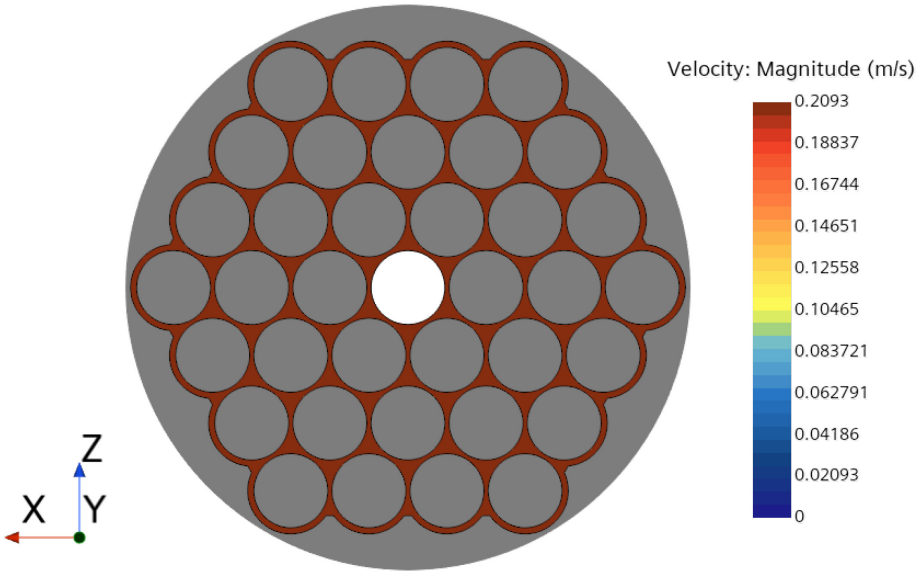

(a) Inlet

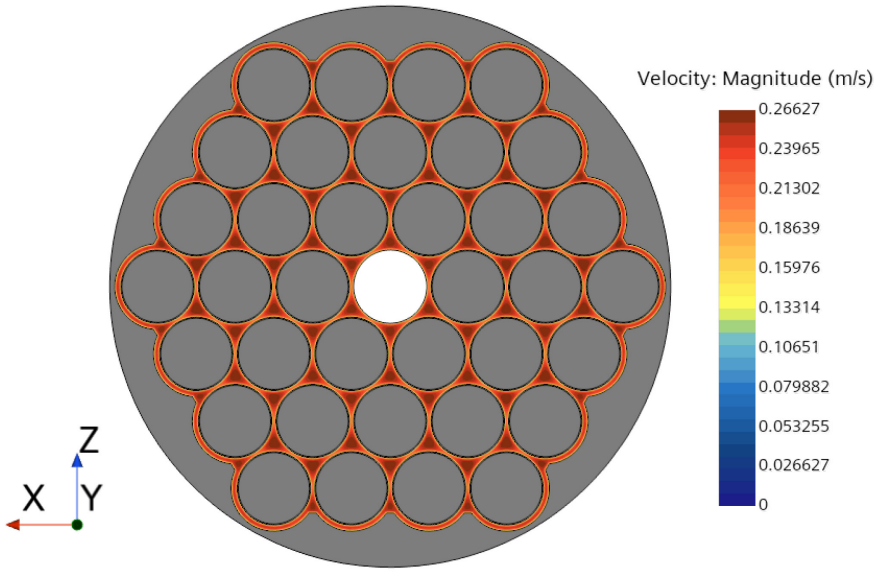

(b) Bottom of fuel (P1)

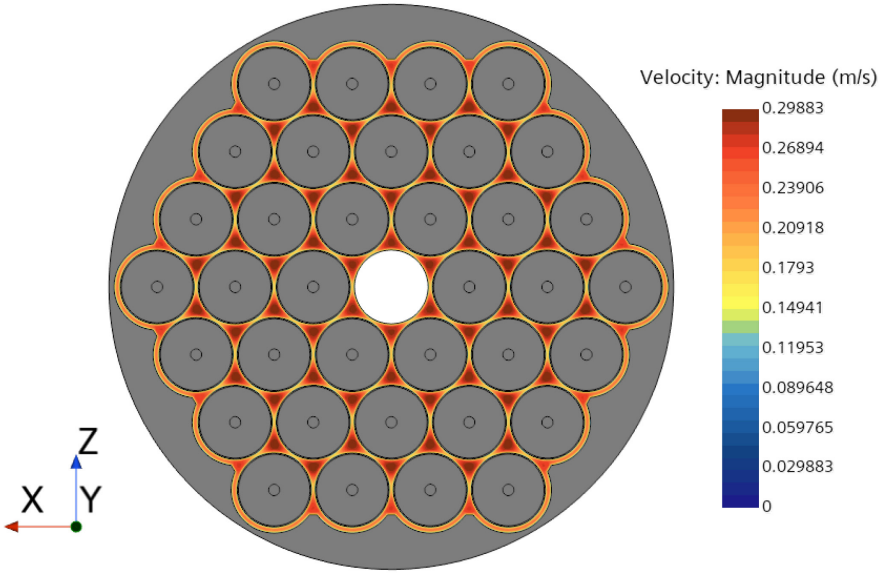

(c) Midpoint of fuel (P2)

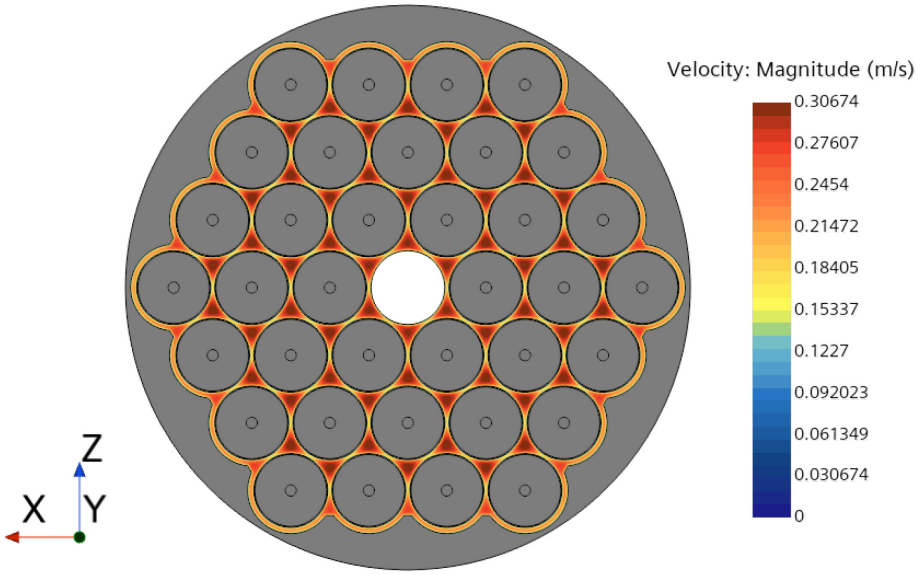

(d) Top of fuel (P3)

Figure 10. Flow velocity distributions at different elevations in the MARVEL reactor core

Figure 11 illustrates the temperature distributions at different elevations. The fuel rod 2-1 was the hottest rod in the core. The peak fuel and cladding temperatures of the fuel rod 2-1 were calculated to be 552.52 °C (825.67 K) and 545.94 °C (819.09K), respectively. Note that the peak temperatures of fuel and cladding were slightly higher than those depicted in Figure 11-(d) because the top of fuel is not the hottest spot due to the heat transfer to the top graphite reflector from the fuel.

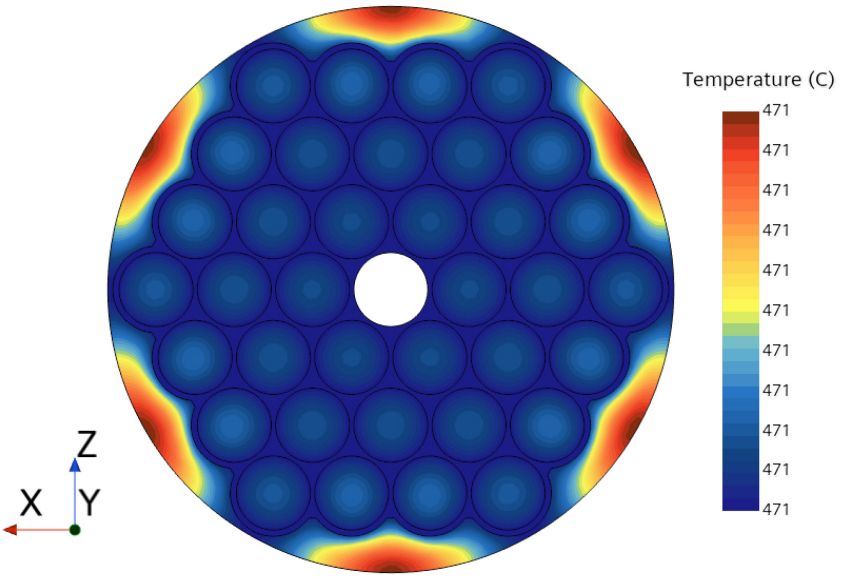

(a) Inlet

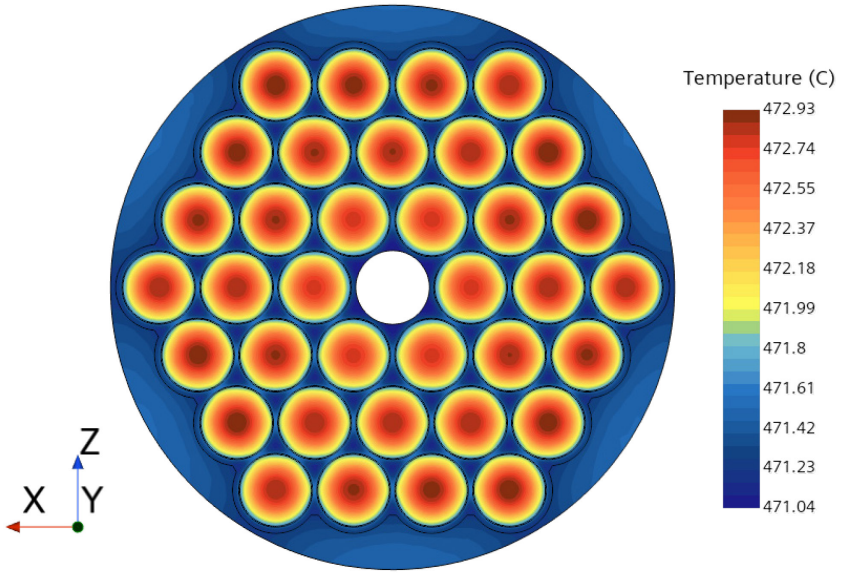

(b) Bottom of fuel (P1)

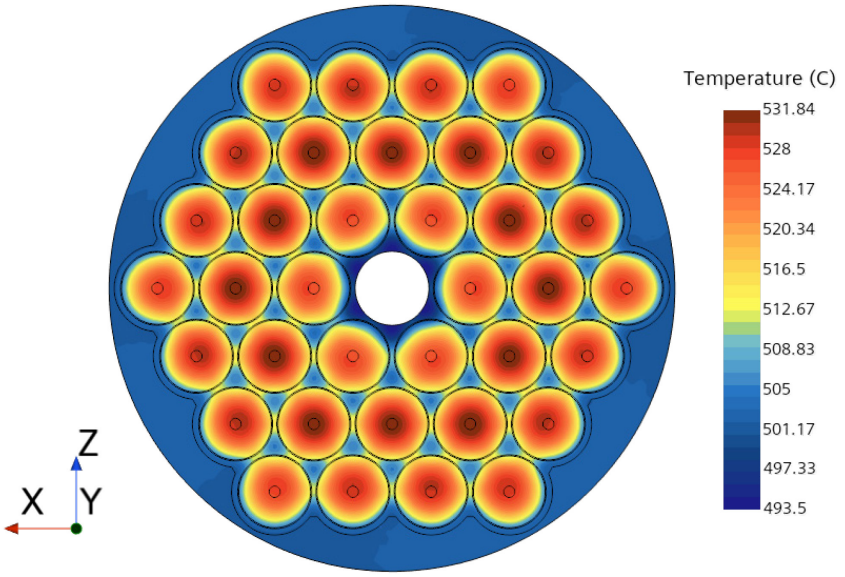

(c) Midpoint of fuel (P2)

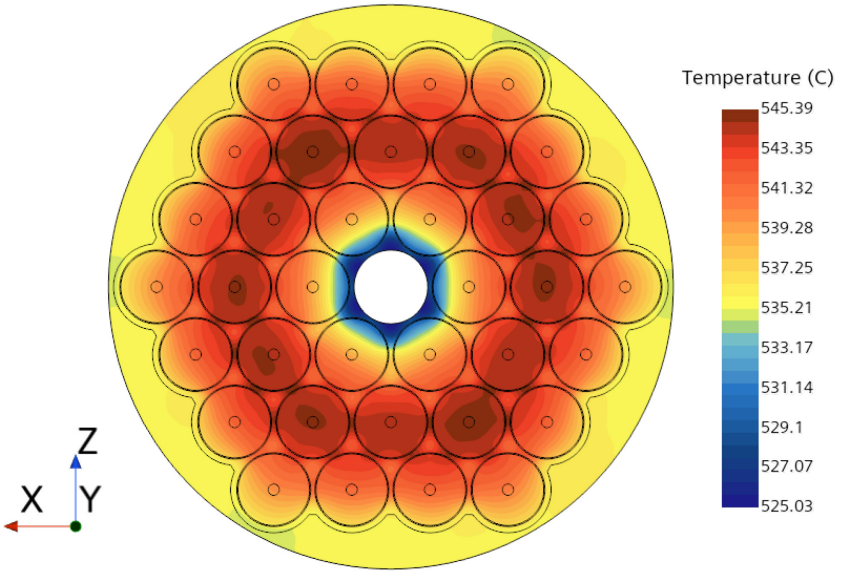

(d) Top of fuel (P3)

Figure 11. Temperature distributions at different elevations in the MARVEL reactor core

The azimuthal temperature profiles of three fuel rods aligned across the reactor core are depicted in Figure 12, Figure 13 and Figure 14. The azimuthal temperature was obtained on the surface interfacing fuel and cladding. It is worth noting that the differences in the maximum value of azimuthal temperature obtained from the fuel-to-cladding interface and the cladding-to-fluid interface were smaller than 1.0 K. The local temperature peaks were observed at the fuel-to-fuel gaps. The fuel rod 1-1 showed a different temperature profile due to the non-heated rod at the middle of the core. In the same manner, the fuel rod 3-1 showed a different temperature profile due to its proximity to the beryllium reflector where is not heated. The maximum azimuthal temperature variation of the cladding was 13.95 K in the 1st ring (fuel

rod 1-4), while the 2nd and 3rd rings showed 5.73 K (fuel rod 2-4) and 9.94 K (fuel rod 3-5), respectively. Fuel rods in the 1st and 3rd rings are adjacent to unheated components with relatively lower temperatures, whereas those in the 2nd ring are surrounded by other fuel rods, resulting in a smaller azimuthal temperature variation. The azimuthal temperature profiles of all fuel rods are attached in **Appendix G**.

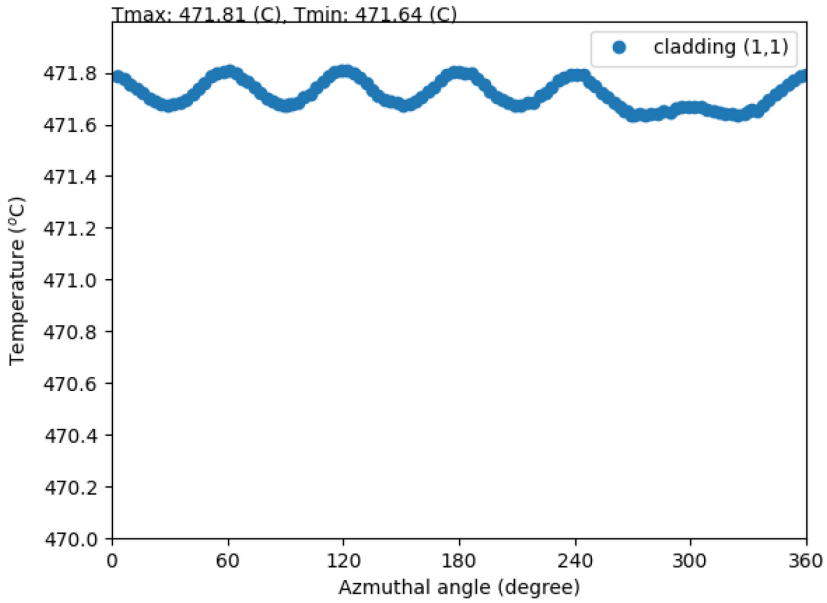

(a) Bottom of fuel (P1)

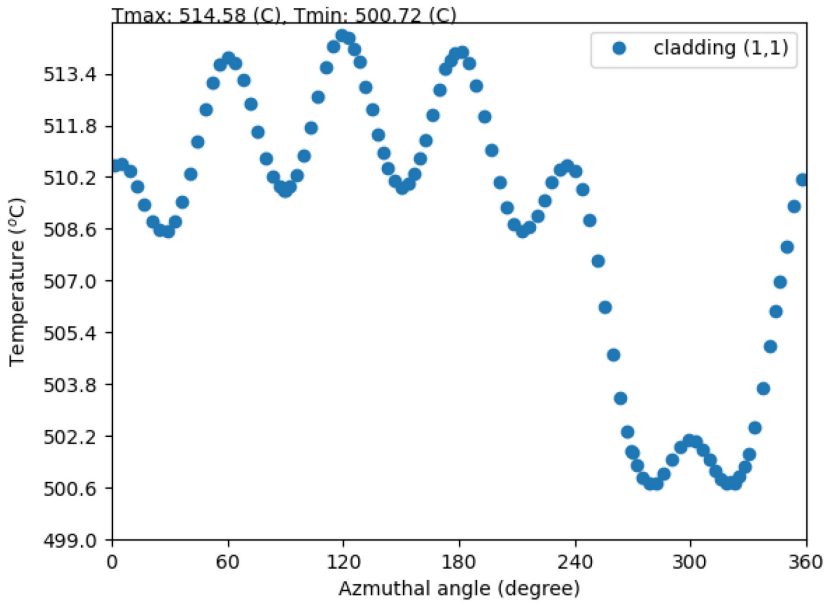

(b) Midpoint of fuel (P2)

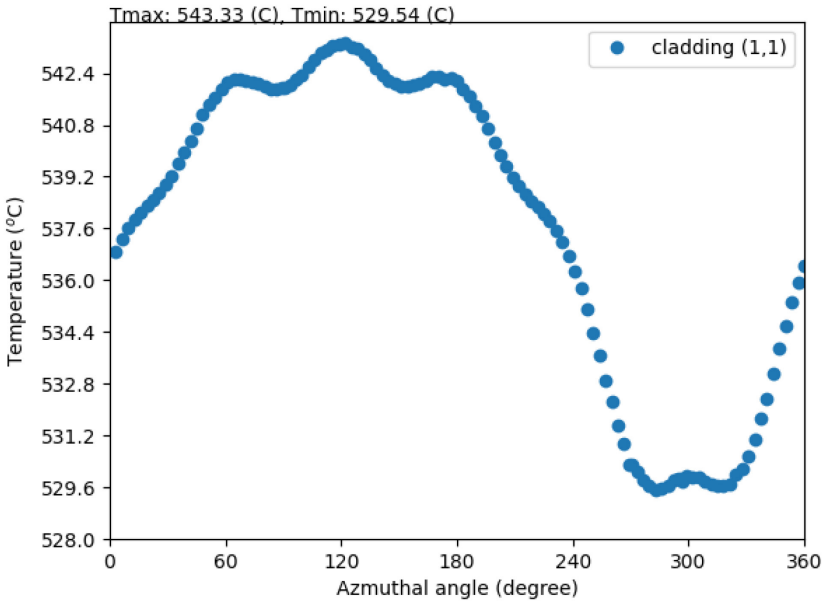

(c) Top of fuel (P3)

Figure 12. Azimuthal temperature profiles of fuel rod 1-1 at three elevations P1, P2 and P3.

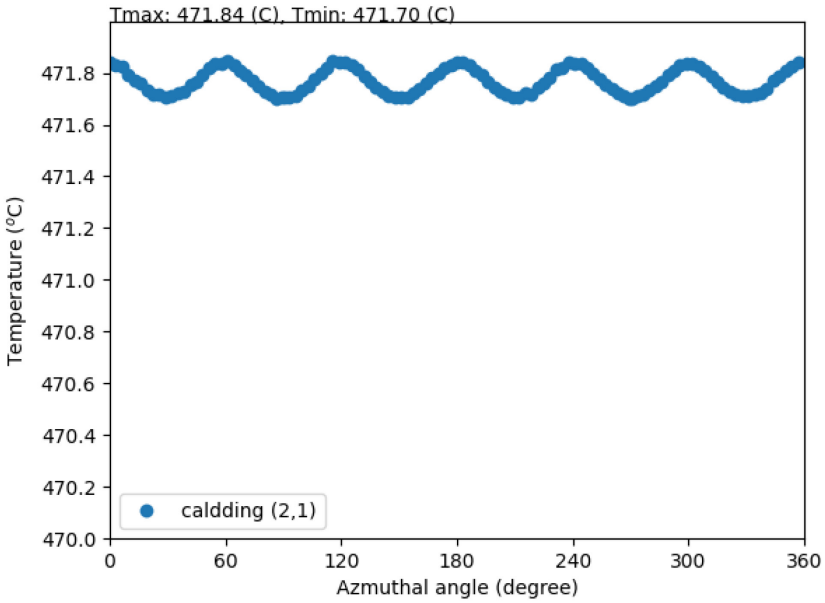

(a) Bottom of fuel (P1)

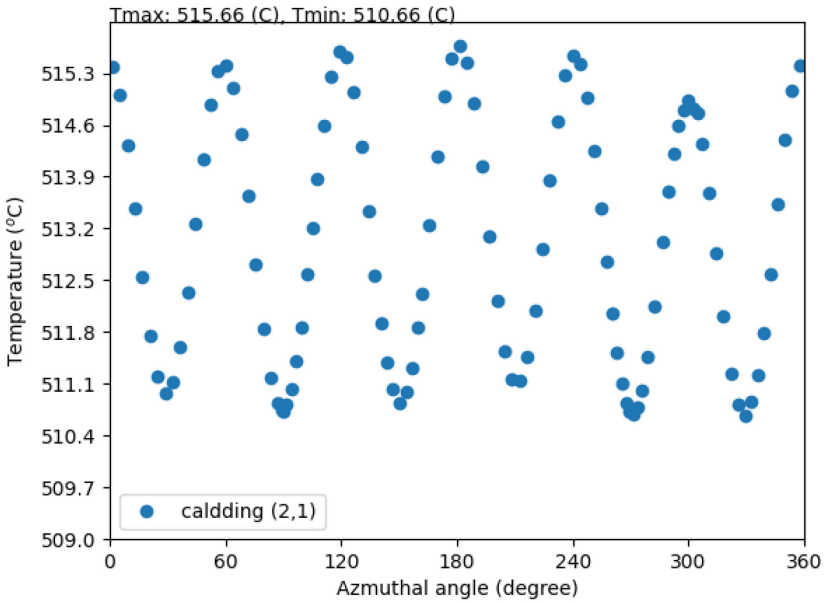

(b) Midpoint of fuel (P2)

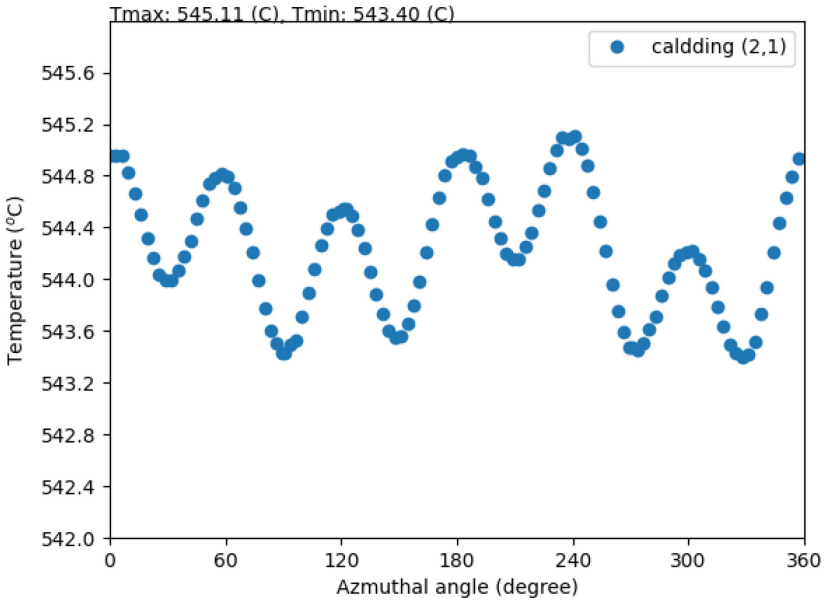

(c) Top of fuel (P3)

Figure 13. Azimuthal temperature profiles of fuel rod 2-1 at three elevations P1, P2 and P3.

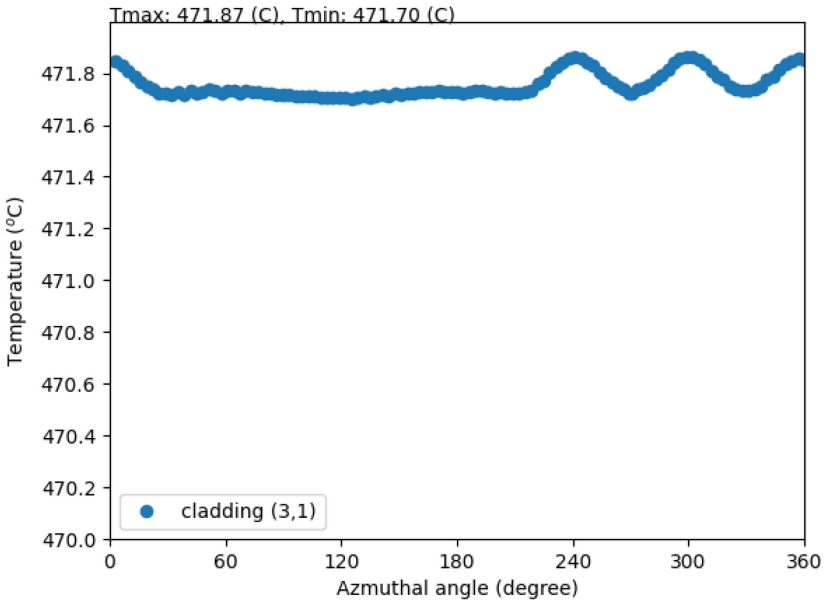

(a) Bottom of fuel (P1)

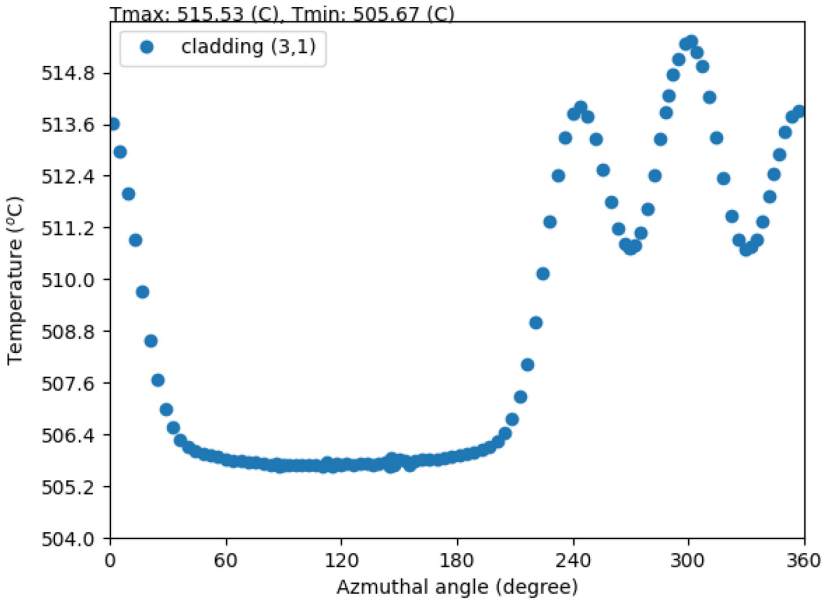

(b) Midpoint of fuel (P2)

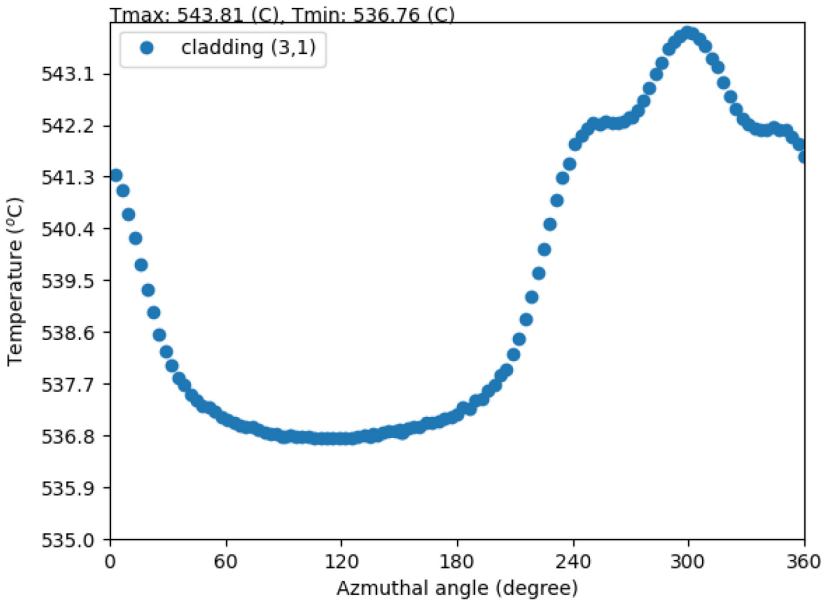

(c) Top of fuel (P3)

Figure 14. Azimuthal temperature profiles of fuel rod 3-1 at three elevations P1, P2 and P3.

The isometric view of the temperatures of fuel and cladding are illustrated in Figure 15. The temperature increment from the inlet to outlet was 68.57 K. Three-dimensional temperature fields depicted in Figure 15-(b) were exported with their X-, Y-, and Z-axial coordinates to specify the boundary condition of finite element model.

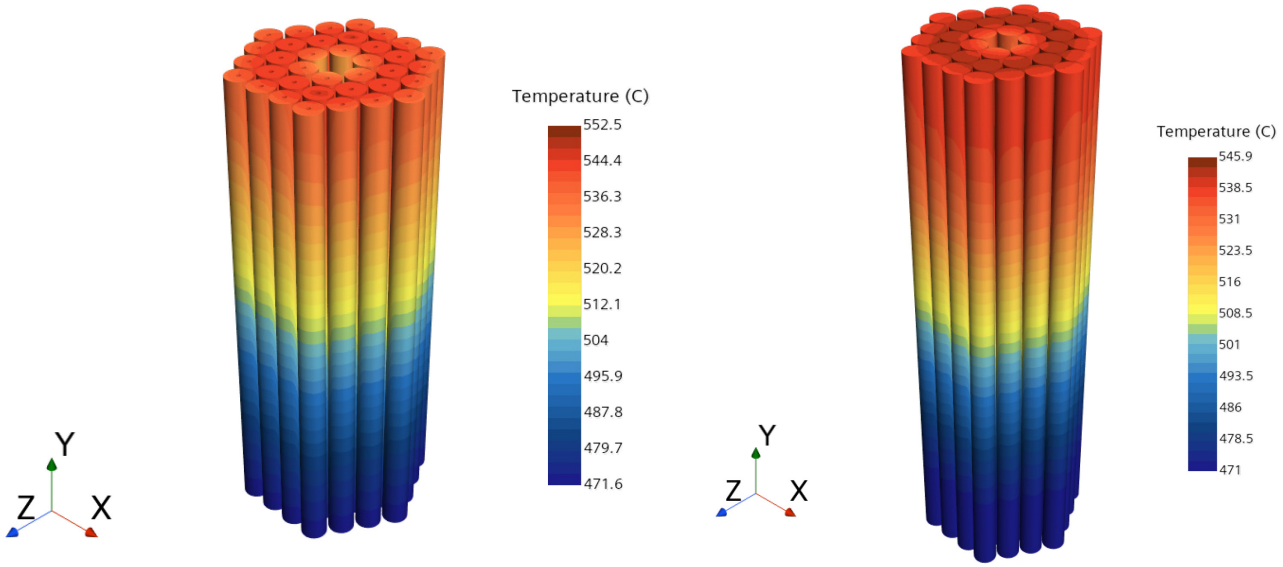

(a) Fuel temperature (b) Cladding temperature

Figure 15. Isometric view of fuel and cladding temperature distributions.

7.2. Data Mapping Process

The flow velocity in the MARVEL reactor core was relatively slow (~0.3m/s) and the differential pressure in both transversal and axial directions were not significant. Since the stress due to the differential pressure on the cladding surface would be negligible, hence, it is not mapped in this work.

7.2.1. External data mapping from STAR-CCM+ to Abaqus

For the external data mapping from STAR-CCM+ to Abaqus, Abaqus input file (*.inp) needs to be prepared first. In this work, the cladding geometry is exported as IGES file from the CFD model. It is worth noting that the STEP file format exported from STAR-CCM+ may not be fully compatible with Abaqus. The following steps describe the external data mapping process:

1. Import cladding geometry into Abaqus: The cladding geometry can be obtained from CAD software or STAR-CCM+ (“File” >> “Import” >> “Part…” in Abaqus).
2. Prepare Abaqus input file: In this step, the mesh of imported cladding geometry is generated to write an Abaqus input file (“Analysis” >> “Jobs” >> “Write Input” in Abaqus).
3. Import Abaqus input file to STAR-CCM+: The Abaqus input file generated in Step-2 is imported to STAR-CCM+ (“File” >> “Import” >> “Import CAE Model” in STAR-CCM+).
4. Data mapping and export mapped data: Temperature field of STAR-CCM+ FVM cells is mapped to Abaqus FEM elements (data type: Vertex) using “Map Data” function of STAR-CCM+ (“Imported Models” >> “Map Data” >> “Volume Data…” in STAR-CCM+). The mapped data can be exported to Abaqus input file (“Imported Models” >> “Export Mapped Data” in STAR-CCM+). The header “*TEMPERATURE” in the exported Abaqus input file needs to be commented out (“*TEMPERATURE” >> “**TEMPERATURE” in mapped Abaqus input file).
5. Data conversion from Abaqus input file to Abaqus output database: The mapped temperature fields in Abaqus input file should be converted to Abaqus output database (*.odb) for the finite element analysis. For this data conversion, “Predefined Fields” in Abaqus needs to be created with an initial condition first. Next step is that editing the model Keyword (“Model” >> “Edit Keywords” >> Edit “Predefined Fields” block) to include the mapped temperature field as shown in Figure 16. It is worth noting that the initial condition should be commented out (e.g., “**SET-1, 294.26” in Figure 16) and the absolute path to the mapped Abaqus input file should be specified. In addition, the thermal expansion coefficient in the Abaqus model for converting the mapped temperature field should set to be zero without any mechanical loads.

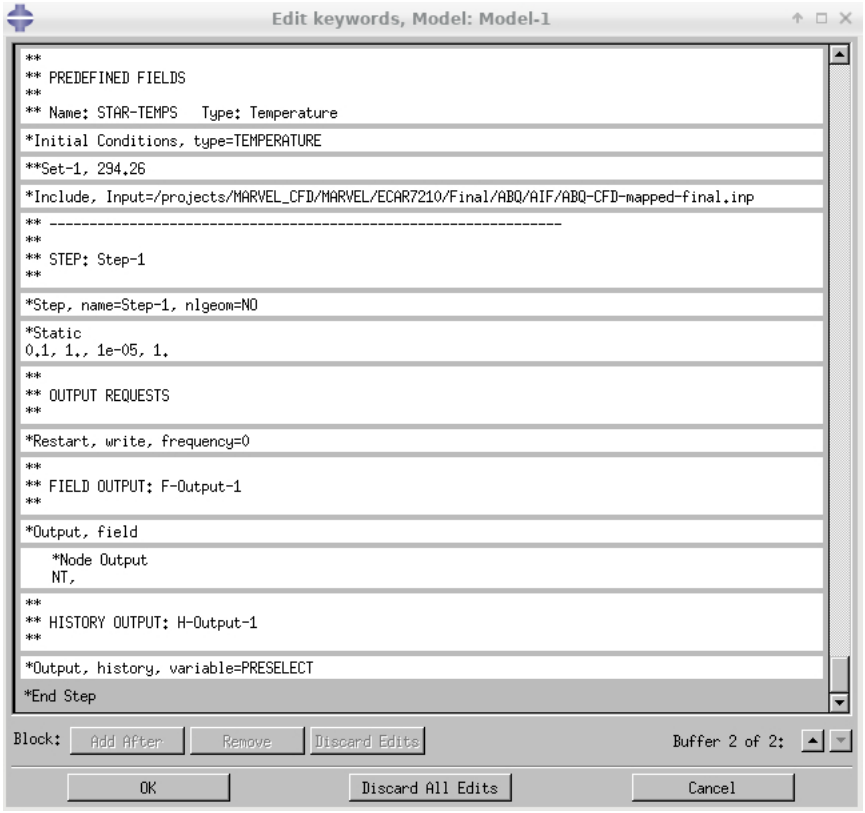

Figure 16. Model Keywords Function in Abaqus to defined Predefined Fields with mapped data.

6. The Abaqus output database can be generated by running the Abaqus model. The mapped temperature field converted to Abaqus output database is shown in Figure 17. In the Abaqus model, the temperature field is in unit of Kelvin. The comparison of the temperature bounds in Figure 17 with those in Figure 15.
7. Figure 15-(b) confirms that the data mapping has been performed appropriately. The Abaqus output database can be loaded to “Predefined Fields” for thermal deformation calculations.

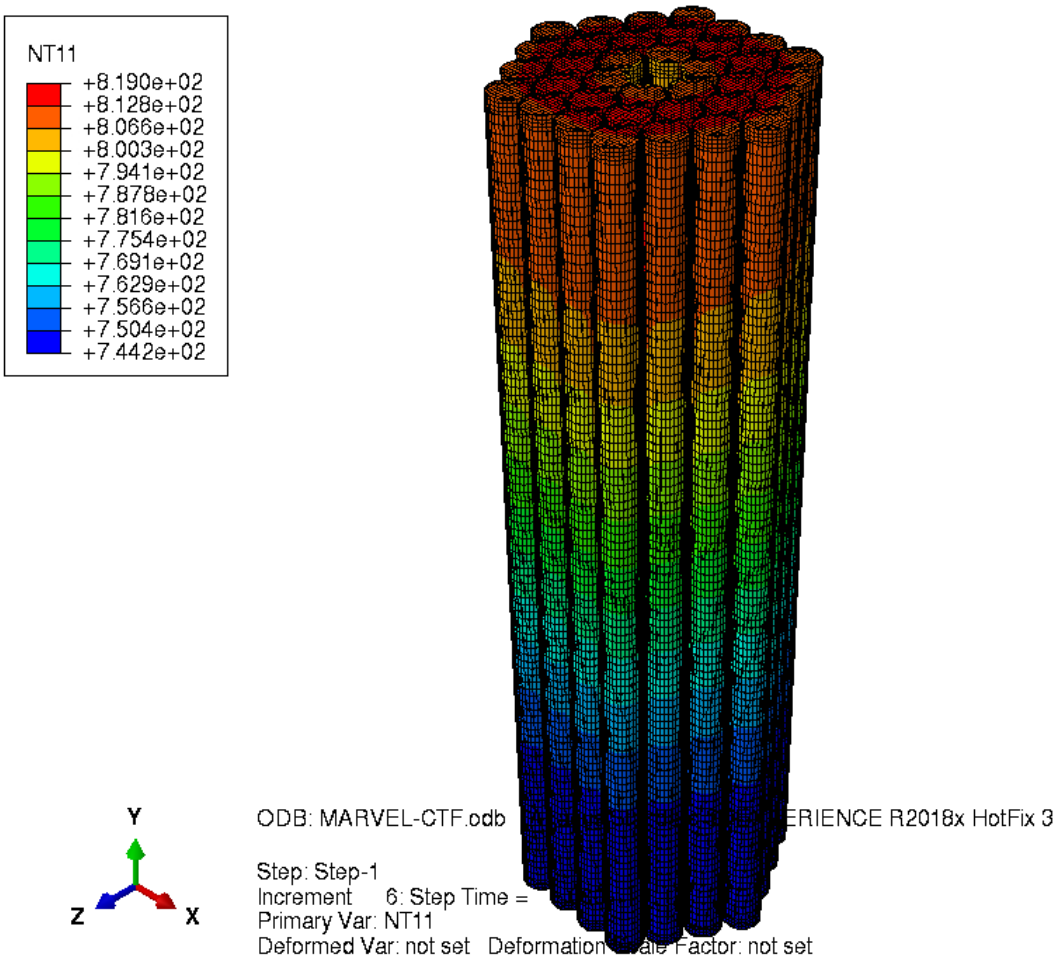

Figure 17. Mapped temperature field of fuel cladding imported into Abaqus [unit: Kelvin].

7.2.2. Internal data mapping from cell to vertex for solid stress analysis in STAR-CCM+

STAR-CCM+ is also capable of running a solid stress analysis. To perform the finite element solids stress analysis in STAR-CCM+, the cladding parts need to be duplicated and re-meshed using the tetrahedral mesh. The base mesh size of tetrahedral element for the solid stress analysis was 10.0 mm. The internal data mapping from polyhedral cell to tetrahedral element can be performed using “Data Mappers” of STAR-CCM+ (“Tools” >> “Data Mappers” >> “New Data Mappers” >> “Volume Data Mappers” in STAR-CCM+). The model properties of “Volume Data Mappers” are tabulated in Table 1. The internal data mapping creates the field variable for the thermal load with the name specified in “Data Mappers”. In this work, the name of the field variable is “CHT-Thermal Load”. This field variable is utilized to specify the temperature field of cladding region (“cladding XX-YY” >> “Physics Values”>> “Specified Temperature” >> “Properties” >> “Method”: “Field Function” and “Scalar Function” “CHT-Thermal Load”). The cladding numbering “XX-YY” can be found in Figure 4-(a). The mesh structure of claddings for the solid stress analysis is illustrated in Figure 18.

Table 1. Model Properties of Data Mappers for STAR-CCM+ Solid Stress Analysis

Properties	Source		Properties	Target
Source Volumes	All cladding parts (original) in conjugate heat transfer analysis		Target Entities	All cladding parts (duplicated) for solid stress analysis
Source Stencil	Cell		Target Stencil	Vertex
Scalar Field Functions	Temperature		Target Source Transform	Identity Transform
Vector Field Functions	N/A		Interpolation Method	Least Squares
Mapped Names	Source Names	Temperature	Limiter	Min/Max of Contributing Stencil
	Mapped Names	CHT-Thermal Load	Boundary Map Option	Map from Boundaries of Source Volumes

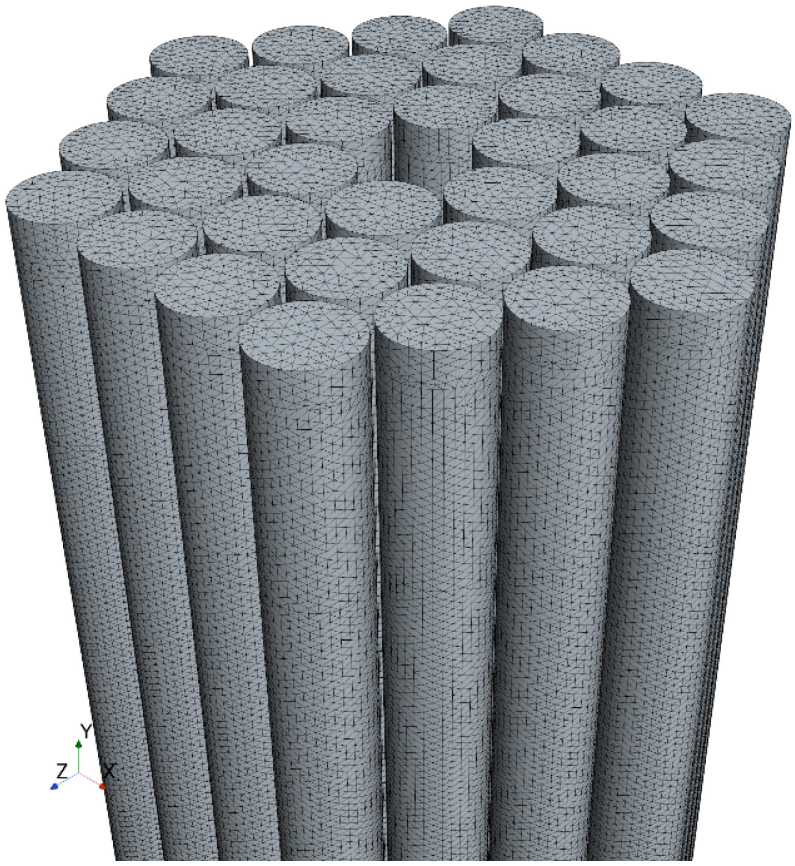

Figure 18. Tetrahedral mesh structure of claddings generated for STAR-CCM+ solid stress analysis

7.3. Finite Element Analysis of MARVEL Reactor Fuel Cladding

As described in Section 5, the core internal structures, once assembled, can restrict the transverse displacement of the fuel rods at both ends while the axial expansion of fuel rods is allowed. The top and bottom boundary conditions of the Abaqus cladding model were specified as shown in Figure 19. The pressure load above the top of the modeled core was calculated to be 13630.79 Pa (**Appendix E**). This pressure load was employed in the Abaqus model. Additionally, a finite element analysis was conducted, assuming free thermal bowing of the fuel rods, to investigate the thermal bowing direction of each fuel rod. The ABAQUS model for claddings were meshed by using the structured linear hexahedral element (C3D8R) for 3D stress analysis. The mesh partitioning was performed to generate the hex elements as shown in Figure 20. Total number of node and element per rod are 18250 and 14692, respectively. A general, static step was created to define to run the finite element thermal deformation simulation.

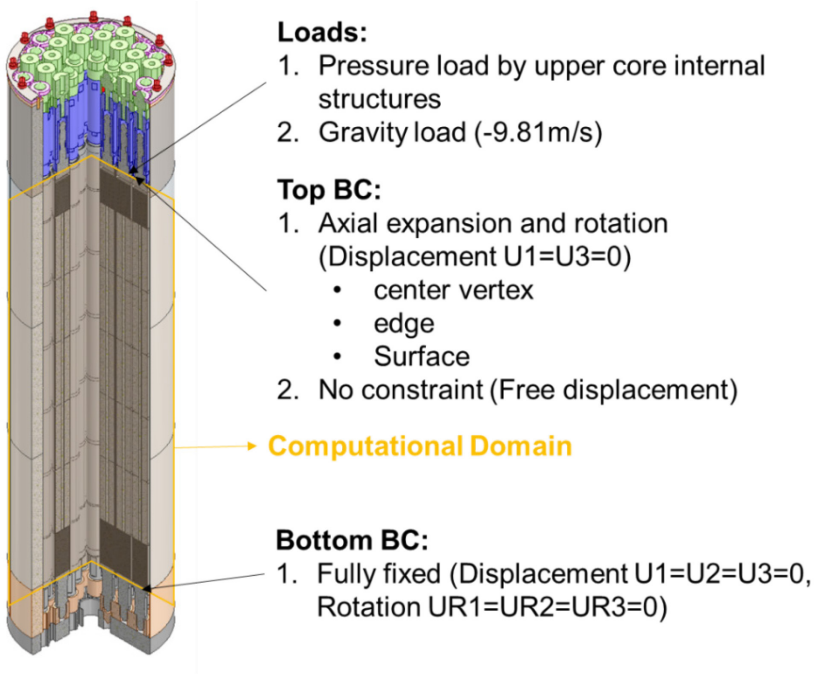

Figure 19. Boundary conditions for finite element analysis

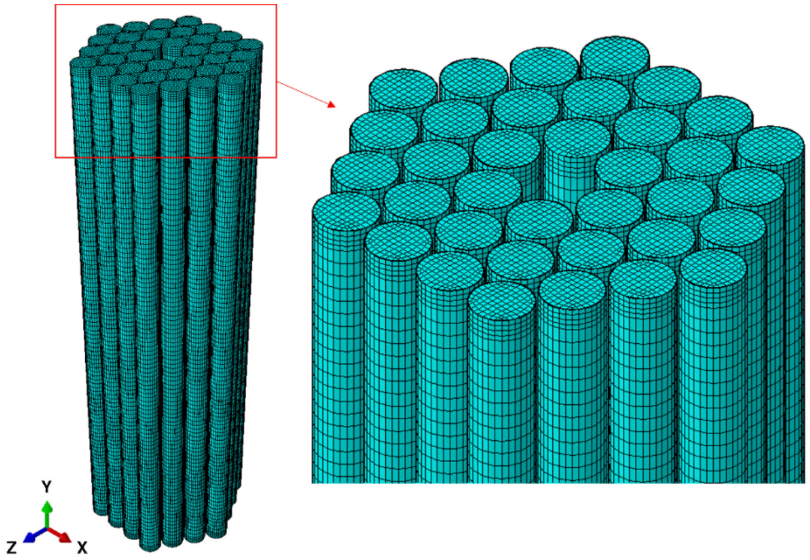

Figure 20. Mesh structure of ABAQUS cladding model.

7.3.1. FEA result in STAR-CCM+

The finite element method-based solid mechanics model in STAR-CCM+ can calculate the thermal expansion of the cladding. The solid stress solver with the isotropic linear elasticity and isotropic thermal expansion solvers were adopted for the analysis.

The thermal strain ε_T in STAR-CCM+ is defined as:

$$\varepsilon_T = \alpha\left(T - T_{ref}\right) \qquad \text{Eqn. (3)}$$

where T_{ref} is the reference temperature at which the thermal strain is assumed to be zero, and α is the thermal expansion coefficient.

For a linear isotropic elastic material and infinitesimal strain ε, the change of volume relative to the deformed volume is calculated by:

$$\frac{V - V_0}{V} = \varepsilon = \alpha\left(T - T_{ref}\right) + \frac{\sigma_m}{K} \qquad \text{Eqn. (4)}$$

where V_0 is the initial volume of body, K is the bulk modulus, and σ_m is the mean stress.

To specify the mechanical properties in STAR-CCM+ FEA model, the polynomial functions for temperature-dependent Young's modulus and thermal expansion coefficient of cladding (Table 9 and in Table 10 in **Appendix C**) were derived as follows:

- α (1/K):

$$-1.537884E\text{-}17\times T^4+5.147804E\text{-}14\times T^3-6.525143E\text{-}11\times T^2+4.069205E\text{-}8\times T+7.722943E\text{-}6 \qquad \text{Eqn. (5)}$$

- Young's Modulus (Pa):

$$-3.9290E+04\times T^2 - 3.1303E+07\times T + 2.0717E+11 \qquad \text{Eqn. (6)}$$

In STAR-CCM+ model, scalar field functions for expansion coefficient and Young's modulus were created using the above equations.

Prior to running the thermal deformation model in STAR-CCM+, existing solvers for conjugate heat transfer analysis must be de-activated by checking "Solver Frozen" or "Freeze Flow" of "Wall Distance", "Segregated Flow", "Segregated Energy", "K-Omega Turbulence", and "K-Omega Turbulent Viscosity" solvers under "Solvers" menu in STAR-CCM+. In the STAR-CCM+ FEA model, only a few iterations were necessary to get a solution with the residuals of solid stress solvers and monitored variables (displacement and force) smaller than 1.0E-6.

Figure 21 illustrates the displacement components of cladding calculated using STAR-CCM+. For the free thermal bowing condition, the axial expansion of cladding (Figure 21-(b)) was 7.44 mm. The maximum values of radial displacements in X-axial direction and Z-axial direction were 1.155 mm and 1.075 mm, respectively. To verify the axial expansion of claddings, the linear expansion of cladding length based on the volume averaged cladding temperature was estimated by:

$$\Delta L = \alpha * L_0\left(T - T_{ref}\right) = 1.83796 \times 10^{-5} \cdot 818.44 \cdot (780.25 - 294.26) = 7.31\ mm \qquad \text{Eqn. (7).}$$

The axial expansion calculated by Eqn. (7) and STAR-CCM+ result showed good agreement. The relative deviation of axial displacement between the hand calculation and STAR-CCM+ was approximately 1.77%. The computational domain in this model is not a complete replica of the actual cladding geometry, but only partially models it. Additionally, the boundary conditions for the finite element analysis were not intended for the stress evaluations, but for evaluating thermal deformation. Therefore, the stress calculation result for claddings of this ECAR should not be used to assess the mechanical integrity of the claddings. In this regard, the stress calculation results will not be discussed in this report.

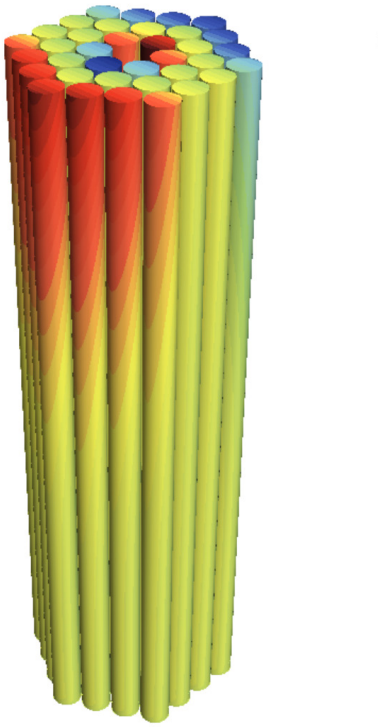

(a) Displacement in X-direction

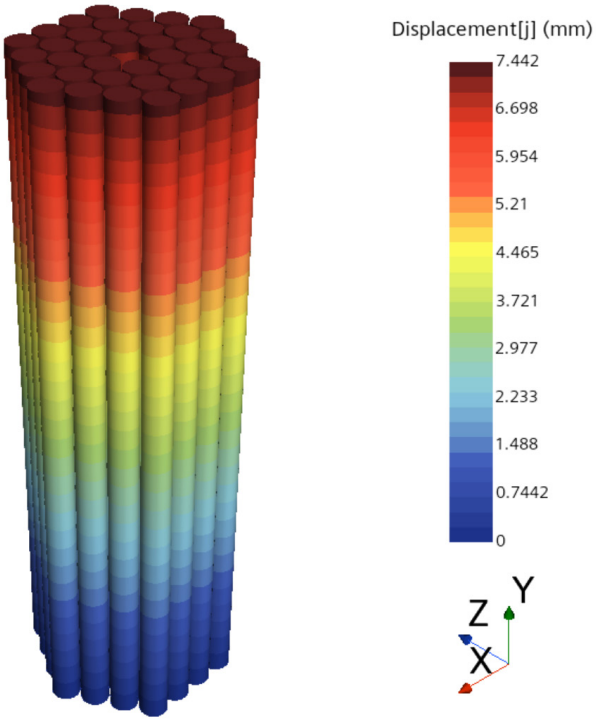

(b) Displacement in Y-direction

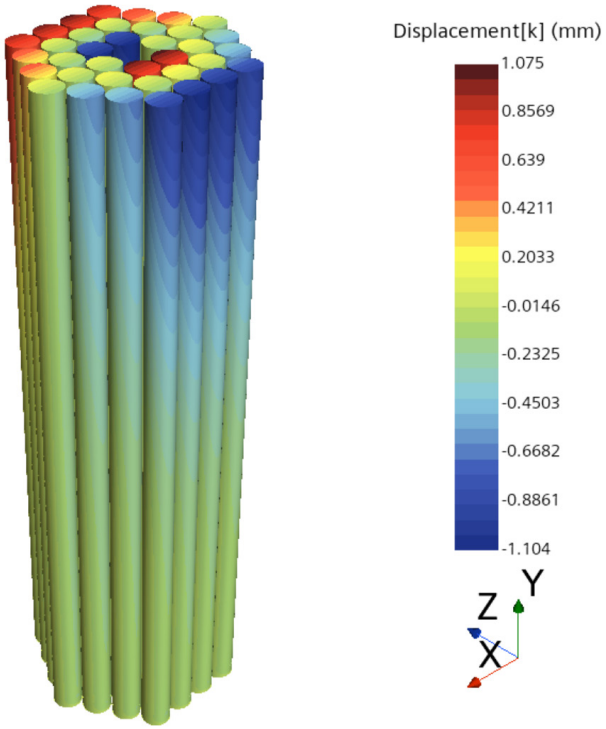

(c) Displacement in Z-direction

Figure 21. Displacement components of claddings calculated by STAR-CCM+ (free thermal bowing).

7.3.2. FEA result: A free thermal bowing

A cladding deformation for the free thermal bowing condition was performed using Abaqus to evaluate the reliability of the simulations. Figure 22 illustrates the displacement magnitude of the claddings. For a better visualization of radial displacement of the claddings, non-uniform deformation scale factors, X:100, Y:1, and Z:100, were applied. The axial expansion of claddings for the free thermal bowing condition was 7.462 mm. The difference in the axial expansion between the hand-calculation and Abaqus result was only 2.07%. The maximum values of radial displacements in X-direction and Z-direction were 1.19 mm and 1.054 mm, respectively. The relative deviations in radial displacements U1, U2 and U3 between Abaqus and STAR-CCM+ were 2.94%, 0.29% and 1.99 %, respectively. It was determined that different mesh types of Abaqus model and STAR-CCM+ model can cause minor differences in the simulation result while a good agreement between the two codes confirmed that the thermal expansion models in this work are reliable.

The radial flowering of the core is clearly observed in Figure 22. The cladding in the 1st ring (see Figure 4-(a)) bowed inward while those in the 2nd and 3rd rings bowed outward. The radial displacement of the claddings in the 1st and 3rd rings were larger than those in the 2nd ring due to the larger temperature gradients across the claddings in 1st and 3rd rings compared to those in the 2nd ring. The radial displacements U1 and U3 are illustrated in Figure 23 and Figure 24, respectively. The maximum value of radial displacements was found in the 1st ring.

In the MARVEL reactor core, the top alignment grid plate and other structures constrain the radial displacement of the fuel rods. Therefore, the FEA results for a free thermal bowing condition in this section and Section 7.3.2 can provide information on a hypothetical situation in which the top alignment grid plate and other structures fail to function properly.

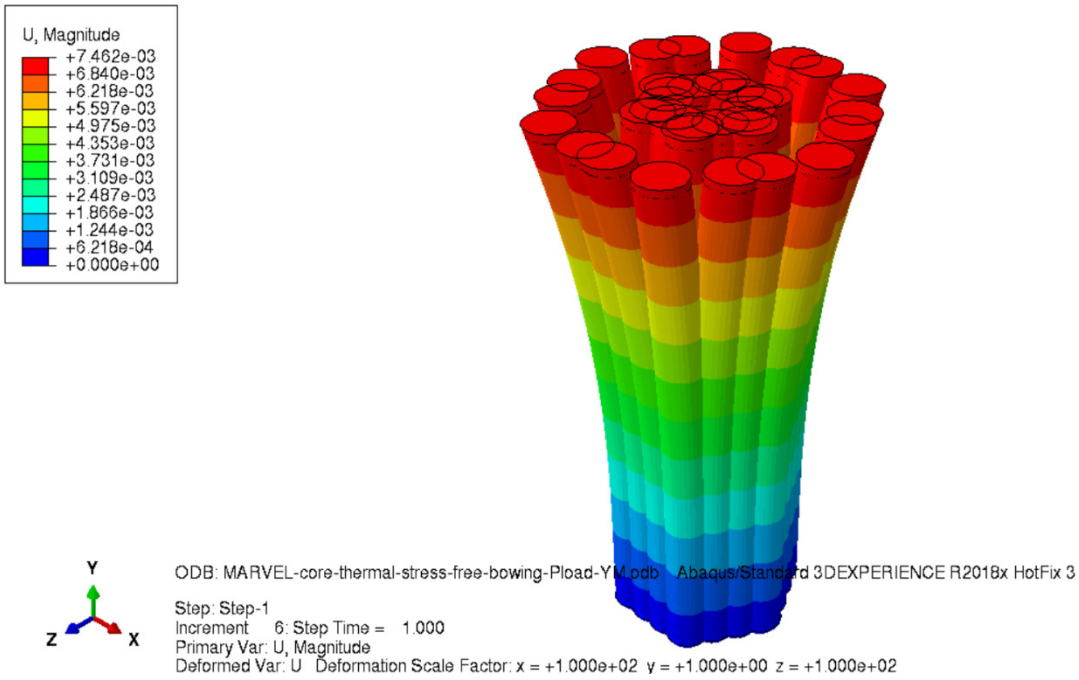

Figure 22. Displacement magnitude of claddings (free thermal bowing condition) [unit: m]

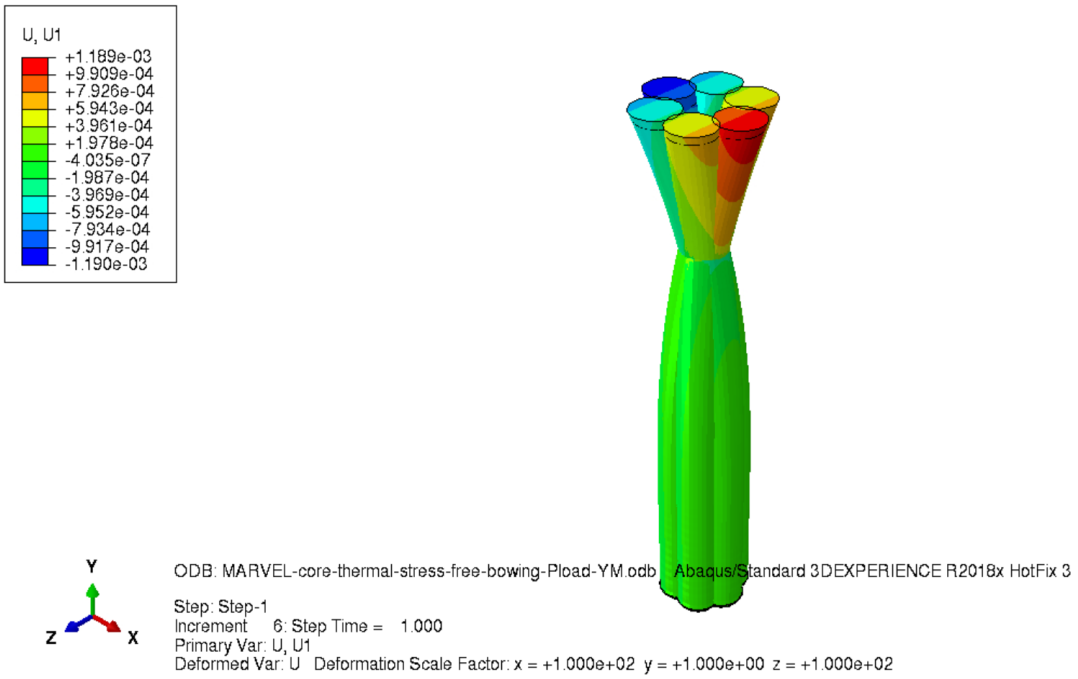

(a) Fuel rods 1-1 ~ 1-6

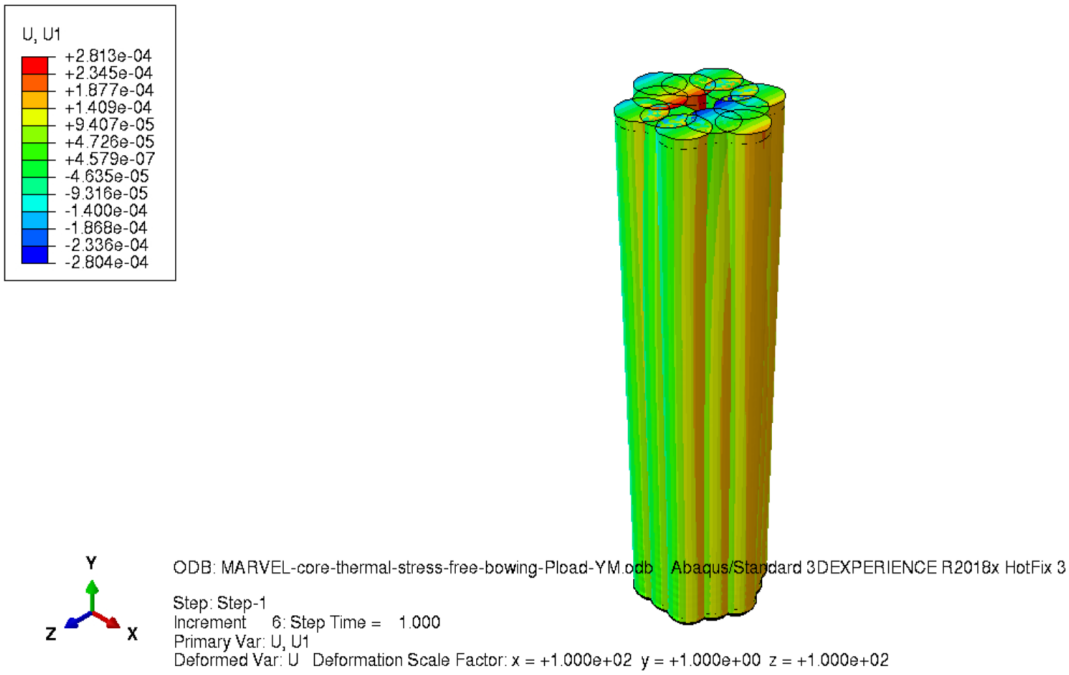

(b) Fuel rods 2-1 ~ 2-12

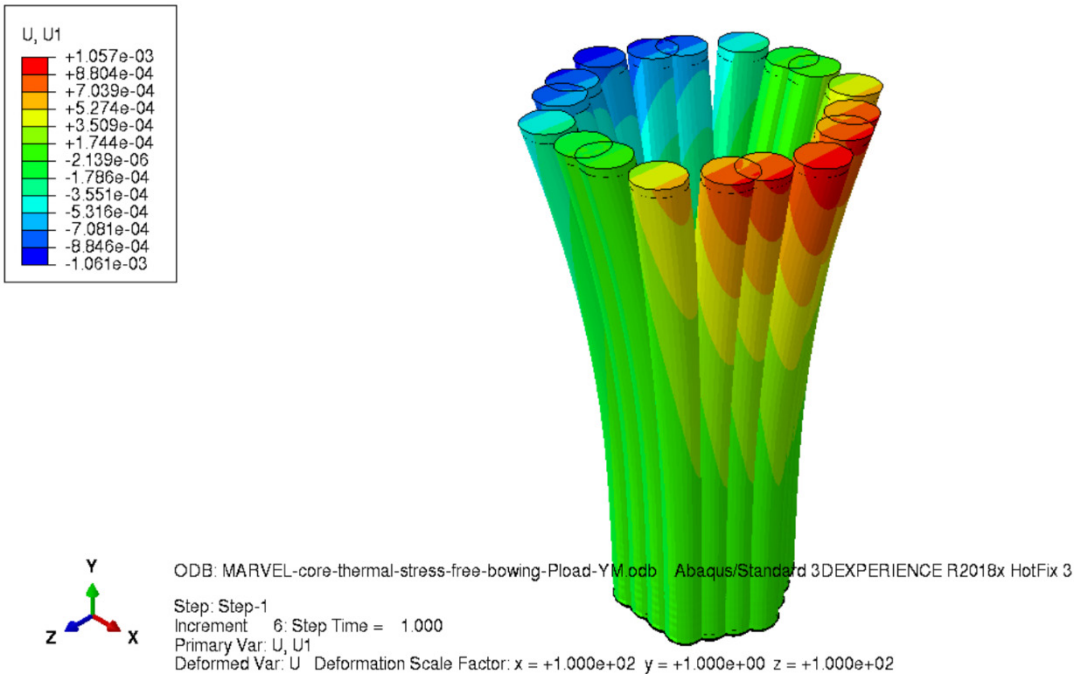

(c) Fuel rod 3-1 ~ 3-18

Figure 23. Spatial displacement component U1 of the claddings in each ring (free thermal bowing condition) [unit: m]

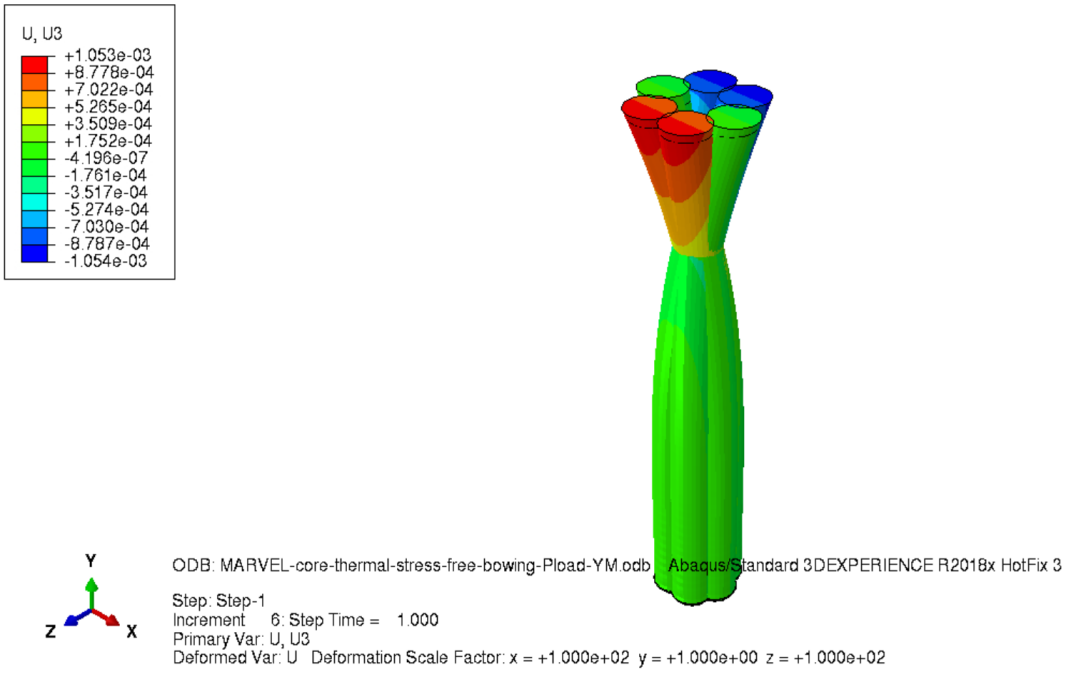

(a) Fuel rods 1-1 ~ 1-6

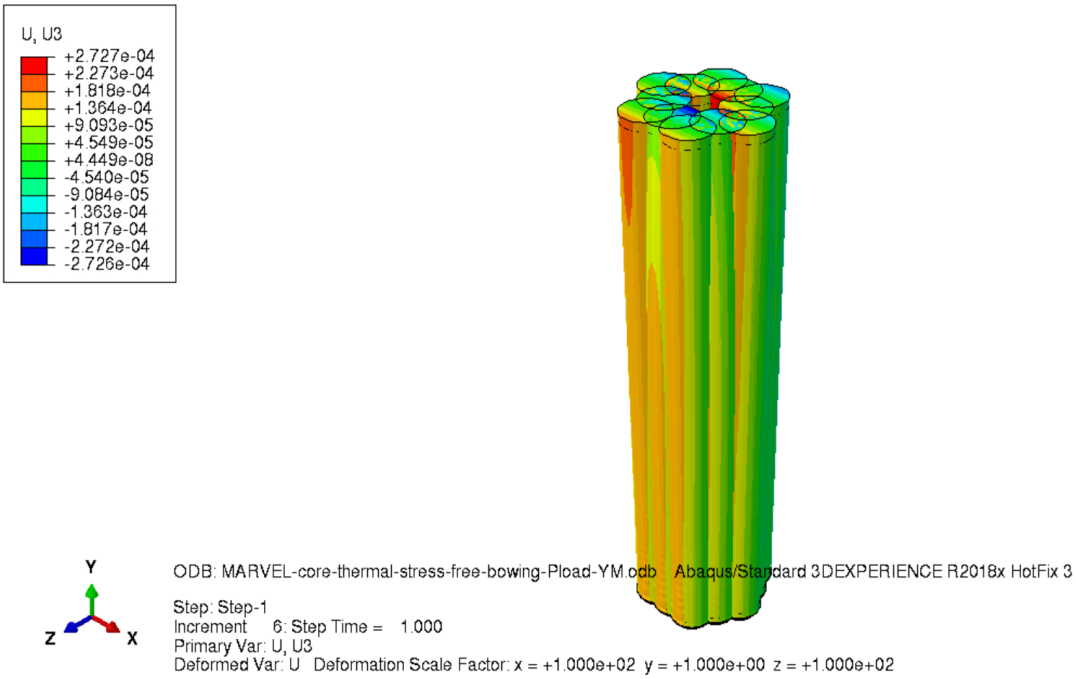

(b) Fuel rods 2-1 ~ 2-12

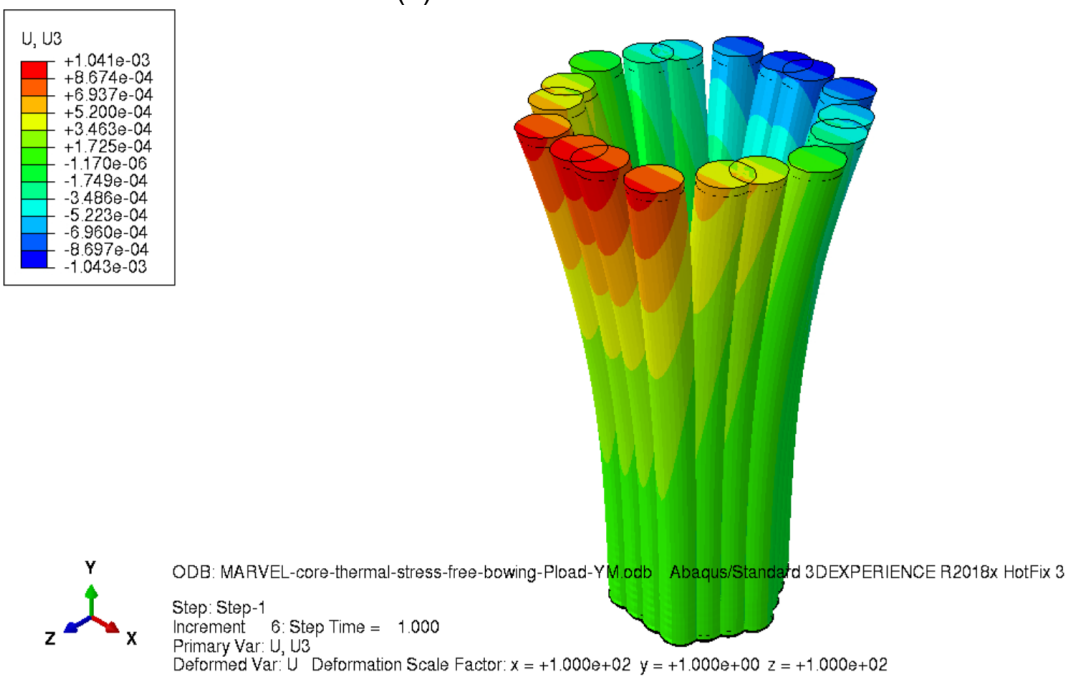

(c) Fuel rod 3-1 ~ 3-18

Figure 24. Spatial displacement component U3 of the claddings in each ring (free thermal bowing condition) [unit: m]

7.3.3. FEA result: Constrained boundary

The displacement magnitude and spatial displacement components U1 and U3 of the claddings are illustrated in Figure 25, Figure 26, and Figure 27, respectively. The maximum value of axial expansion (displacement magnitude) was 7.51 mm. Compared to the free thermal bowing result, the effect of top

constraint on the axial expansion of claddings was negligible. When the top constraint was applied, the fuel rods in the 1st ring of the core bowed outward while those in the 2nd and the 3rd rings bowed inward. For the fuel rods located in the first ring, the side facing the center of the core has a lower temperature than the opposite side due to the central insurance absorber (CIA) rod. In contrast, for the fuel rods located in the second and third rings, the side facing the center of the core has a higher temperature than the side facing outward. Since the thermal expansion on the higher-temperature side is greater than the lower-temperature side, when the top and bottom ends are fixed, the fuel rods in the first ring undergoes deformation in the outward direction, while those in the second and third rings undergoes deformation in the inward direction.

The Abaqus calculation result for constrained boundary condition provides information on the variation in fuel-to-fuel gap distribution. It is worth noting that the thermal deformation of the fuel rod is three-dimensional while the displacement component U1, U2 or U3 is only the vector component of three-dimensional displacement. This means that the maximum values reported in Figure 26 and Figure 27 do not directly represent the variation in the fuel-to-fuel gap distance. Hence, to evaluate the minimum value of fuel-to-fuel gap distance, the minimum distance between the elements of two adjacent fuel rods must be calculated based on the element coordinates of the deformed geometry. The calculation method to get the minimum distance between two fuel rods is discussed in Section 7.3.4.

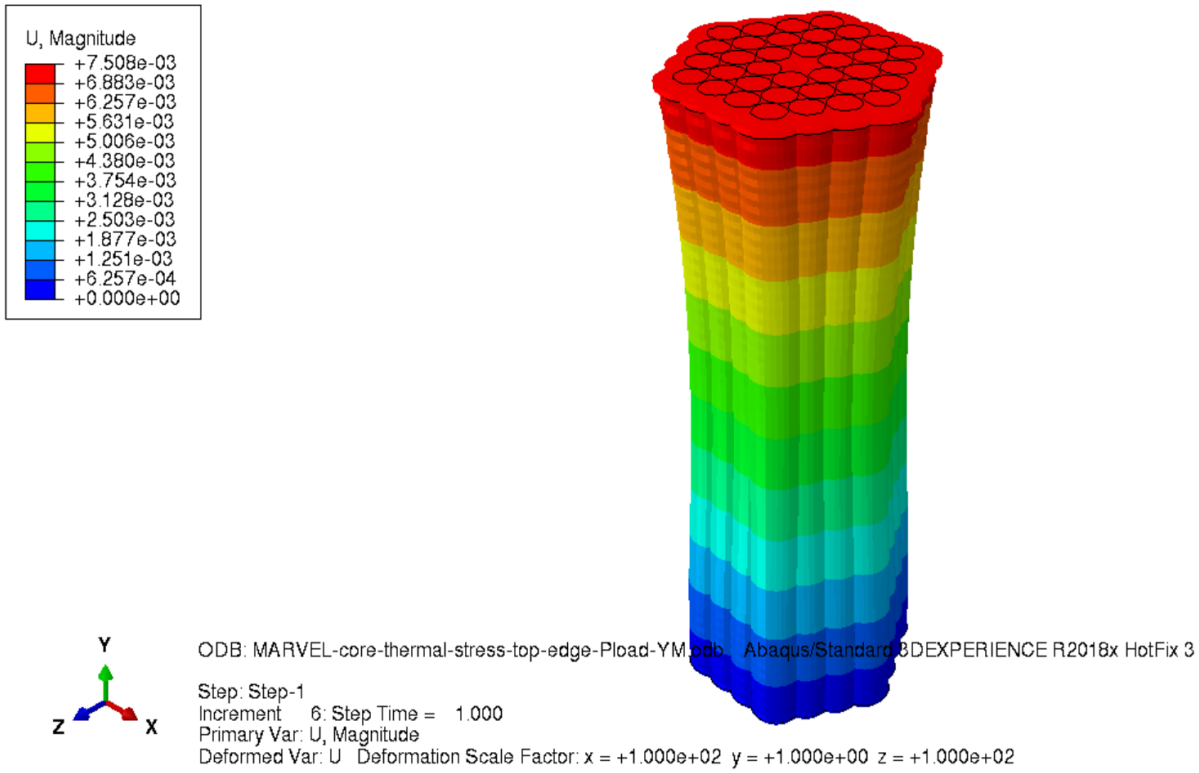

Figure 25. Isometric view of thermal deformation (displacement magnitude) of claddings [unit: m].

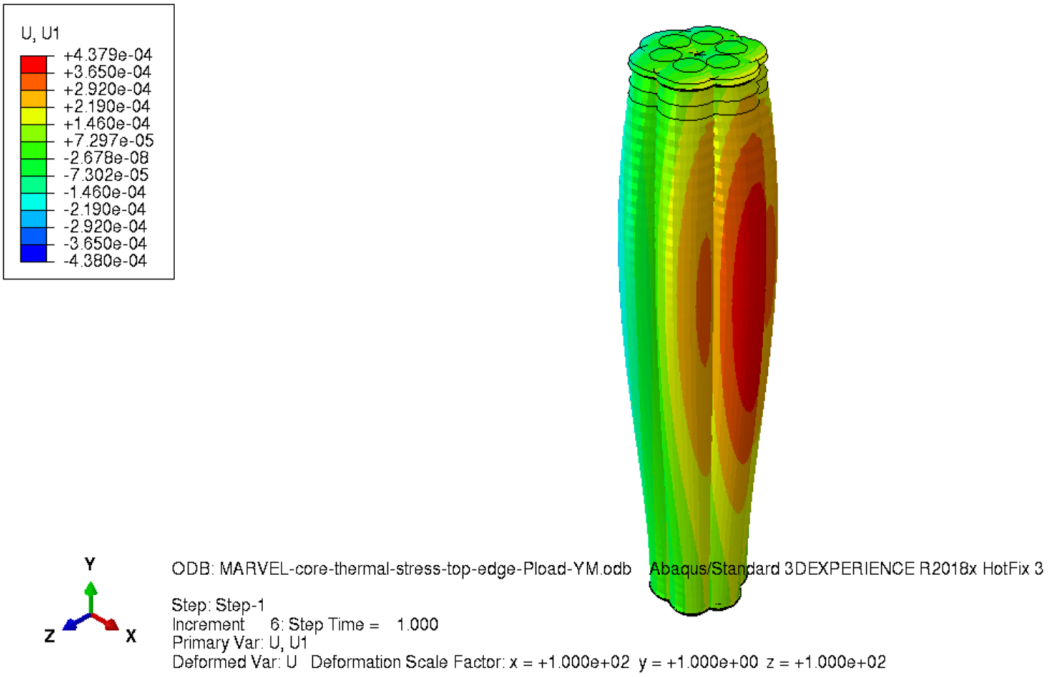

(d) Fuel rods 1-1 ~ 1-6

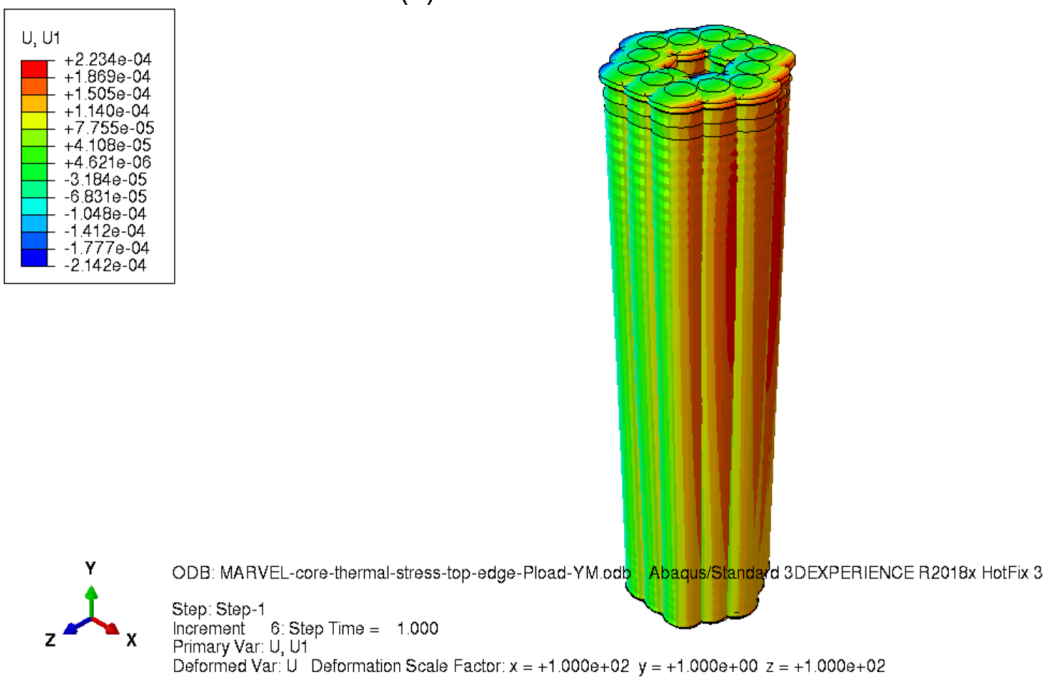

(e) Fuel rods 2-1 ~ 2-12

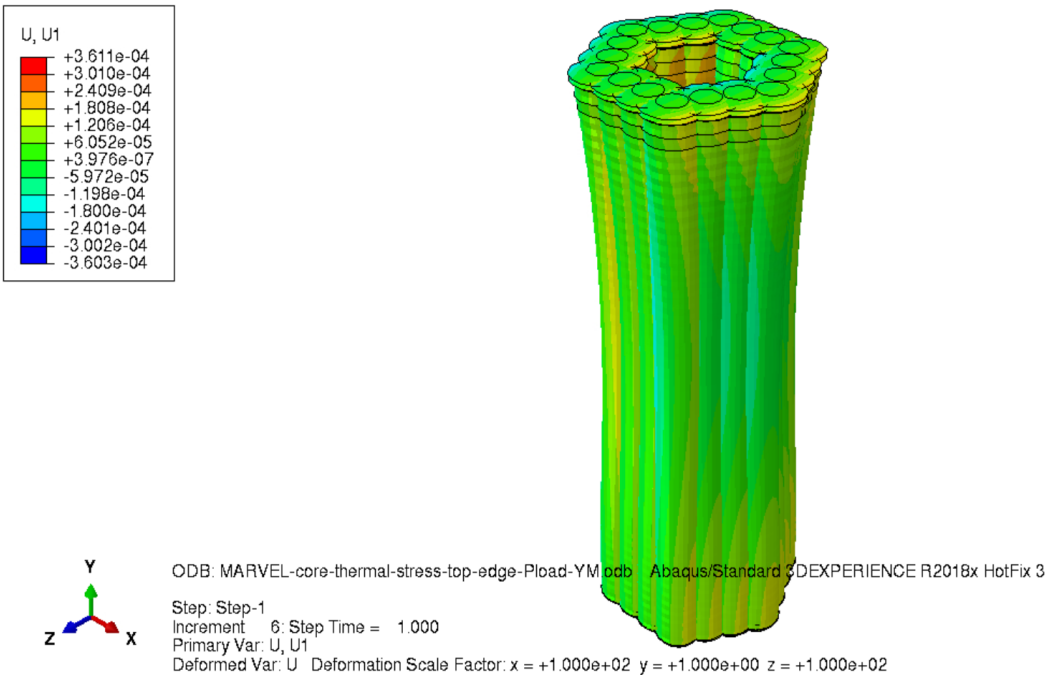

(f) Fuel rod 3-1 ~ 3-18

Figure 26. Spatial displacement component U1 of the claddings in each ring [unit: m].

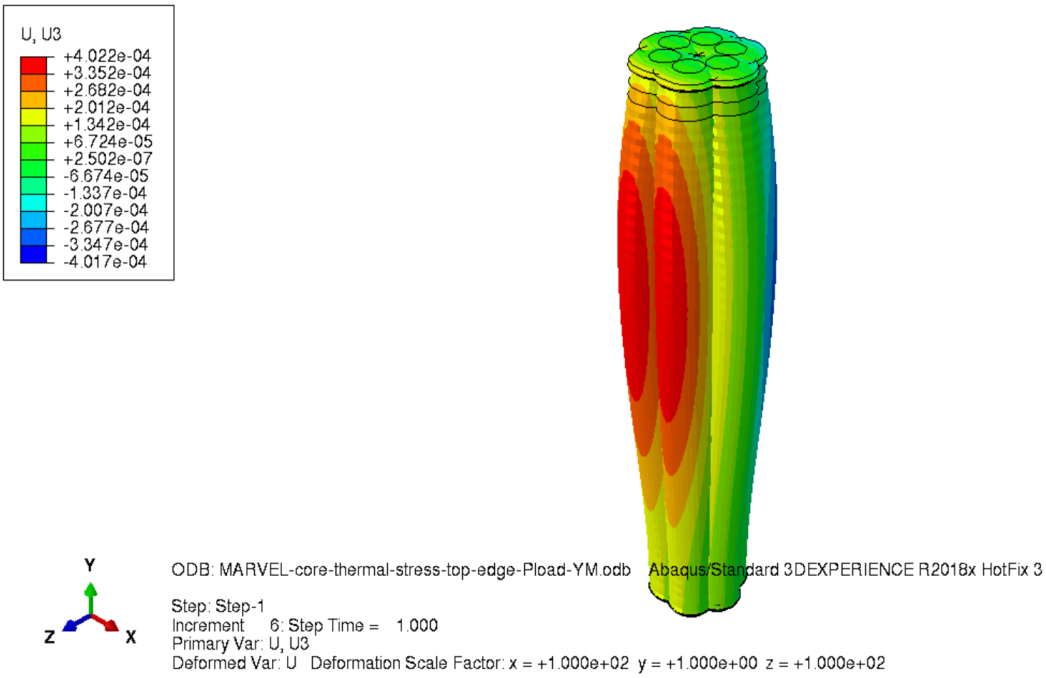

(d) Fuel rods 1-1 ~ 1-6

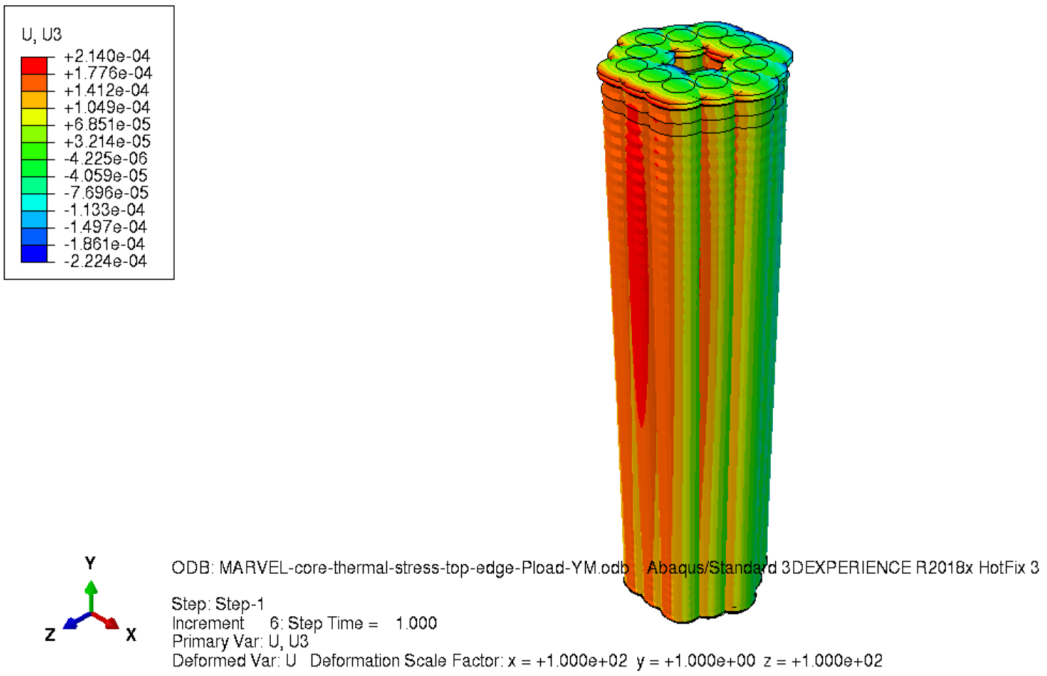

(e) Fuel rods 2-1 ~ 2-12

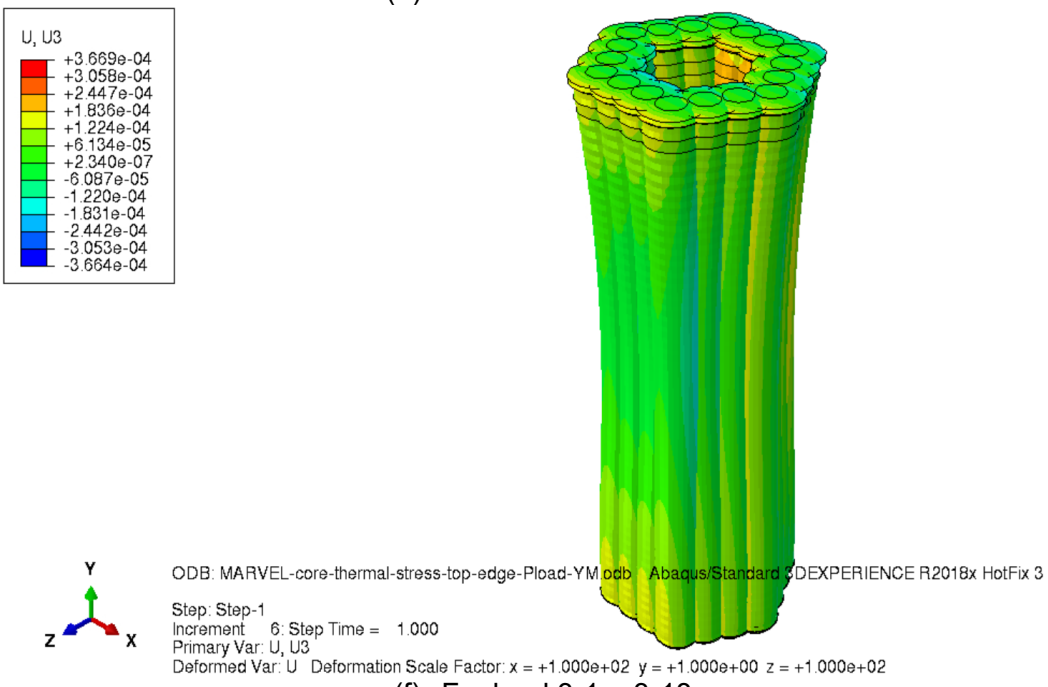

(f) Fuel rod 3-1 ~ 3-18

Figure 27. Spatial displacement component U3 of the claddings in each ring [unit: m].

7.3.4. Evaluation of fuel-to-fuel gap distance

The finite element coordinates of the deformed fuel rods can be calculated using their original coordinates with displacement components. The spatial displacement components (U1, U2, and U3) of

claddings can be exported from the Abaqus result. Figure 28 shows “Report Field Output” function of Abaqus code to export the output (“Report” >> “Field Output...”). The Abaqus input file for the data mapping process includes the coordinates of original fuel cladding elements. A python script has been developed to process the Abaqus input file and output report file. This script reads two files, calculates the coordinates of deformed claddings, and finally determines the minimum value of fuel-to-fuel gap between two fuel rods. A python script and the calculated changes in fuel-to-fuel gap distances are attached in **Appendix H**.

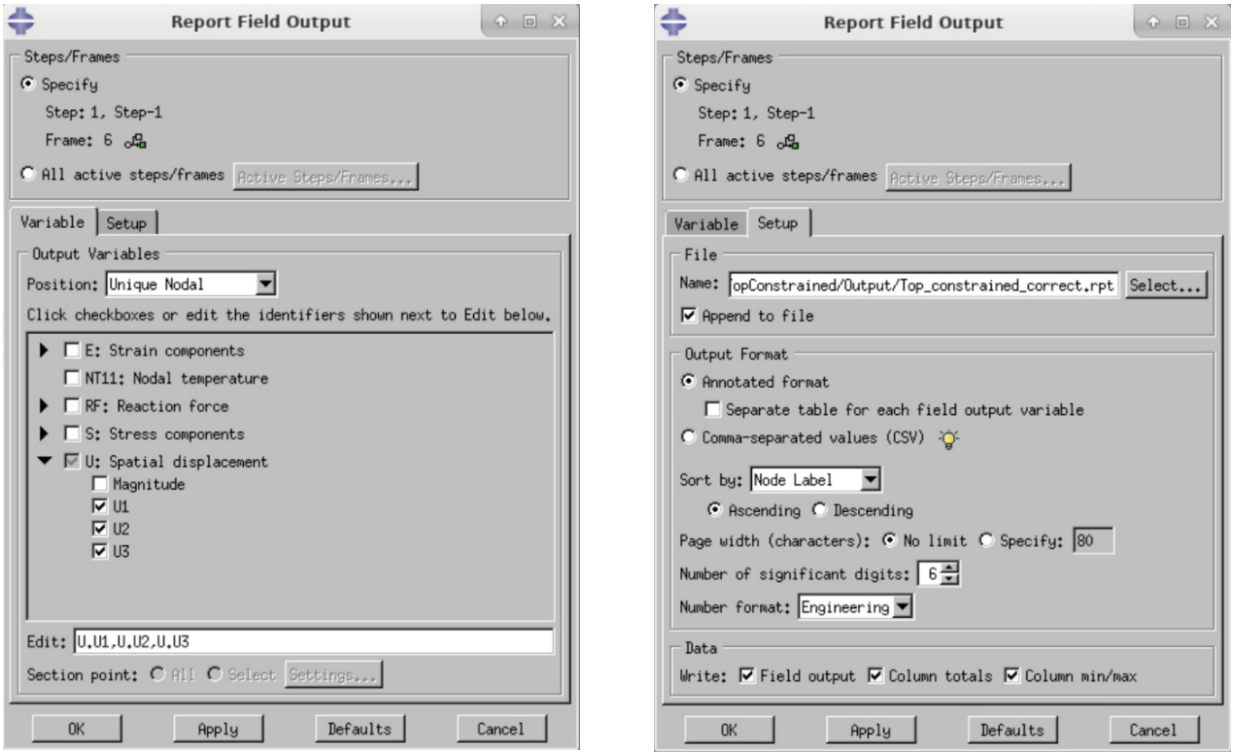

Figure 28. Exporting the field output from Abaqus (“Report” >> “Field Output…”).

For the top constrained condition, the minimum fuel-to-fuel gap distance by the thermal bowing was calculated to be 1.358 mm, which is 0.642 mm or 32.1% reduction from the nominal gap of 2 mm (undeformed). This minimum gap was found between the fuel rod 1-6 and fuel rod 2-11. The minimum distance of fuel-to-fuel gap between the fuel rod 2-1 and adjacent rods was 1.541 mm (0.459 mm or 23% reduction), which was found between the fuel rod 2-1 and fuel rod 3-18.

7.3.5. Thermal-hydraulic Assessment of Deformed Fuel Rods

The straightness tolerances of the fuel rod illustrated in Figure 29 may lead to the fuel-to-fuel contact in the reactor core. For 32” (818.438 mm)-long fuel rod, a straightness tolerance of 0.1mm/100mm (**Appendix I**) can reduce the fuel-to-fuel gap distance to 0.363 mm (2-0.8184*2=0.363 mm) in the worst-case scenario. In this case, if the change in the fuel-to-fuel gap distance is greater than 0.363 mm, the fuels in contact can happen. Since the thermal deformation of cladding, which implies the change in the fuel-to-fuel gap thickness, could be 0.642 mm in maximum and it could be 0.459 mm for the hottest pin as described in Section 7.3.4, the thermal bowing of the fuel rods can result in a very tight fuel-to-fuel gap or the fuels in contact that will increase the peak temperatures of cladding and fuel

meat. From the standpoint of nuclear reactor safety, the temperature increase in the fuel and cladding by changes in the fuel-to-fuel gap is undesirable as it may cause the fuel rods to overheat beyond the safety criteria. To assess the impact of the changes in fuel-to-fuel gap distance, the CFD simulation taking into account the straightness tolerance and thermal bowing of fuel rods was performed. If the peak temperatures of fuel and cladding exceeds the safety criteria, the fuel spacer must be adopted to prevent fuel-to-fuel contact in the reactor.

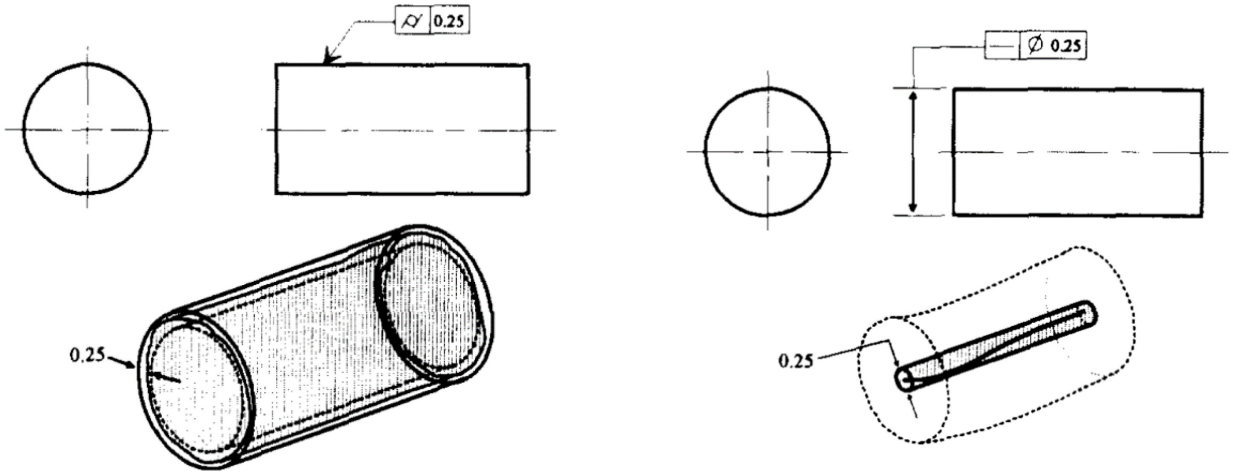

(a) Cylindricity tolerance (b) Straightness of median line tolerance

Figure 29. Tolerance definitions given in the GD&T Y14.5 Standard [13].

In this work, it was assumed that the fuel-to-fuel gap between the fuel rod 2-1, which was the hottest one found in the conjugate heat transfer CFD analysis, and the gap between adjacent fuel rods (1-1, 2-2, 2-12, 3-1, 3-2, 3-18) was reduced to 0.05 mm. To reduce the fuel-to-fuel gap distance, the adjacent fuel rods were moved toward the fuel rod 2-1, while the fuel rod 2-1 remained in its original position as seen in Figure 30. Since the current CFD model does not include the inlet plenum, modeling the contacting fuel rods will result in the separated flow subchannels where the inlet flow distribution is not currently available. Therefore, the fuel-to-fuel gap of 0.05 mm allows the CFD model to calculate the flow distribution for a given geometry while it restrains the flow mixing among the flow subchannels and the convective heat transfer at the gap region.

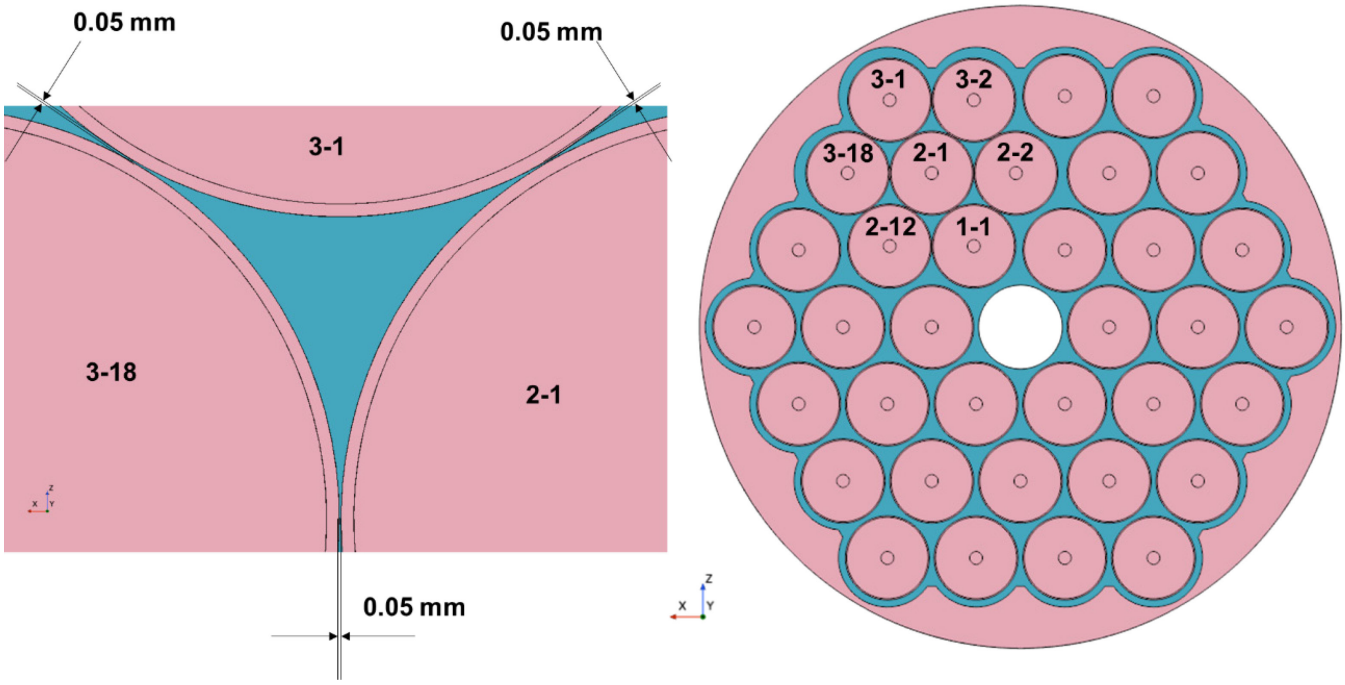

Figure 30. Cross-sectional view of MARVEL reactor core with 0.05 mm gap between fuel rod 2-1 and the fuel rods adjacent to it (1-1, 2-2, 2-12, 3-1, 3-2, and 3-18).

Figure 31 shows the temperature distribution on the cladding surface of fuel rod 2-1 and the cross-sectional temperature distributions of the reactor core at three elevations. The peak temperatures of cladding and fuel of the fuel rod 2-1 were 586.66 °C and 596.49 °C, respectively. The peak temperatures of cladding and fuel were found to be slightly lower than the top elevation of the fuel (P3) due to the heat transfer to the top graphite reflector. The PCT of the fuel rod 2-1 increased 40.76 K by reducing the gap distance, but it is still lower than 764 °C, which is a safety criterion for cladding internal temperature defined in Section 1.3 of ECAR-6332 [11]. In addition, the peak temperature of fuel centerline was lower than the normal operation safety limit of 925 °C [11]. The bulk temperature of NaK coolant, which is a surface averaged temperature at the core outlet, was calculated to be 539.73 °C. The NaK outlet temperature was slightly higher than the acceptance criterion of 539 °C for a normal operation [11].

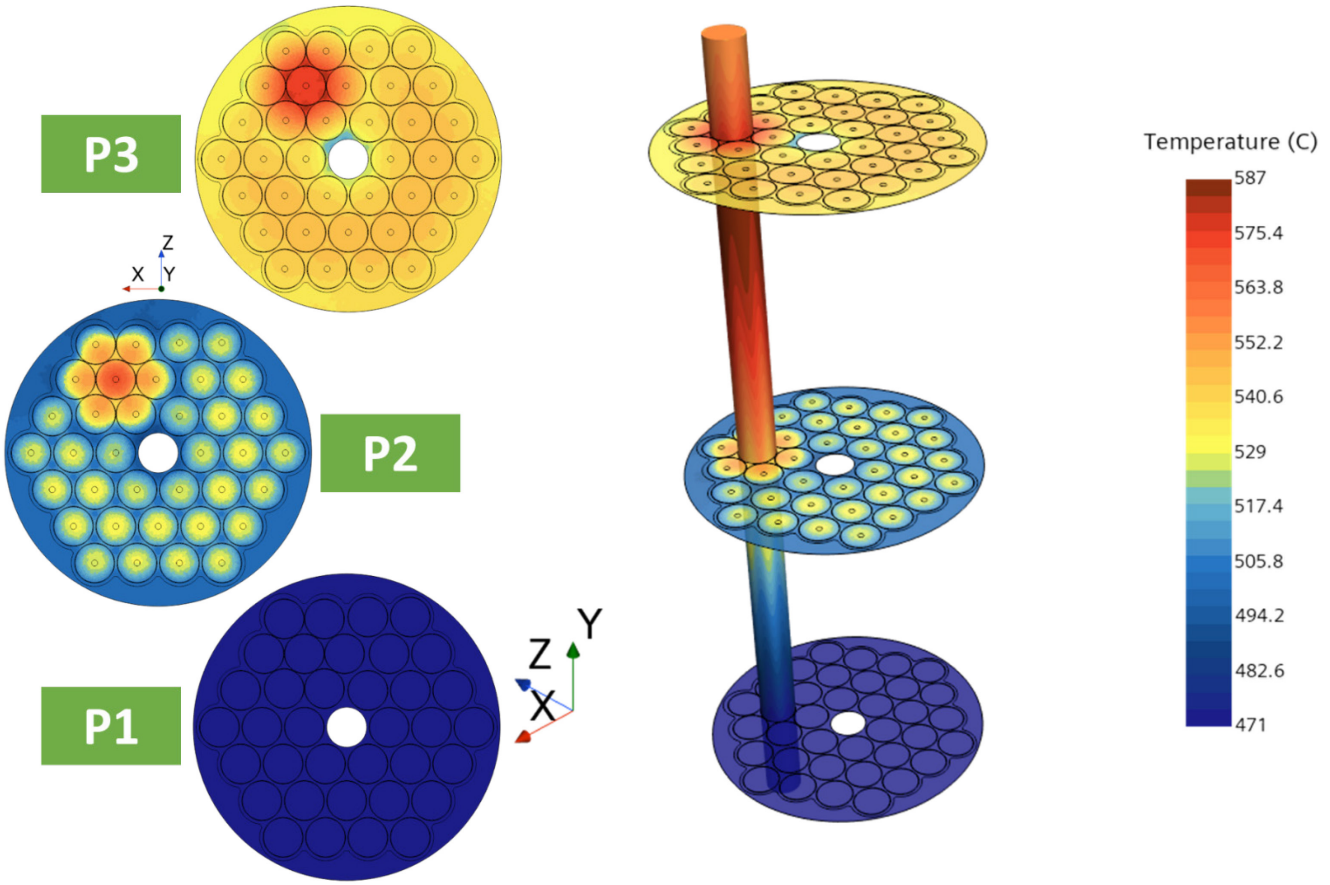

Figure 31. The temperature distribution on the cladding surface of fuel rod 2-1 and the cross-sectional temperature distribution of the reactor core at three elevations by modifying the positions of fuel rods adjacent to the fuel rod 2-1.

It is worth noting that the fuel-to-fuel gap of 0.05 mm, along with the entire length of the fuel rod, is very conservative due to presence of the top and bottom alignment grid plates, which prevent such a gap. Therefore, it can be concluded that the MARVEL reactor could be operated below the safety criteria during normal operation even without installing the fuel spacers. While a reduction in the fuel-to-fuel gap by the straightness tolerance and thermal deformation deteriorates the convective heat transfer of NaK coolant, a high thermal conductive NaK coolant and stainless-steel cladding can effectively remove the heat from the fuel rods, preventing the temperature from rising above the safety criteria.

However, it should be noted that the steady-state calculations in this report may not ensure the reactor safety under the transients. The peak temperatures of reactor components can be changed during the transients due to unbalanced heat generation and removal in the system. Therefore, unsteady CFD analysis of the reactor core with fuel rods in contact is necessary to assess whether the reactor system can meet the safety criteria during the reactor transients. Additionally, the hot channel factor of system safety analysis should take into account the temperature increase by the changes in the fuel-to-fuel gap distance.

Storage Locations of STAR-CCM+/ABAQUS Models

- Base CAD file for the CFD model is stored in:
  "/projects/MARVEL_CFD/MARVEL/ECAR7210/Final/CAD/"
  - MARVEL-NaK-SIMPLE.stp
- The STAR-CCM+ model for conjugate heat transfer analysis is stored in:
  "/projects/MARVEL_CFD/MARVEL/ECAR7210/Final/CFD/"
  - MARVEL_core_CHT_RANS_SST_base_10mm_ECAR6332base.sim
  - MARVEL_core_CHT_RANS_SST_base_20mm_ECAR6332base.sim
  - MARVEL_core_CHT_RANS_SST_base_40mm_ECAR6332base.sim
- The STAR-CCM+ model for deformed fuel rods is stored in:
  "/projects/MARVEL_CFD/MARVEL/ECAR7210/Final/CFD/HCF/"
  - MARVEL_core_HCF_RANS_SST_gap_0.05mm_ECAR6332base.sim
- The STAR-CCM+ model for solid mechanical analysis is stored in:
  "/projects/MARVEL_CFD/MARVEL/ECAR7210/Final/CFD/solid_stress/"
  - MARVEL_core_CHT_RANS_SST_base_10mm_ECAR6332base_stress_freebowing_pressure_load.sim
- Abaqus input files for data mapping are stored in:
  "/projects/MARVEL_CFD/MARVEL/ECAR7210/Final/ABQ/AIF/"
  - ABQ-CFD-mapped-final.inp (mapped data)
  - ABQ-CFD.inp (initial input file)
- Abaqus model for converting the mapped data to Abaqus output database is stored in:
  "/projects/MARVEL_CFD/MARVEL/ECAR7210/Final/ABQ/AOD/"
  - MARVEL-CTF.odb
- Abaqus model for free thermal bowing condition is stored in:
  "/projects/MARVEL_CFD/MARVEL/ECAR7210/Final/ABQ/FreeThermalBowing/"
  - marvel_core_iges-free-bowing-Pload-2018-HF3-YM.cae
  - MARVEL-core-thermal-stress-free-bowing-Pload-YM.odb
- Abaqus model for top constrained condition is stored in :
  "/projects/MARVEL_CFD/MARVEL/ECAR7210/Final/ABQ/TopConstrained/"
  - marvel_core_iges-top-edge-Pload-2018-HF3-YM.cae
  - MARVEL-core-thermal-stress-top-edge-Pload-YM.odb

8. REFERENCES

[1] T. L. Lange, ""Neutronics Analyses for the MARVEL Preliminary Documented Safety Analysis," ECAR-6099, rev. 0, Idaho National Laboratory, Idaho Falls, 2023.

[2] Nuclear Energy Agency Nuclear Science Committee, "NEA Benchmark of the Modular High-Temperature Gas-Cooled Reactor-350MW Core Design Volumes I and II," OECD-NEA, 2018.

[3] Siemens PLM Software, "STAR-CCM+® Documentations, Version 2020.3.1," 16 December 2020. [Online]. Available: https://docs.sw.siemens.com/en-US/product/226870983/doc/PL20201113103827399.starccmp_userguide_pdf/pdf/.

[4] Siemens PLM Software, "STAR-CCM+ Software Completes ASME NQA-1 Compliance Press Release, New York and London," 11 July 2017. [Online]. Available: https://www.plm.automation.siemens.com/global/en/our-story/newsroom/siemens-press-release/43868. [Accessed 4 March 2020].

[5] Siemens PLM Software, *Simcenter STAR-CCM+ Verification Suite,* Siemens Digital Industries Software, 2020.

[6] ECAR-3020, "STARCCM MULTI-PHYSICS VALIDATION," Idaho National Laboratory, Idaho Falls, 2017.

[7] Dassault Systèmes Simulia Corp., *ABAQUS/Standard Version 2018.HF3,* 2018.

[8] ECAR-3845, "Software Validation Report for ABAQUS Standard and Explicit Version 2018.HF3 for Structural Analyses," Idaho National Laboratory, Idaho Falls, 2019.

[9] MatWeb, "MatWeb Material Property Data, Molybdenum, Mo, Annealed," [Online]. Available: https://www.matweb.com/search/datasheet.aspx?matguid=ef57c33963404798ad0301a05692312a&ckck=1. [Accessed 24 4 2023].

[10] J. A. Evans, R. T. Sweet and D. D. Keiser, "MARVEL Reactor Fuel Performance Report," INL/RPT-22-68555, Rev.0, Idaho National Laboratory, Idaho Falls, 2023.

[11] ECAR-6332, "RELAP5-3D THERMAL-HYDRAULIC ANALYSIS OF MARVEL MICROREACTOR - FINAL DESIGN," Idaho National Laboratory, Idaho Falls, 2023.

[12] ECAR-6581, "Hydraulic Assessment of Conceptual Design of Ring-type Spacer for MARVEL Reactor," Idaho National Laboratory, Idaho Falls, 2023.

[13] K. Carr and P. Ferreira, "Verification of form tolerances Part II: Cylindricity and straightness of a median line," *Precision Engineering,* vol. 17, pp. 144-156, 1995.

[14] J. H. Keenan, J. Chao and J. Kaye, Gas Tables - International Version, 2nd ed., New York: John Wiley & Sons, 1980 (English Units) and 1983 (SI Units).

[15] Y. S. Touloukian, S. C. Saxena and P. Hestermans, Thermophysical Properties of Matter - the TPRC Data Series. Volume 11. Viscosity, New York, N.Y.: Purdue Research Foundation, 1975.

[16] Y. S. Touloukian and T. Makita, Thermophysical Properties of Matter - The TPRC Data Series. Volume 6. Specific Heat - Nonmetallic Liquids and Gases, New York, N.Y.: Purdue Research Foundation, 1970.

[17] Y. S. Touloukian, P. E. Liley and S. C. Saxena, Thermophysical Properties of Matter - The TPRC Data Series. Volume 3. Thermal Conductivity - Nonmetallic Liquids and Gases, New York, N.Y.: Purdue Research Foundation, 1970.

[18] D. R. Olander, E. Greenspan, H. D. Garkisch and B. Petrovic, "Uranium-zirconium hydride fuel properties," *Nuclear Engineering and Design,* vol. 239, no. 8, pp. 1406-1424, 2009.

[19] S. Yamanaka, K. Yamada, K. Kurosaki, M. Uno, K. Takeda, H. Anada, T. Matsuda and S. Kobayashi, "Thermal properties of zirconium hydride," *Journal of Nuclear Materials,* vol. 294, no. 1-2, pp. 94-98, 2001.

[20] RELAP5-3D Code Development Team, "RELAP5-3D Code Manual Volume I," Idaho National Laboratory, Idaho Falls, 2018.

[21] G. Atomics, "Graphite Design Handbook," DOE-HTGR-8811, 1988.

[22] INTERNATIONAL ATOMIC ENERGY AGENCY, *Thermophysical Properties of Materials for Nuclear Engineering: A Tutorial and Collection Data,* Vienna: IAEA, 2008.

[23] American Iron and Steel Institute, HIGH-TEMPERATURE CHARACTERISTICS OF STAINLESS STEELs, Republished in 2020 by Nickel Institute, 1979.

[24] British Stainless Steel Association, "ELEVATED TEMPERATURE PHYSICAL PROPERTIES OF STAINLESS STEELS," British Stainless Steel Association, 2023. [Online]. Available: https://bssa.org.uk/bssa_articles/elevated-temperature-physical-properties-of-stainless-steels/. [Accessed 3 5 2023].

[25] ASME Standard, 2021 ASME Boiler & Pressure Vessel Code, Section II Materials, Part D Properties (Customary), ASME, 2021.

Appendix A

Abaqus Validation Test Report (Thermal)

ABQ EXE: Abaqus
COMPUTER: r6i0n31
OS: Linux
OS TYPE: 3.10.0-1160.76.1.el7.x86_64
t1

ODB: Test-1
dictTest[Test-1].Keys: ['Grp1']
NT11-n325
Max error: 1.20% ←--------
Max1: 37.3320 Min1: 10.5200 Range: 26.8120
Abq Max2: 37.7813 Abq Min2: 10.6362 Range: 27.1451
NT11-n281
Max error: 1.48% <----------
Max1: 55.1070 Min1: 13.9970 Range: 41.1100
Abq Max2: 54.7760 Abq Min2: 14.2043 Range: 40.57==

==
ODB: Test-2
dictTest[Test-2].Keys:' ['G'p2', 'G'p1']
NT15-n61
Max error: 1.34% <----------
Max1: 37.3320 Min1: 10.5200 Range: 26.8120
Abq Max2: 37.7366 Abq Min2: 10.6609 Range: 27.0756
NT11-n61
Max error: 1.54% <----------
Max1: 55.1070 Min1: 13.9970 Range: 41.1100
Abq Max2: 54.7444 Abq Min2: 14.2131 Range: 40.53==

==
ODB: Test-3
dictTest[Test-3].Keys:' ['G'p1']
NT11-n130
Max error: 1.65% <----------
Max1: 44.5920 Min1: 12.5210 Range: 32.0710
Abq Max2: 44.7825 Abq Min2: 12.7270 Range: 32.0555
NT11-n59
Max error: 1.85% <----------
Max1: 55.3390 Min1: 14.7770 Range: 40.5620
Abq Max2: 55.0396 Abq Min2: 15.0511 Range: 39.98==

==
ODB: Test-4
dictTest[Test-4].Keys:' ['G'p1']
NT11-n281
Error: 0.00% <----------
Ans: 13.7600 Abq: 13.7600
NT11-n303
Error: 0.00% <----------
Ans: 11.3200 Abq: 11.3200
NT11-n325
Error: 0.00% <----------
Ans: 4.0000 Abq: 4.0000
NT11-n314
Error: 0.00% <----------
Ans: 8.2700 Abq: 8.2700

```
        NT11-n292
Error: 0.00%       <----------
Ans:      13.1500 Abq:      13.15==
```

```
==
ODB: Test-5
dictTest[Test-5].Keys:‘ ['G’p3‘, 'G’p2‘, 'G’p1‘, 'G’p5‘, 'G’p4']
        NT13-n62
Error: 0.00%       <----------
Ans:      11.3200 Abq:      11.3200
        NT12-n62
Error: 0.00%       <----------
Ans:      13.1500 Abq:      13.1500
        NT11-n62
Error: 0.00%       <----------
Ans:      13.7600 Abq:      13.7600
        NT15-n62
Error: 0.00%       <----------
Ans:       4.0000 Abq:       4.0000
        NT14-n62
Error: 0.00%       <----------
Ans:       8.2700 Abq:       8.27==
```

```
==
ODB: Test-6
dictTest[Test-6].Keys:‘ ['G’p1']
        NT11-n533
Max error: 0.39% <----------
   Max1:  80.7640    Min1:  61.8970 Range:  18.8670
Abq Max2:  80.4914 Abq Min2:  61.7364 Range:  18.7551
        NT11-n803
Max error: 0.38% <----------
   Max1:  94.5930    Min1:  71.5310 Range:  23.0620
Abq Max2:  94.3007 Abq Min2:  71.2781 Range:  23.02==
```

```
==
ODB: Test-7
dictTest[Test-7].Keys:‘ ['G’p1']
        HFL-e56
Error: 0.19%       <----------
Ans:      -0.1700 Abq:      -0.16==
```

```
==
ODB: Test-8
dictTest[Test-8].Keys:‘ ['G’p1']
        HFL-e1121
Error: 1.74%       <----------
Ans:       0.1710 Abq:       0.1740
        HFL-e3678
Error: 2.25%       <----------
Ans:      -0.1620 Abq:      -0.16==
```

```
==
ODB: Test-9
dictTest[Test-9].Keys:‘ ['G’p1']
        NT11-n13
Error: 0.01%       <----------
Ans:      50.0010 Abq:      50.0036
        NT11-n17
```

Error: 0.00% <----------
Ans: 55.5500 Abq: 55.5500
NT11-n328
Error: 0.20% <----------
Ans: 51.6040 Abq: 51.7074
NT11-n38
Error: 0.05% <----------
Ans: 50.0890 Abq: 50.1148
NT11-n28
Error: 0.11% <----------
Ans: 50.7010 Abq: 50.7550
NT11-n218
Error: 0.01% <----------
Ans: 50.0110 Abq: 50.0176
NT11-n32
Error: 0.10% <----------
Ans: 50.3060 Abq: 50.3555
NT11-n324
Error: 0.20% <----------
Ans: 52.4260 Abq: 52.5321
NT11-n4
Error: 0.08% <----------
Ans: 51.0600 Abq: 51.1006
NT11-n320
Error: 0.16% <----------
Ans: 53.6690 Abq: 53.75==

t==
ODB: Test-10
dictTest[Test-10].Keys:‘ ['G’p1']
NT11-n325
Error: 0.15% <----------
Ans: 215.7130 Abq: 216.03==

t==
ODB: Test-11
dictTest[Test-11].Keys:‘ ['G’p1']
HFL-e55
Error: 0.02% <----------
Ans: -5.5000 Abq: -5.49==

t==
ODB: Test-12
dictTest[Test-12].Keys:‘ ['G’p1']
NT11-n336
Error: 0.00% <----------
Ans: 406.6667 Abq: 406.66==

Appendix B

Abaqus Validation Test Report (Standard)

ABQ EXE: Abaqus
COMPUTER: r6i0n31
OS: Linux
OS TYPE: 3.10.0-1160.76.1.el7.x86_64
s1

---------- U ----------

N-185	%err	N-122	%err	N-121	%err	N-120	%err	N-119	%err	N-118	%err
0.6500	0.00	0.1600	0.00	0.1447	0.00	0.1048	0.00	0.0537	0.00	0.0000	0.00

---------- RF ----------

N-154	%err	N-158	%err	N-162	%err	N-126	%err	N-90	%err	N-86	%err	N-82	%err	N-118	%err
334.4081	0.00	447.8178	0.00	334.4081	0.00	447.8176	-0.00	334.4081	0.00	447.8177	-0.00	334.4081	0.00	447.8176	-0.00

s2

---------- EIGVAL ----------

Mode-1	%err	Mode-2	%err	Mode-3	%err	Mode-4	%err	Mode-5	%err	Mode-6	%err
-0.0000	0.00	-0.0000	0.00	0.0000	0.00	0.0000	0.00	0.6340	0.00	2.3660	0.00

---------- EIGFREQ ----------

Mode-1	%err	Mode-2	%err	Mode-3	%err	Mode-4	%err	Mode-5	%err	Mode-6	%err
0.0000	0.00	0.0000	0.00	0.0000	0.00	0.0000	0.00	0.1267	-0.24	0.2448	-0.08

s4

----------plastic_std.odb----------

Max Stress in dir mises: 50000.0000 psi0.00%

s5

----------std_beam_*.odb----------

Element	Max. Stress sig11 (ksi)	Difference (%%)	Max Deflection (in)	Difference (%%)	Input File std_beam_+
B31	29.2500	-2.50	-0.3334	0.02	beam.odb
SR3	30.7117	2.37	-0.3303	-0.92	shell3.odb
S4R	29.2500	-2.50	-0.3328	-0.15	shell4.odb
STRI65	30.5289	1.76	-0.3322	-0.34	shell6.odb
S8R	30.0000	0.00	-0.3324	-0.29	shell8.odb
C3D6	21.4954	-28.35	-0.2006	-39.82	sol06.odb
C3D8	18.1044	-39.65	-0.2051	-38.47	sol08.odb
C3D8I	29.6562	-1.15	-0.3311	-0.67	sol08i.odb
C3D8R	24.6824	-17.73	-0.3461	3.83	sol08r.odb
C3D10M	37.7092	25.70	-0.3440	3.19	sol10.odb
C3D15	35.4466	18.16	-0.3321	-0.38	sol15.odb
C3D20R	33.5220	11.74	-0.3322	-0.33	sol20.odb

s6

----------thermal_stress.odb----------

Max Stress in dir 11: -30000.5996 psi 0.00%

s7

----------thick_cyl4.odb----------

Max Stress in dir 33: 52790.2266 psi 1.52%

s8

----------thick_cyl8.odb----------

Max Stress in dir 33: 51935.8359 psi -0.12%

Appendix C

Thermo-physical Properties of MARVEL Reactor Core Internal Structures and Working Fluid

Table 2. Thermo-physical Properties of liquid NaK (Fluid) [11]

Temperature (K)	Density	Viscosity	Specific Heat	Thermal Conductivity
	ρ (kg/m^3)	μ (kg/m-sec)	Cp (J/kg-K)	k (W/m-k)
300.00	839.54	7.2154E-04	843.88	21.94
350.00	827.00	5.6182E-04	831.04	22.86
400.00	814.77	4.5526E-04	821.79	23.67
450.00	802.76	3.8092E-04	815.23	24.37
500.00	790.93	3.2729E-04	810.79	24.96
550.00	779.24	2.8742E-04	808.07	25.45
573.15	773.86	2.7232E-04	807.49	25.63
598.15	768.07	2.5788E-04	806.87	25.80
600.00	767.64	2.5688E-04	806.82	25.82
623.15	762.30	2.4505E-04	806.7	25.95
648.15	756.54	2.3359E-04	806.85	26.07
650.00	756.11	2.3279E-04	806.87	26.08
673.15	750.80	2.2327E-04	807.28	26.16
698.15	745.06	2.1392E-04	807.98	26.22
700.00	744.63	2.1327E-04	808.04	26.23
723.15	739.33	2.0542E-04	808.95	26.26
748.15	733.60	1.9763E-04	810.19	26.27
750.00	733.18	1.9708E-04	810.29	26.27
773.15	727.87	1.9048E-04	811.68	26.25
798.15	722.14	1.8389E-04	813.42	26.20
800.00	721.72	1.8342E-04	813.56	26.20
823.15	716.41	1.7778E-04	815.41	26.13
848.15	710.67	1.7212E-04	817.64	26.03
850.00	710.24	1.7172E-04	817.81	26.02
873.15	704.92	1.6686E-04	820.12	25.90
898.15	699.15	1.6196E-04	822.84	25.74
900.00	698.73	1.6161E-04	823.05	25.73
923.15	693.38	1.5738E-04	825.81	25.56
948.15	687.59	1.5310E-04	829.03	25.35
950.00	687.16	1.5280E-04	829.28	25.33
973.15	681.78	1.4910E-04	832.51	25.11
998.15	675.95	1.4534E-04	836.25	24.84
1000.00	675.51	1.4507E-04	836.54	24.82
1023.00	670.13	1.4182E-04	840.24	24.55
1023.15	670.09	1.4180E-04	840.26	24.55

1050.00	663.78	1.3823E-04	844.87	24.20
1059.00	661.65	1.3709E-04	846.5	24.08

The polynomial function for the density of NaK implemented in the STAR-CCM+ is given by:

$$\rho_{NaK}\left[{}^{kg}/_{m^3}\right] = -0.23206 \cdot T[K] + 907.37272 \quad 300K \leq T \leq 1059K.$$

Table 3. Thermo-physical Properties of Air (Fuel Plenum)

Temperature (K)	Density [14]	Dynamic Viscosity [15]	Specific Heat [16]	Thermal Conductivity [17]
	ρ (kg/m^3)	μ (kg/m-sec)	Cp (J/kg-K)	k (W/m-k)
293.15	1.204	1.83E-05	1007	0.02514
298.15	1.184	1.85E-05	1007	0.02551
303.15	1.164	1.87E-05	1007	0.02588
308.15	1.145	1.90E-05	1007	0.02625
313.15	1.127	1.92E-05	1007	0.02662
318.15	1.109	1.94E-05	1007	0.02699
323.15	1.092	1.96E-05	1007	0.02735
333.15	1.059	2.01E-05	1007	0.02808
343.15	1.028	2.05E-05	1007	0.02881
353.15	0.9994	2.10E-05	1008	0.02953
363.15	0.9718	2.14E-05	1008	0.03024
373.15	0.9458	2.18E-05	1009	0.03095
393.15	0.8977	2.26E-05	1011	0.03235
413.15	0.8542	2.35E-05	1013	0.03374
433.15	0.8148	2.42E-05	1016	0.03511
453.15	0.7788	2.50E-05	1019	0.03646
473.15	0.7459	2.58E-05	1023	0.03779
523.15	0.6746	2.76E-05	1033	0.04104
573.15	0.6158	2.93E-05	1044	0.04418
623.15	0.5664	3.10E-05	1056	0.04721
673.15	0.5243	3.26E-05	1069	0.05015
723.15	0.488	3.42E-05	1081	0.05298
773.15	0.4565	3.56E-05	1093	0.05572
873.15	0.4042	3.85E-05	1115	0.06093
973.15	0.3627	4.11E-05	1135	0.06581
1073.15	0.3289	4.36E-05	1153	0.07037
1173.15	0.3008	4.60E-05	1169	0.07465
1273.15	0.2772	4.83E-05	1184	0.07868
1773.15	0.199	5.82E-05	1234	0.09599
2273.15	0.1553	6.63E-05	1264	0.11113

Table 4. Thermo-physical Properties of Uranium-Zirconium Hydride (Fuel) [18] [19]

Temperature (K)	Density	Specific Heat	Thermal Conductivity
	ρ (kg/m^3)	Cp (J/kg-K)	k (W/m-k)
300	8298.273	178.75	18.0
400		235.32	
500		272.88	
600		302.95	
700		329.49	
800		354.15	
900		377.71	
1000		400.59	

Table 5. Thermo-physical Properties of Stainless Steel 304 (Cladding) [20]

Temperature (K)	Density	Specific Heat	Thermal Conductivity
	ρ (kg/m^3)	Cp (J/kg-K)	k (W/m-k)
300	7800.0	477.491	13.25
400		504.785	15.14
500		528.544	17.03
600		549.663	18.92
700		568.697	20.81
800		586.024	22.70
900		601.913	24.59
1000		616.567	26.48
1100		630.142	28.37
1200		642.763	30.26
1300		654.531	32.15
1400		665.528	34.04
1500		675.826	35.93
1600		685.483	37.82
1671		691.978	39.16

Table 6. Thermo-physical Properties of Graphite H-451 (Top and Bottom Reflectors) [2]

Temperature (K)	Density	Specific Heat	Thermal Conductivity	
	ρ (kg/m^3)	Cp (J/kg-K)	Temperature (K)	k (W/m-k)
300.0	1780.0 [21]	712.763	500.0	114.976
400.0		990.362	600.0	106.097
500.0		1217.634	700.0	97.876
600.0		1389.860	800.0	90.310
700.0		1519.837	900.0	83.402
800.0		1619.440	1000.0	77.149
900.0		1697.261	1001.0	77.090

1000.0		1759.228	1100.0	71.554
1001.0		1759.782	1200.0	66.614
1100.0		1809.429	1300.0	62.331
1200.0		1850.726	1400.0	58.705
1300.0		1885.157	1500.0	55.735
1400.0		1914.205	1600.0	53.422
1500.0		1938.966	1700.0	51.765
1600.0		1960.266	1800.0	50.765
1700.0		1978.737		
1800.0		1994.869		
1900.0		2009.048		
2000.0		2021.582		
2100.0		2032.717		
2200.0		2042.654		
2300.0		2051.559		
2400.0		2059.567		
2500.0		2066.792		
2600.0		2073.331		
2700.0		2079.264		
2800.0		2084.659		
2900.0		2089.576		
3000.0		2094.066		

Table 7. Thermo-physical Properties of Beryllium (internal reflector) [22]

Temperature (K)	Density	Specific Heat	Thermal Conductivity
	ρ (kg/m^3)	Cp (J/kg-K)	k (W/m-k)
293.15	1847.4	2398.5	156.7
373.15	1840.8	2477.3	145.8
473.15	1832.3	2575.8	133.2
573.15	1823.5	2674.3	121.7
673.15	1814.3	2772.8	111.3
773.15	1804.8	2871.3	102.0
873.15	1794.9	2969.8	93.7
973.15	1784.8	3068.3	86.6
1073.15	1774.3	3166.8	80.6
1173.15	1763.5	3265.3	75.6
1273.15	1752.4	3363.8	71.8
1373.15	1741.0	3462.3	69.0
1473.15	1729.2	3560.8	67.3
1560.15	1718.7	3646.4	66.8

Table 8. Thermo-physical Properties of Zirconium (Zirconium rod) [22]

Temperature (K)	Density [14]	Viscosity [15]	Specific Heat [16]	Thermal Conductivity [17]
	ρ (kg/m^3)	μ (kg/m-sec)	Cp (J/kg-K)	k (W/m-k)
298	6500	285.0	1.852E+06	21.2
300	6499	285.2	1.854E+06	21.2
400	6483	297.9	1.931E+06	19.6
500	6466	309.6	2.002E+06	19.0
600	6449	320.4	2.066E+06	19.0
700	6432	330.6	2.127E+06	19.3
800	6415	340.4	2.184E+06	19.9
900	6398	350.0	2.240E+06	20.6
1000	6382	359.7	2.295E+06	21.5
1100	6365	369.6	2.352E+06	22.4
1200	6348	307.4	1.952E+06	23.5
1300	6331	313.1	1.982E+06	24.6
1400	6314	319.5	2.018E+06	25.9
1500	6297	326.8	2.058E+06	27.2
1600	6280	335.0	2.104E+06	28.5
1700	6264	344.1	2.155E+06	30.0
1800	6247	354.3	2.213E+06	31.5
1900	6230	365.5	2.277E+06	33.0
2000	6213	377.9	2.348E+06	34.6
2100	6196	391.6	2.426E+06	36.3

The polynomial function for the density of zirconium rod implemented in the STAR-CCM+ is given by:

$$\rho_{Zr}\left[{}^{kg}/_{m^3}\right] = -0.1685 \cdot T[K] + 6550.0 \quad 298K \leq T \leq 2100K.$$

Table 9. Young's Modulus (Modulus of Elasticity) and Poisson's Ratio of SS-304 (Cladding)

Young's Modulus (Modulus of Elasticity) [23]		Poisson's Ratio [24]	
Temperature (K)	E (Pa)	Temperature (K)	Poisson's Ratio
300.15	1.93E+11	423.15	0.28
366.15	1.92E+11	533.15	0.30
422.15	1.87E+11	643.15	0.32
477.15	1.83E+11	753.15	0.28
533.15	1.79E+11	863.15	0.29
589.15	1.77E+11	973.15	0.28
644.15	1.70E+11	1093.15	0.25

700.15	1.66E+11		
755.15	1.60E+11		
811.15	1.55E+11		
866.15	1.50E+11		
922.15	1.45E+11		
977.15	1.41E+11		
1033.15	1.34E+11		
1089.15	1.25E+11		

Table 10. Thermal Expansion Coefficient of SS-304(Cladding) [25]

Temperature (K)	CTE (1E-05 1/K)	Temperature (K)	CTE (1E-05 1/K)
294.26	1.530	699.82	1.818
310.93	1.548	727.59	1.836
338.71	1.584	755.37	1.836
366.48	1.602	783.15	1.854
394.26	1.638	810.93	1.854
422.04	1.656	838.71	1.872
449.82	1.692	866.48	1.872
477.59	1.710	894.26	1.890
505.37	1.728	922.04	1.908
533.15	1.746	949.82	1.908
560.93	1.764	977.59	1.926
588.71	1.782	1005.37	1.926
616.48	1.782	1033.15	1.944
644.26	1.800	1060.93	1.944
672.04	1.800	1088.71	1.944

The polynomial functions for the mechanical properties of SS-304 implemented in the STAR-CCM+ are as follows:

Young's Modulus (Pa):

$$E_{SS-304}[Pa] = -3.929 \cdot 10^4 T^2 - 3.1303 \cdot 10^7 T + 2.0717 \cdot 10^{11} \quad 300.15K \leq T \leq 1089.15K$$

Coefficient of Thermal Expansion (1/K):

$$\alpha_{SS-304}\left[{}^{1}/_{K}\right] = -1.537884 \cdot 10^{-17} T^4 + 5.147804 \cdot 10^{-14} T^3 - 6.525143 \cdot 10^{-11} T^2 + 4.069205 \cdot 10^{-8} T + 7.722943 \cdot 10^{-17} \quad 294.26K \leq T \leq 1088.71K.$$

Appendix D

Boundary Condition Inputs for CFD Model

Fuel Pin Power Distribution

Axial power distribution has been provided by Carlo Parisi on March 3, 2023.

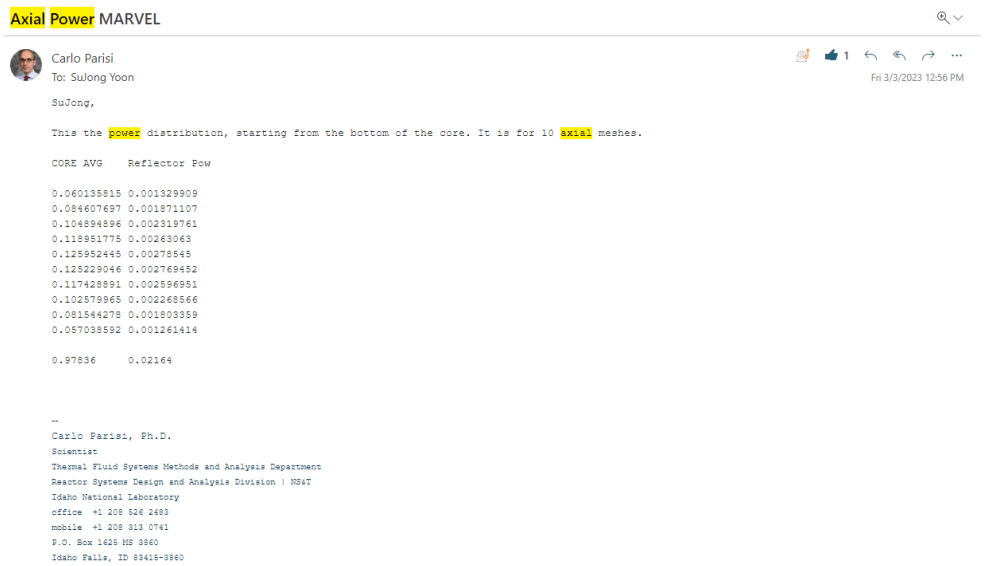

Axial Power MARVEL

Carlo Parisi
To: SuJong Yoon
Fri 3/3/2023 12:56 PM

SuJong,

This the power distribution, starting from the bottom of the core. It is for 10 axial meshes.

CORE AVG Reflector Pow

0.060135815 0.001329909
0.084607697 0.001871107
0.104894896 0.002319761
0.118951775 0.00263063
0.125952445 0.00278545
0.125229046 0.0027694452
0.117428891 0.002596951
0.102579965 0.002268566
0.081544278 0.001803359
0.057038592 0.001261414

0.97836 0.02164

--
Carlo Parisi, Ph.D.
Scientist
Thermal Fluid Systems Methods and Analysis Department
Reactor Systems Design and Analysis Division | NS&T
Idaho National Laboratory
office +1 208 526 2483
mobile +1 208 313 0741
P.O. Box 1625 MS 3860
Idaho Falls, ID 83415-3860

The user-defined field functions for polynomial fitting curve of axial power profile in Eqn. (1) was implemented as follows:

$${Position}[1]<-1.8069?0.0:$${Position}[1]<-1.1719? 14.080*pow($${Position}[1],4) + 84.258*pow($${Position}[1],3) + 179.597*pow($${Position}[1],2) + 160.240*$${Position}[1] + 50.625:0.0 Eqn. (D.1)

where $${Position}[1] represents the axial elevation (m), and the values -1.8069 and -1.1719 represent the bottom and top elevations of the fuel volume in the CFD model, respectively.

The definition of user-defined field function “Volumetric heat generation rate XX-YY” (W/m^3) is given by:

${Fuel power}/${Fuel volume XX-YY}${Axial power profile}*${RPF XX-YY}* Eqn.(D.2)

where “XX-YY” is the fuel pin identification number (Figure 4-(a)), ${RPF XX-YY} is a power peaking factor of fuel pin XX-YY (Figure 4-(b)), ${Axial power profile} is the axial power profile (Figure 4-(c)), ${Fuel volume XX-YY} is the volume of fuel meat ($5.881 \cdot 10^{-4}$ m^3), and ${Fuel power} is a unit pin power (=85,000/36 W).

Appendix E

Pressure Load for ABAQUS Finite Element Analysis

It is assumed that the pressure load due to the weight of the components above the reactor core is uniformly distributed to the fuel pins.

Table 11. The weight of the component above the MARVEL reactor

Drawing No.	Component	Material	Estimated Weight (lbs)	# per sub-assembly	Total Weight (lbs)
1014679	Upper Alignment Grid Plate	SS316H SST ASME SA-240	1.8	1	1.8
1014587	Fuel pin to Upper Grid Adapter	SS316H SST ASME SA-241	1.3	6	7.56
1014593	Upper grid Adapter	SS316H SST ASME SA-240	0.6	1	0.6
1014594	Alignment Pin	SS316H SST ASME SA-240	0.3	3	0.9
1014595	Top Screw Pin	SS316H SST ASME SA-240	0.4	3	1.2
Total					10.8

Since each subassembly contains 6 fuel pins, the weight of the upper internal structure per pin is 1.8 lbs (=0.816 kg). The cross-sectional area of the fuel pin is 1.0066E-3 m^2. The pressure load per pin is calculated by:

$$P_{upper\_structure} = \frac{9.81 \times 0.816}{1.0066 \times 10^{-3}} \approx 7955.56 \ \frac{kg}{m \cdot s^2}.$$

The height NaK volume above the upper internal structure is 0.805m. The hydrostatic pressure due to the NaK volume above the core is calculated by:

$$P_{NaK} = \rho \times g \times H = 718.76 \times 9.81 \times 0.805 = 5675.23 = \frac{kg}{m \cdot s^2}$$

where the density of NaK is 718.76 kg/m^3 at the NaK outlet temperature (539.6°C).

The total pressure load is calculated to be:

$$P_{total} = P_{NaK} + P_{upper\_structure} = 13630.79 \ \frac{kg}{m \cdot s^2}$$

Appendix F

Mesh Sensitivity Test Results of MARVEL Reactor Core CFD Model

To evaluate the mesh dependency of the solution, the CFD models with three base mesh sizes of 10.0 mm, 20.0 mm and 40.0 mm were compared. In this mesh sensitivity test, the numbers and total thickness of prism boundary layers were fixed to 4 and 1.67E-3 m, respectively. The PCT was selected to evaluate the mesh sensitivity as seen in Figure 32. The maximum deviation of the PCT among three mesh refinements was only 0.36%. This ECAR reported the calculation results obtained from the CFD model meshed by the base mesh size of 10.0 mm (finest model) because it predicted the most conservative PCT among three mesh refined models.

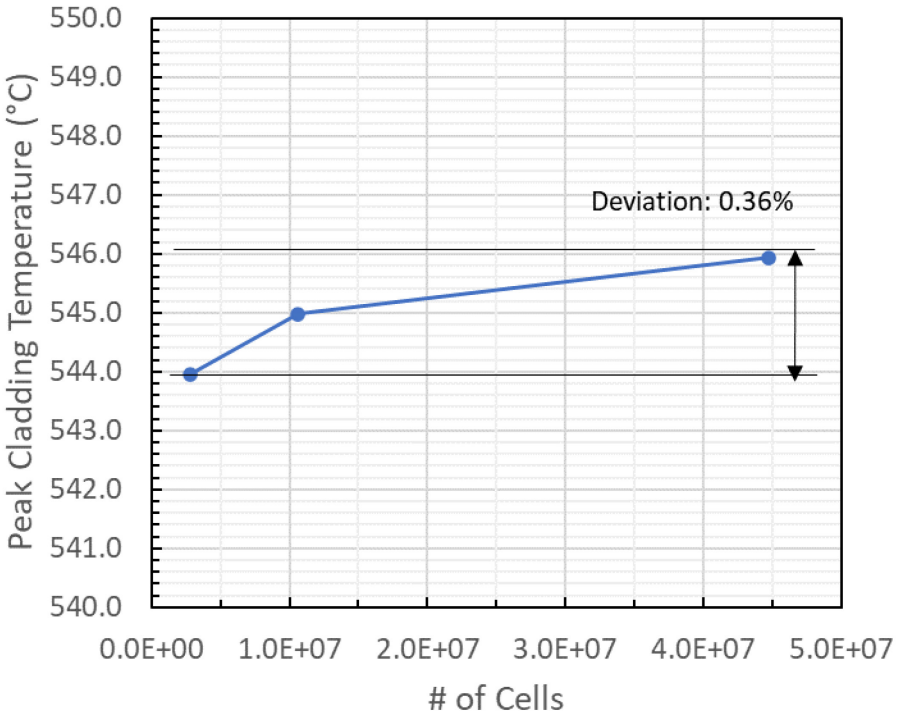

Figure 32. Mesh sensitivity test result for the PCT

Appendix G

Azimuthal Temperature Profiles of Claddings

The azimuthal temperature profiles of claddings were obtained along with the counterclockwise direction from the reference angle as seen in Figure 33. The data was extracted at the interface between the cladding and fuel meat, and at the top elevation of the fuel (P3). Figure 34, Figure 35, and Figure 36 illustrate the azimuthal temperature profiles of the fuel rods in each ring.

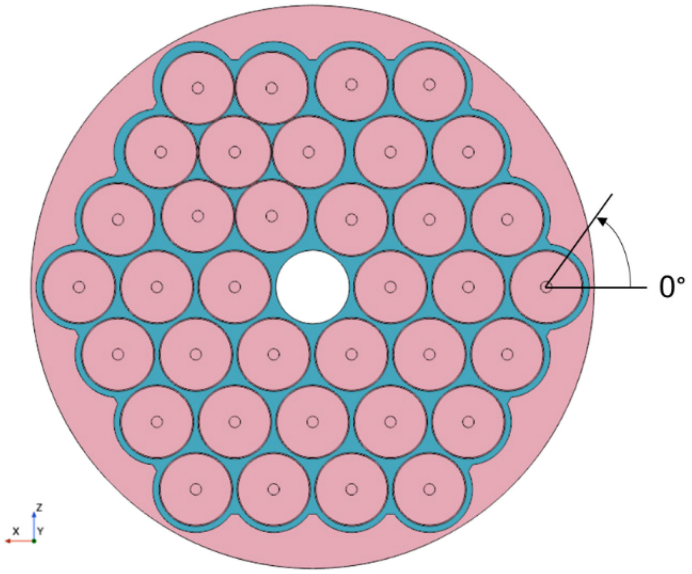

Figure 33. Reference angle of azimuthal temperature profile.

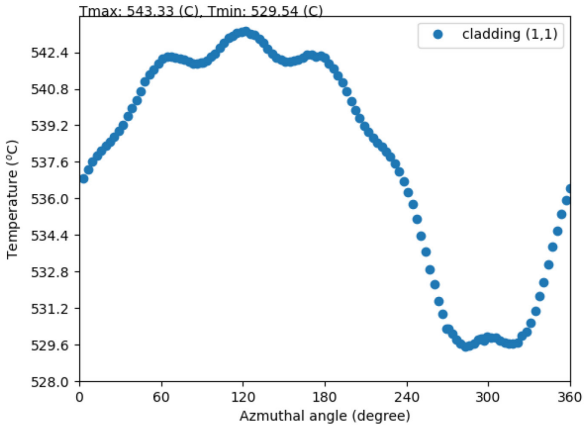

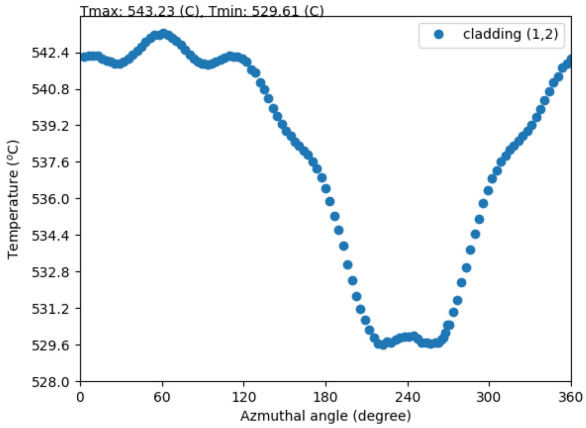

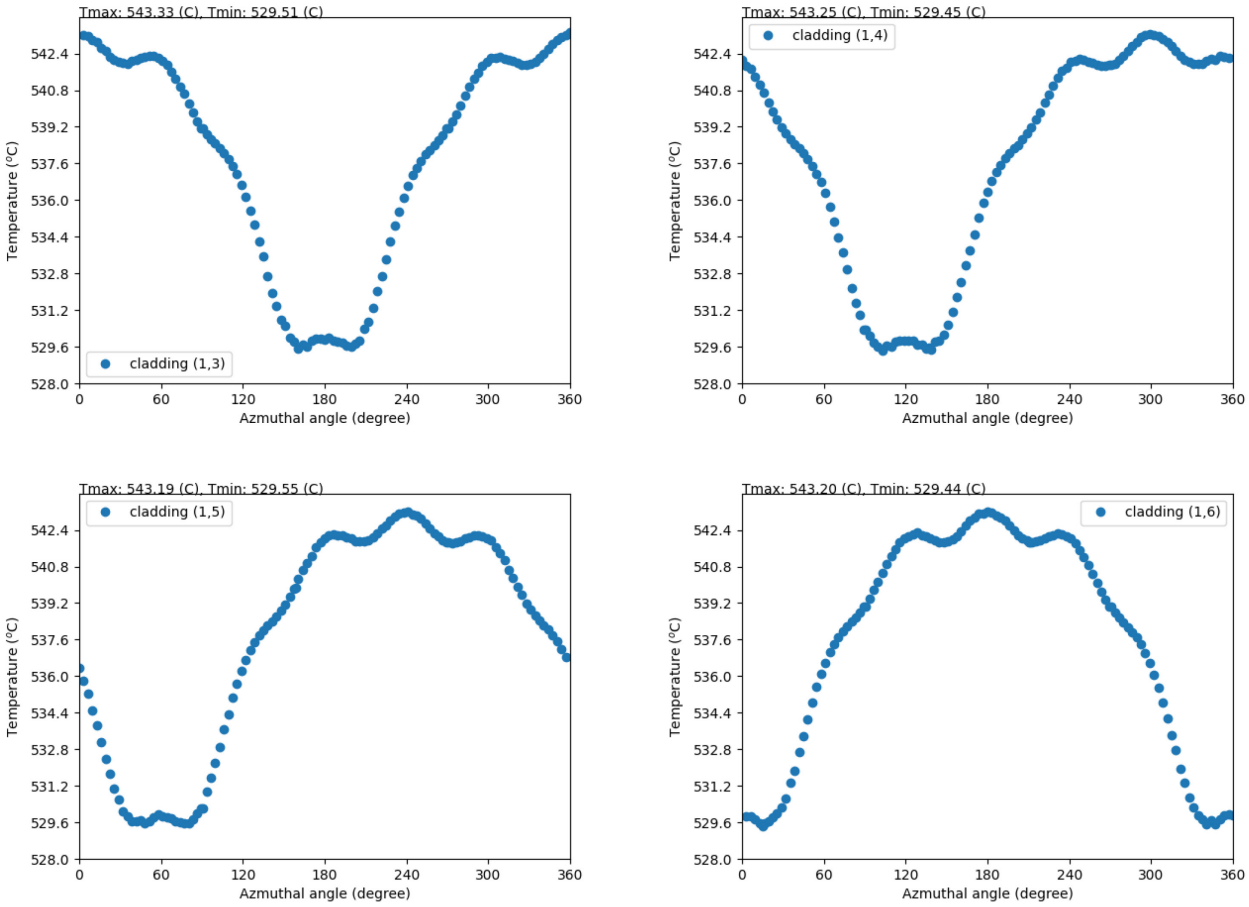

Figure 34. Azimuthal temperature profiles of the claddings in the first ring (Elevation: P3)

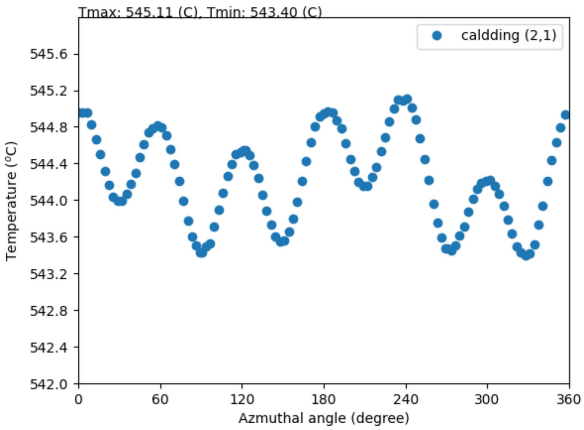
Tmax: 545.11 (C), Tmin: 543.40 (C)
caldding (2,1)
Temperature (°C)
Azmuthal angle (degree)

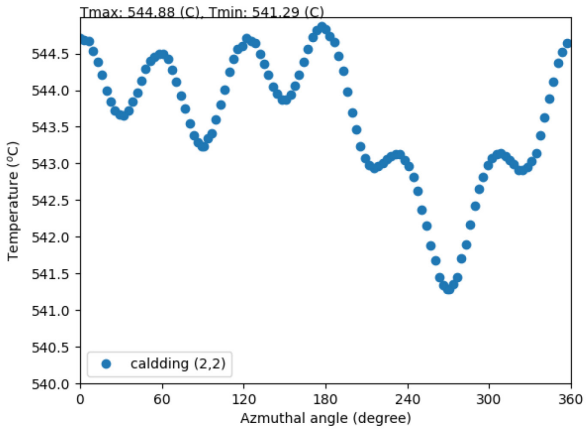
Tmax: 544.88 (C), Tmin: 541.29 (C)
caldding (2,2)
Temperature (°C)
Azmuthal angle (degree)

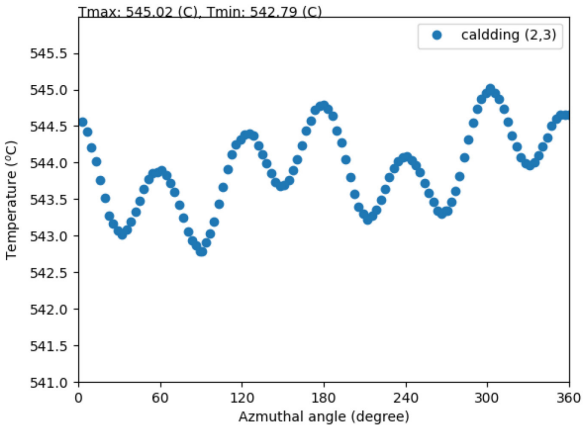
Tmax: 545.02 (C), Tmin: 542.79 (C)
caldding (2,3)
Temperature (°C)
Azmuthal angle (degree)

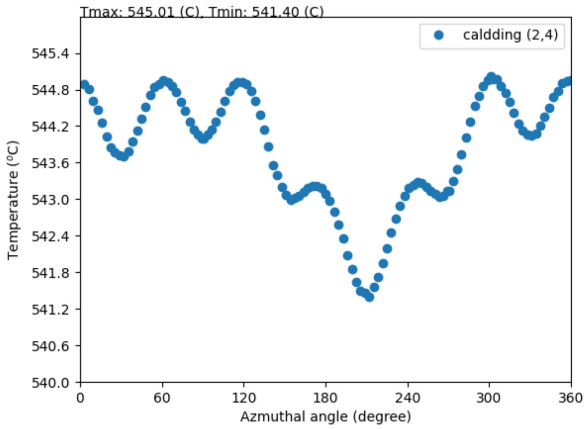
Tmax: 545.01 (C), Tmin: 541.40 (C)
caldding (2,4)
Temperature (°C)
Azmuthal angle (degree)

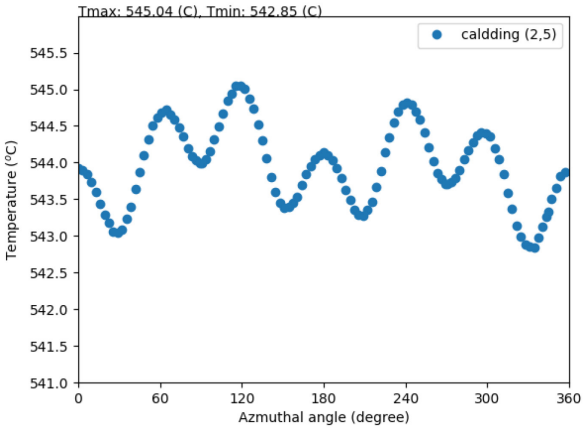
Tmax: 545.04 (C), Tmin: 542.85 (C)
caldding (2,5)
Temperature (°C)
Azmuthal angle (degree)

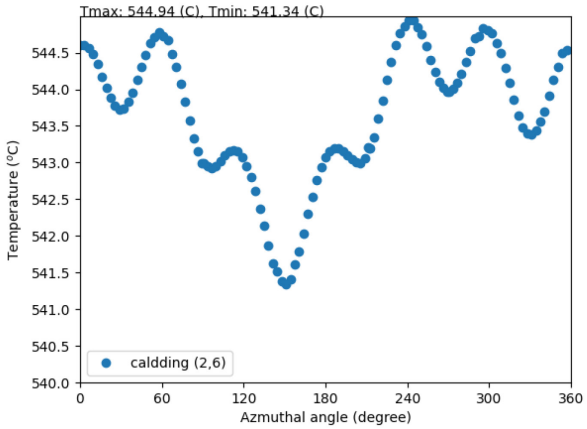
Tmax: 544.94 (C), Tmin: 541.34 (C)
caldding (2,6)
Temperature (°C)
Azmuthal angle (degree)

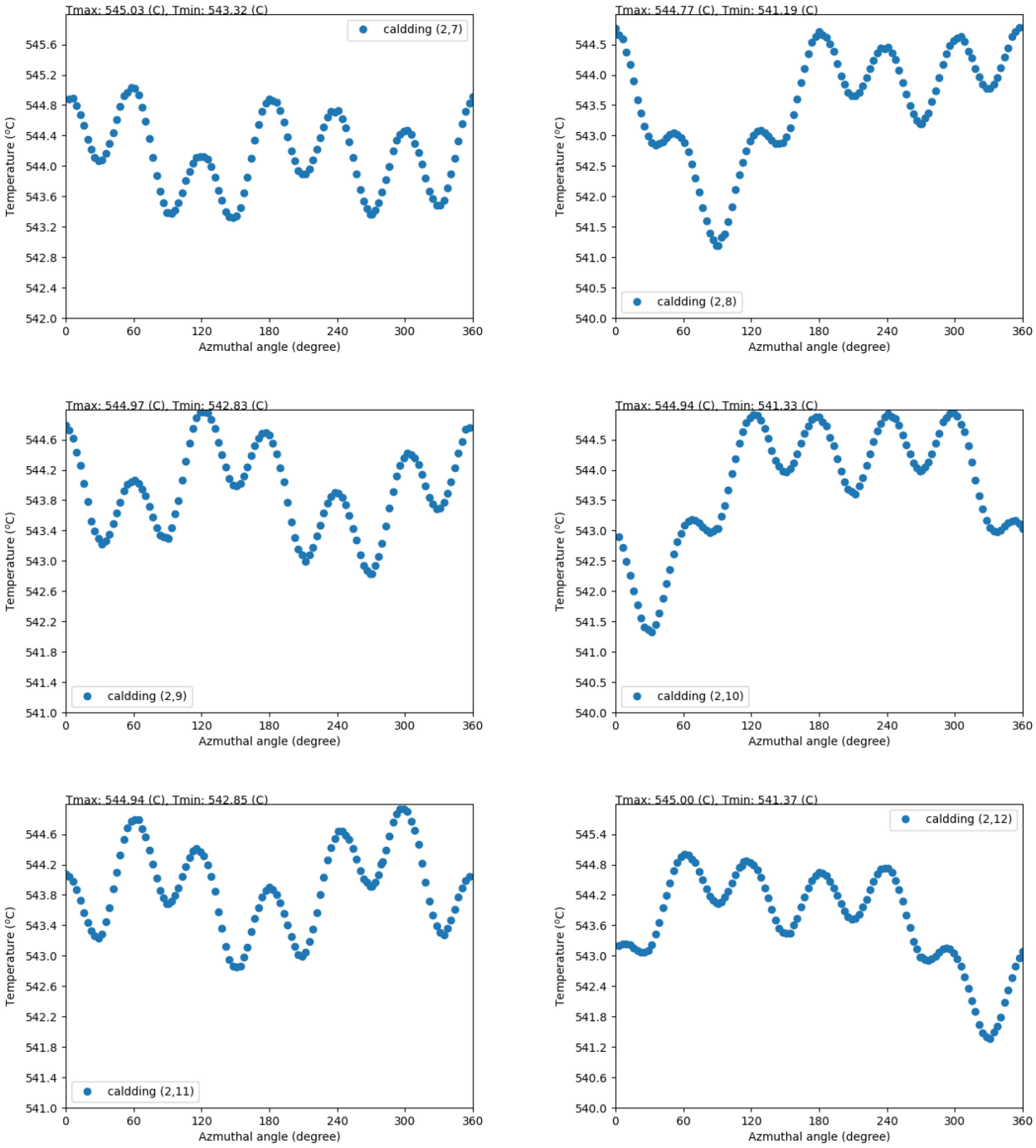

Figure 35. Azimuthal temperature profiles of the claddings in the second ring (Elevation: P3)

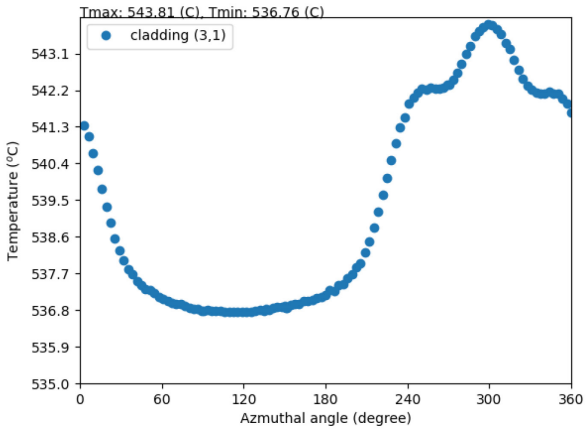
Tmax: 543.81 (C), Tmin: 536.76 (C)
cladding (3,1)
Temperature (°C)
Azmuthal angle (degree)

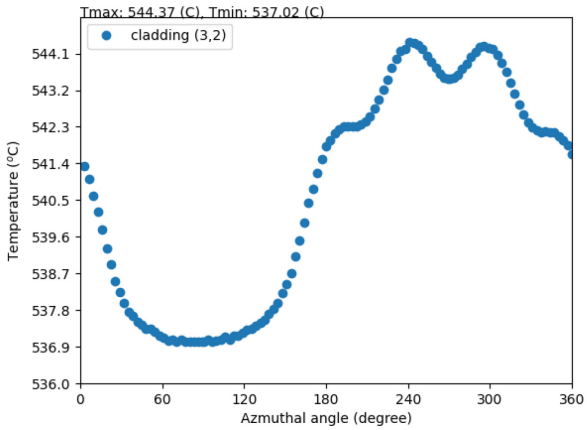
Tmax: 544.37 (C), Tmin: 537.02 (C)
cladding (3,2)
Temperature (°C)
Azmuthal angle (degree)

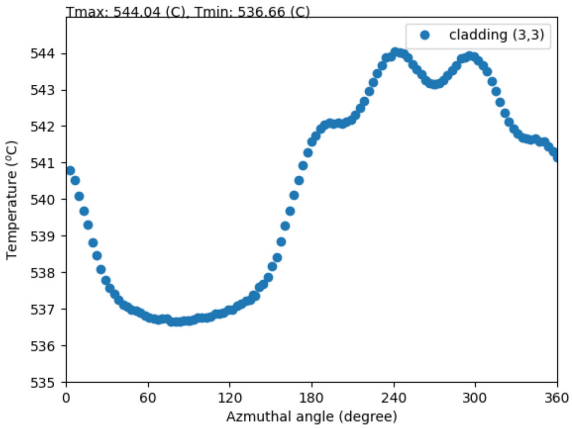
Tmax: 544.04 (C), Tmin: 536.66 (C)
cladding (3,3)
Temperature (°C)
Azmuthal angle (degree)

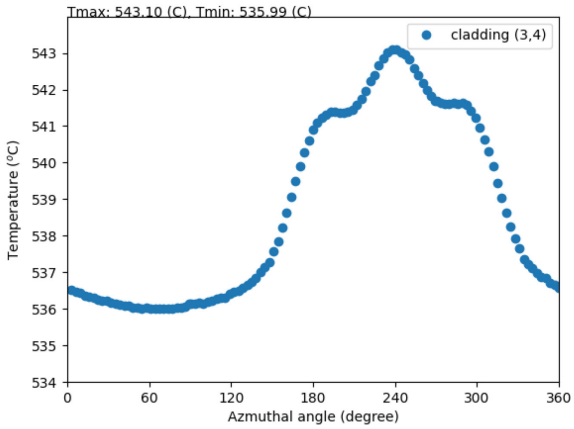
Tmax: 543.10 (C), Tmin: 535.99 (C)
cladding (3,4)
Temperature (°C)
Azmuthal angle (degree)

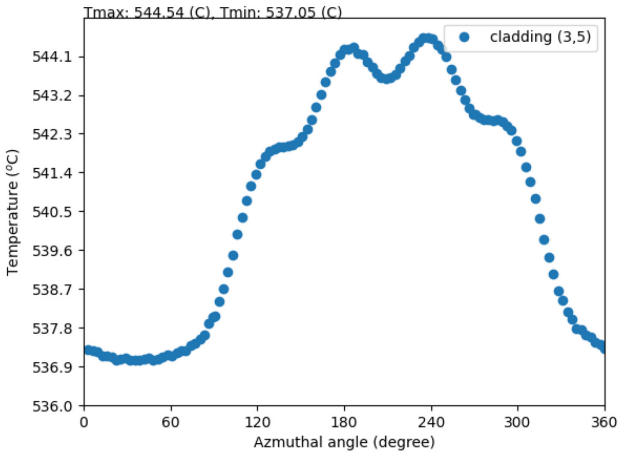
Tmax: 544.54 (C), Tmin: 537.05 (C)
cladding (3,5)
Temperature (°C)
Azmuthal angle (degree)

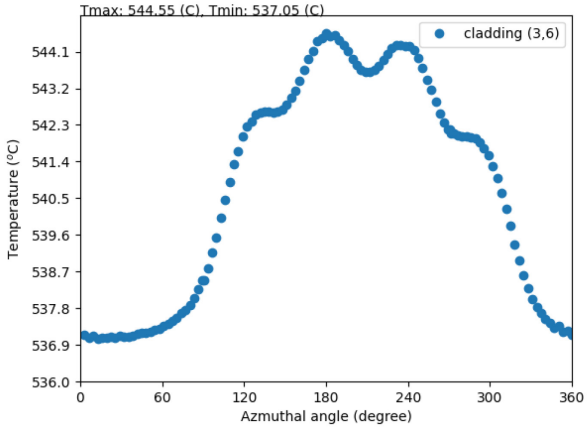
Tmax: 544.55 (C), Tmin: 537.05 (C)
cladding (3,6)
Temperature (°C)
Azmuthal angle (degree)

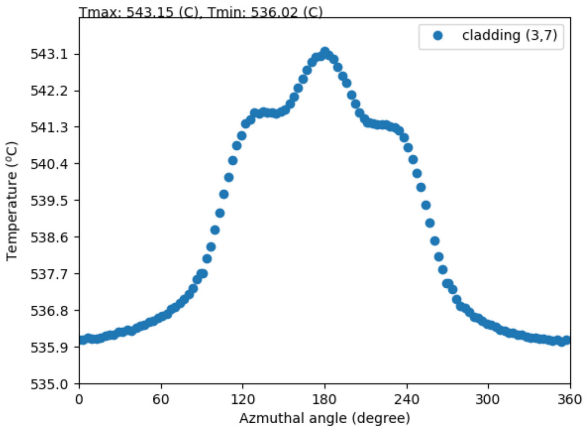
Tmax: 543.15 (C), Tmin: 536.02 (C)
cladding (3,7)
Temperature (°C)
Azmuthal angle (degree)

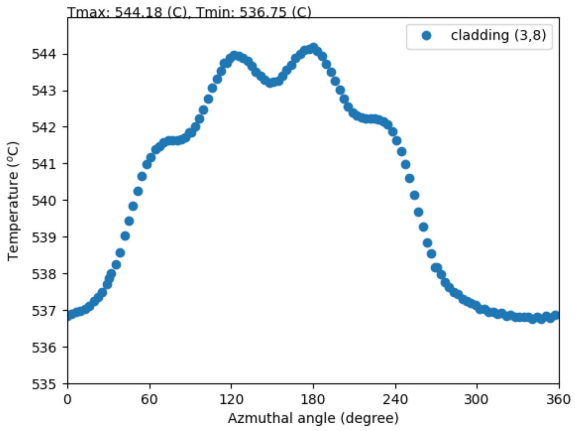
Tmax: 544.18 (C), Tmin: 536.75 (C)
cladding (3,8)
Temperature (°C)
Azmuthal angle (degree)

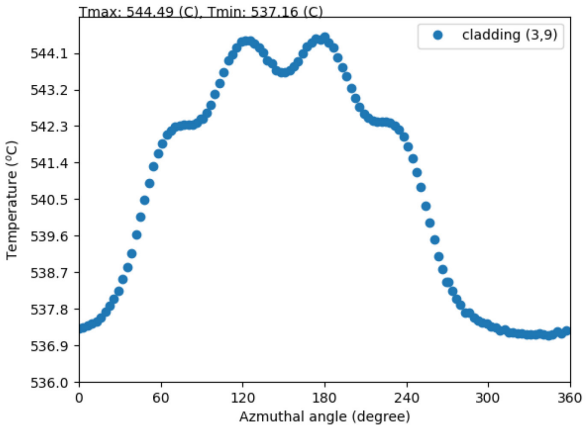
Tmax: 544.49 (C), Tmin: 537.16 (C)
cladding (3,9)
Temperature (°C)
Azmuthal angle (degree)

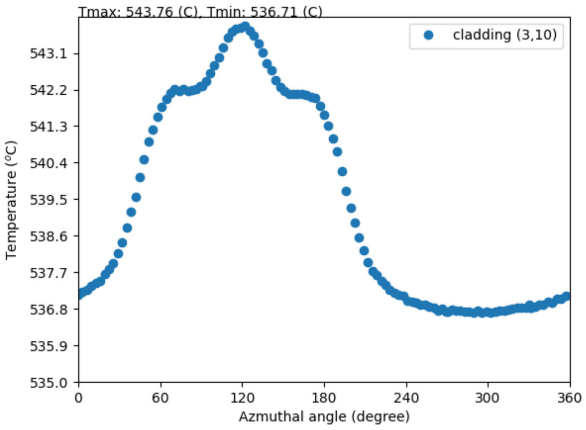
Tmax: 543.76 (C), Tmin: 536.71 (C)
cladding (3,10)
Temperature (°C)
Azmuthal angle (degree)

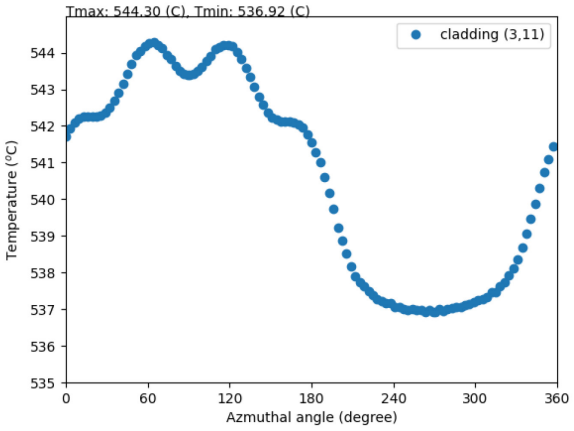
Tmax: 544.30 (C), Tmin: 536.92 (C)
cladding (3,11)
Temperature (°C)
Azmuthal angle (degree)

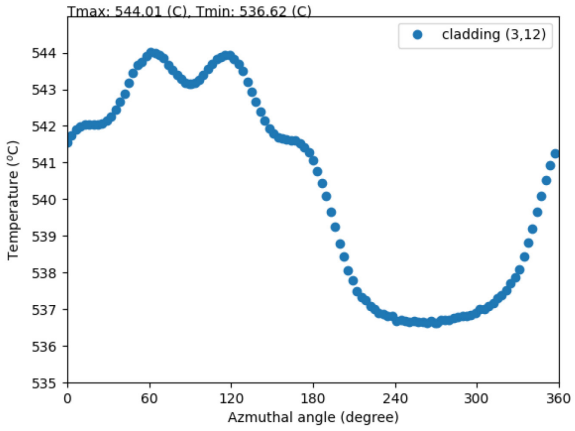
Tmax: 544.01 (C), Tmin: 536.62 (C)
cladding (3,12)
Temperature (°C)
Azmuthal angle (degree)

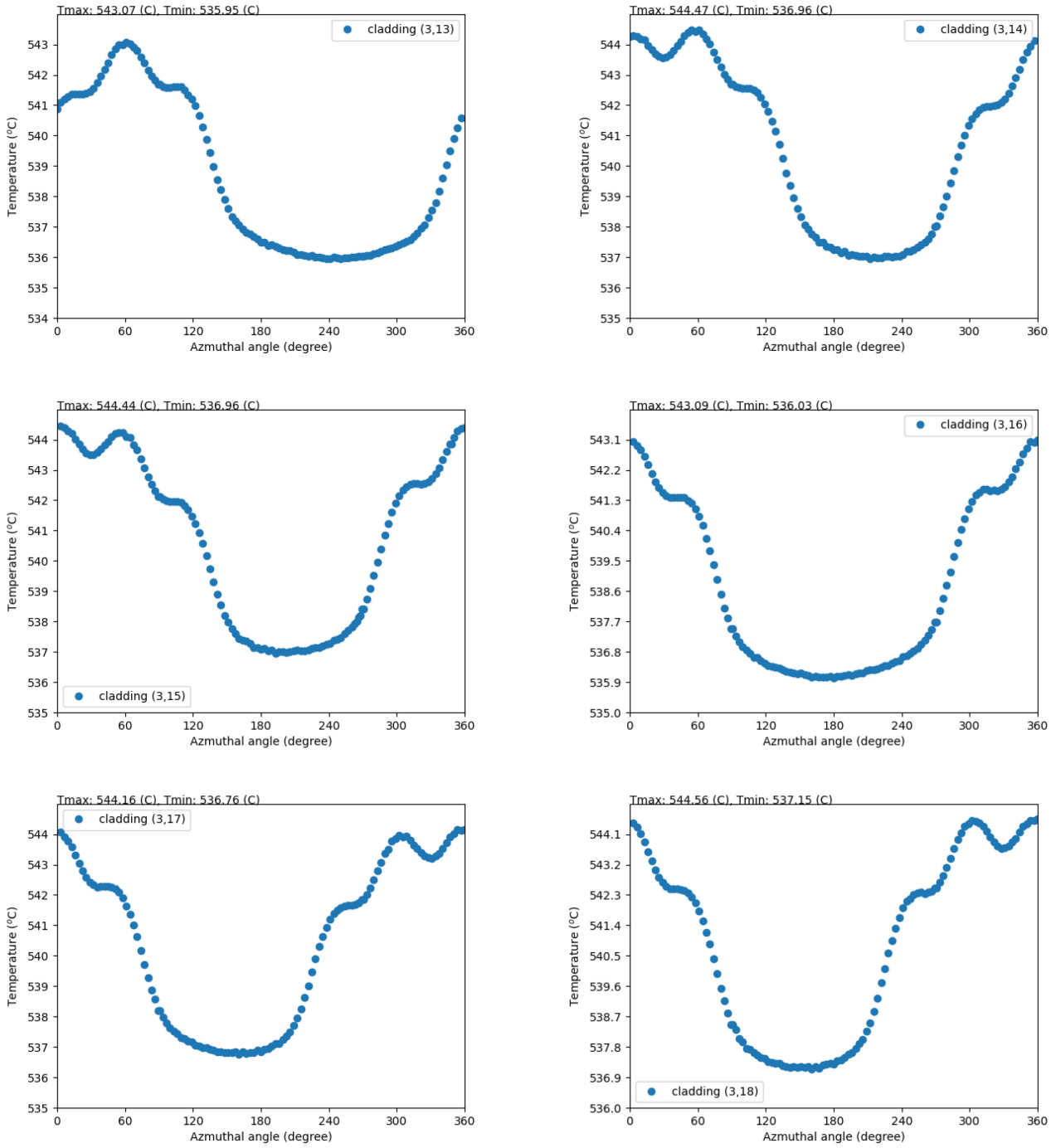

Figure 36. Azimuthal temperature profiles of the claddings in the third ring. (Elevation: P3)

Table 12. Maximum and minimum azimuthal temperature of fuel cladding at elevation P1(-1.80693m), P2 (-1.48943m) and P3 (-1.17193m).

Elevation (m)	Rod ID	T_{max} (°C)	T_{min} (°C)	dT (°C)	Rod ID	T_{max} (°C)	T_{min} (°C)	dT (°C)
-1.17193	1-1	543.33	529.54	13.79	3-1	543.81	536.76	7.05
-1.48943	1-1	514.58	500.72	13.86	3-1	515.53	505.67	9.86
-1.80693	1-1	471.81	471.64	0.17	3-1	471.87	471.7	0.17
-1.17193	1-2	543.23	529.61	13.62	3-2	544.37	537.02	7.35
-1.48943	1-2	514.45	500.68	13.77	3-2	515.48	505.58	9.9
-1.80693	1-2	471.81	471.63	0.18	3-2	471.86	471.71	0.15
-1.17193	1-3	543.33	529.51	13.82	3-3	544.04	536.66	7.38
-1.48943	1-3	514.5	500.65	13.85	3-3	515.19	505.3	9.89
-1.80693	1-3	471.81	471.64	0.17	3-3	471.84	471.7	0.14
-1.17193	1-4	543.25	529.45	13.8	3-4	543.1	535.99	7.11
-1.48943	1-4	514.6	500.65	13.95	3-4	514.79	504.94	9.85
-1.80693	1-4	471.81	471.63	0.18	3-4	471.84	471.68	0.16
-1.17193	1-5	543.19	529.55	13.64	3-5	544.54	537.05	7.49
-1.48943	1-5	514.42	500.68	13.74	3-5	515.69	505.75	9.94
-1.80693	1-5	471.81	471.63	0.18	3-5	471.87	471.72	0.15
-1.17193	1-6	543.2	529.44	13.76	3-6	544.55	537.05	7.5
-1.48943	1-6	514.49	500.7	13.79	3-6	515.58	505.72	9.86
-1.80693	1-6	471.81	471.64	0.17	3-6	471.87	471.71	0.16
-1.17193	2-1	545.11	543.4	1.71	3-7	543.15	536.02	7.13
-1.48943	2-1	515.66	510.66	5	3-7	514.84	504.98	9.86
-1.80693	2-1	471.84	471.7	0.14	3-7	471.84	471.68	0.16
-1.17193	2-2	544.88	541.29	3.59	3-8	544.18	536.75	7.43
-1.48943	2-2	515.48	509.79	5.69	3-8	515.25	505.37	9.88
-1.80693	2-2	471.84	471.7	0.14	3-8	471.85	471.7	0.15
-1.17193	2-3	545.02	542.79	2.23	3-9	544.49	537.16	7.33
-1.48943	2-3	515.54	510.32	5.22	3-9	515.55	505.76	9.79
-1.80693	2-3	471.84	471.7	0.14	3-9	471.86	471.71	0.15
-1.17193	2-4	545.01	541.4	3.61	3-10	543.76	536.71	7.05
-1.48943	2-4	515.66	509.93	5.73	3-10	515.46	505.65	9.81
-1.80693	2-4	471.85	471.7	0.15	3-10	471.87	471.7	0.17
-1.17193	2-5	545.04	542.85	2.19	3-11	544.3	536.92	7.38
-1.48943	2-5	515.61	510.32	5.29	3-11	515.39	505.56	9.83
-1.80693	2-5	471.84	471.7	0.14	3-11	471.86	471.71	0.15
-1.17193	2-6	544.94	541.34	3.6	3-12	544.01	536.62	7.39
-1.48943	2-6	515.56	509.9	5.66	3-12	515.18	505.29	9.89
-1.80693	2-6	471.85	471.7	0.15	3-12	471.85	471.7	0.15
-1.17193	2-7	545.03	543.32	1.71	3-13	543.07	535.95	7.12
-1.48943	2-7	515.57	510.63	4.94	3-13	514.79	504.88	9.91

-1.80693	2-7	471.84	471.7	0.14	3-13	471.84	471.68	0.16
-1.17193	2-8	544.77	541.19	3.58	3-14	544.47	536.96	7.51
-1.48943	2-8	515.38	509.7	5.68	3-14	515.64	505.71	9.93
-1.80693	2-8	471.84	471.7	0.14	3-14	471.86	471.71	0.15
-1.17193	2-9	544.97	542.83	2.14	3-15	544.44	536.96	7.48
-1.48943	2-9	515.53	510.34	5.19	3-15	515.52	505.68	9.84
-1.80693	2-9	471.85	471.7	0.15	3-15	471.86	471.71	0.15
-1.17193	2-10	544.94	541.33	3.61	3-16	543.09	536.03	7.06
-1.48943	2-10	515.58	509.87	5.71	3-16	514.8	505.01	9.79
-1.80693	2-10	471.84	471.7	0.14	3-16	471.84	471.68	0.16
-1.17193	2-11	544.94	542.85	2.09	3-17	544.16	536.76	7.4
-1.48943	2-11	515.49	510.38	5.11	3-17	515.29	505.4	9.89
-1.80693	2-11	471.84	471.7	0.14	3-17	471.85	471.7	0.15
-1.17193	2-12	545	541.37	3.63	3-18	544.56	537.15	7.41
-1.48943	2-12	515.62	509.9	5.72	3-18	515.63	505.71	9.92
-1.80693	2-12	471.85	471.7	0.15	3-18	471.86	471.71	0.15

Appendix H

Python Script to Calculate Coordinates of Deformed Claddings and Minimum Fuel-to-fuel Gap Distance

```
import os
import numpy as np
from scipy.spatial import KDTree

num_node = 18250
original_dict = {}
displace_dict = {}

# Create the original_dict from the file input
with open('ABQ-CFD.inp', 'r') as f:
    component_id = ''
    for line in f:
        if line.startswith('*Part, name='):
            component_id = line.split('=')[1].strip()
            original_dict[component_id] = {'nodes': []}
        elif line.startswith('*Node'):
            for line in f:
                if line.startswith('*'):
                    break
                node_data = line.strip().split(',')
                if len(node_data) == 4:
                    node_id = float(node_data[0])
                    if node_id > num_node:
                        break
                    node_dict = {'node_id': node_id, 'x': float(node_data[1]), 'y': float(node_data[2]), 'z':
float(node_data[3])}
                    original_dict[component_id]['nodes'].append(node_dict)

## This subroutine is to print the coordinates of original geometry, comment out if it is not necessary:
# for component_id, component_dict in original_dict.items():
#   print(f"Component ID: {component_id}")
#   for node_dict in component_dict['nodes']:
#       print(f"Node ID: {node_dict['node_id']}, x: {node_dict['x']}, y: {node_dict['y']}, z: {node_dict['z']}")

# Create the displace_dict from the ABAQUS report
with open('Top_constrained_correct.rpt', 'r') as f:
    component_id = ''
    for line in f:
        if line.startswith('Field Output reported at nodes for part: '):
            component_id = line.split(': ')[1].strip()[:-4].lower()
            displace_dict[component_id] = {'nodes': []}
        elif line.startswith('---------------------------------------------------------------------'):
            for line in f:
                if not line.strip():
                    break
                node_data = line.strip().split()
                if len(node_data) == 4 and node_data[0] != 'Minimum' and node_data[0] != 'Maximum' and
node_data[0] != 'At' and node_data[0] !='Total':
                    node_id = float(node_data[0])
```

```
                if node_id > num_node:
                    break
                node_dict = {'node_id': node_id, 'x': float(node_data[1]), 'y': float(node_data[2]), 'z':
float(node_data[3])}
                displace_dict[component_id]['nodes'].append(node_dict)

# calculate x, y, z coordinates of deformed fuel pins
deformed_dict = {}
for component in original_dict:
    deformed_dict[component] = {'nodes': []}
    for node1, node2 in zip(original_dict[component]['nodes'], displace_dict[component]['nodes']):
        x_sum = node1['x'] + node2['x']
        y_sum = node1['y'] + node2['y']
        z_sum = node1['z'] + node2['z']
        deformed_dict[component]['nodes'].append({'node_id': node1['node_id'], 'x': x_sum, 'y': y_sum, 'z': z_sum})

min_distance_f_f = []
min_distance_1_2 = []
min_distance_2_3 = []

for i in range(1,4,1):
    if i == 1:
        for j in range(1,7,1):
            if j < 6:
                component_id1 = 'pin_'+str(i)+'_'+str(j)
                component_id2 = 'pin_'+str(i)+'_'+str(j+1)
                # # Extract the coordinates of the two components
                component1_coords = [[node['x'], node['y'], node['z']] for node in
deformed_dict[component_id1]['nodes']]
                component2_coords = [[node['x'], node['y'], node['z']] for node in
deformed_dict[component_id2]['nodes']]

                # Build KD trees from the two sets of coordinates
                component1_tree = KDTree(component1_coords)
                component2_tree = KDTree(component2_coords)

                # Find the minimum distance between the two trees
                min_distance_ins = component1_tree.query(component2_coords)[0].min()*1000
                if min_distance_ins <= 4.0:
                    min_distance_f_f.append(min_distance_ins) # unit: mm
                    print(f"The minimum distance between {component_id1} and {component_id2} is
{min_distance_ins:.3f} mm")
                else:
                    continue
            if j == 6:
                component_id1 = 'pin_1_1'
                component_id2 = 'pin_1_6'
                # # Extract the coordinates of the two components
                component1_coords = [[node['x'], node['y'], node['z']] for node in
deformed_dict[component_id1]['nodes']]
                component2_coords = [[node['x'], node['y'], node['z']] for node in
deformed_dict[component_id2]['nodes']]

                # Build KD trees from the two sets of coordinates
```

```
            component1_tree = KDTree(component1_coords)
            component2_tree = KDTree(component2_coords)

            # Find the minimum distance between the two trees
            min_distance_ins = component1_tree.query(component2_coords)[0].min()*1000
            if min_distance_ins <= 4.0:
                min_distance_f_f.append(min_distance_ins) # unit: mm
                print(f"The minimum distance between {component_id1} and {component_id2} is
{min_distance_ins:.3f} mm")
            else:
                continue
    if i == 2:
        for j in range(1,13,1):
            if j < 12:
                component_id1 = 'pin_'+str(i)+'_'+str(j)
                component_id2 = 'pin_'+str(i)+'_'+str(j+1)
                # # Extract the coordinates of the two components
                component1_coords = [[node['x'], node['y'], node['z']] for node in
deformed_dict[component_id1]['nodes']]
                component2_coords = [[node['x'], node['y'], node['z']] for node in
deformed_dict[component_id2]['nodes']]

                # Build KD trees from the two sets of coordinates
                component1_tree = KDTree(component1_coords)
                component2_tree = KDTree(component2_coords)

                # Find the minimum distance between the two trees
                min_distance_ins = component1_tree.query(component2_coords)[0].min()*1000
                if min_distance_ins <= 4.0:
                    min_distance_f_f.append(min_distance_ins) # unit: mm
                    print(f"The minimum distance between {component_id1} and {component_id2} is
{min_distance_ins:.3f} mm")
                else:
                    continue
            if j == 12:
                component_id1 = 'pin_2_1'
                component_id2 = 'pin_2_12'
                # # Extract the coordinates of the two components
                component1_coords = [[node['x'], node['y'], node['z']] for node in
deformed_dict[component_id1]['nodes']]
                component2_coords = [[node['x'], node['y'], node['z']] for node in
deformed_dict[component_id2]['nodes']]

                # Build KD trees from the two sets of coordinates
                component1_tree = KDTree(component1_coords)
                component2_tree = KDTree(component2_coords)

                # Find the minimum distance between the two trees
                min_distance_ins = component1_tree.query(component2_coords)[0].min()*1000
                if min_distance_ins <= 4.0:
                    min_distance_f_f.append(min_distance_ins) # unit: mm
                    print(f"The minimum distance between {component_id1} and {component_id2} is
{min_distance_ins:.3f} mm")
                else:
```

```
                continue
    if i == 3:
        for j in range(1,19,1):
            if j < 18:
                component_id1 = 'pin_'+str(i)+'_'+str(j)
                component_id2 = 'pin_'+str(i)+'_'+str(j+1)
                # # Extract the coordinates of the two components
                component1_coords = [[node['x'], node['y'], node['z']] for node in
deformed_dict[component_id1]['nodes']]
                component2_coords = [[node['x'], node['y'], node['z']] for node in
deformed_dict[component_id2]['nodes']]

                # Build KD trees from the two sets of coordinates
                component1_tree = KDTree(component1_coords)
                component2_tree = KDTree(component2_coords)

                # Find the minimum distance between the two trees
                min_distance_ins = component1_tree.query(component2_coords)[0].min()*1000
                if min_distance_ins <= 4.0:
                    min_distance_f_f.append(min_distance_ins) # unit: mm
                    print(f"The minimum distance between {component_id1} and {component_id2} is
{min_distance_ins:.3f} mm")
                else:
                    continue
            if j == 18:
                component_id1 = 'pin_3_1'
                component_id2 = 'pin_3_18'
                # # Extract the coordinates of the two components
                component1_coords = [[node['x'], node['y'], node['z']] for node in
deformed_dict[component_id1]['nodes']]
                component2_coords = [[node['x'], node['y'], node['z']] for node in
deformed_dict[component_id2]['nodes']]

                # Build KD trees from the two sets of coordinates
                component1_tree = KDTree(component1_coords)
                component2_tree = KDTree(component2_coords)

                # Find the minimum distance between the two trees
                min_distance_ins = component1_tree.query(component2_coords)[0].min()*1000
                if min_distance_ins <= 4.0:
                    min_distance_f_f.append(min_distance_ins) # unit: mm
                    print(f"The minimum distance between {component_id1} and {component_id2} is
{min_distance_ins:.3f} mm")
                else:
                    continue

for i in range(1,3,1):
    if i == 1:
        for j in range(1,7,1):
            for k in range(1,13,1):
                component_id1 = 'pin_'+str(i)+'_'+str(j)
                component_id2 = 'pin_'+str(i+1)+'_'+str(k)

                # # Extract the coordinates of the two components
```

```
            component1_coords = [[node['x'], node['y'], node['z']] for node in
deformed_dict[component_id1]['nodes']]
            component2_coords = [[node['x'], node['y'], node['z']] for node in
deformed_dict[component_id2]['nodes']]

            # Build KD trees from the two sets of coordinates
            component1_tree = KDTree(component1_coords)
            component2_tree = KDTree(component2_coords)

            # Find the minimum distance between the two trees
            min_distance_ins = component1_tree.query(component2_coords)[0].min()*1000
            if min_distance_ins <= 4.0:
                min_distance_1_2.append(min_distance_ins) # unit: mm
                print(f"The minimum distance between {component_id1} and {component_id2} is
{min_distance_ins:.3f} mm")
            else:
                continue
    if i == 2:
        for j in range(1,13,1):
            for k in range(1,19,1):
                component_id1 = 'pin_'+str(i)+'_'+str(j)
                component_id2 = 'pin_'+str(i+1)+'_'+str(k)

                # # Extract the coordinates of the two components
                component1_coords = [[node['x'], node['y'], node['z']] for node in
deformed_dict[component_id1]['nodes']]
                component2_coords = [[node['x'], node['y'], node['z']] for node in
deformed_dict[component_id2]['nodes']]

                # Build KD trees from the two sets of coordinates
                component1_tree = KDTree(component1_coords)
                component2_tree = KDTree(component2_coords)

                # Find the minimum distance between the two trees
                min_distance_ins = component1_tree.query(component2_coords)[0].min()*1000
                if min_distance_ins <= 4.0:
                    min_distance_2_3.append(min_distance_ins) # unit: mm
                    print(f"The minimum distance between {component_id1} and {component_id2} is
{min_distance_ins:.3f} mm")
                else:
                    continue

# minimum distance between the fuel rod 2-1 and adjacent fuel rods
host = [(2,1)]
neighbors = [(1,1), (2,2), (2,12), (3,1), (3,2),(3,18)]

for i,j in neighbors:
    component_id1 = 'pin_2_1'
    component_id2 = 'pin_'+str(i)+'_'+str(j)

    # # Extract the coordinates of the two components
    component1_coords = [[node['x'], node['y'], node['z']] for node in deformed_dict[component_id1]['nodes']]
    component2_coords = [[node['x'], node['y'], node['z']] for node in deformed_dict[component_id2]['nodes']]
```

```
# Build KD trees from the two sets of coordinates
component1_tree = KDTree(component1_coords)
component2_tree = KDTree(component2_coords)

# Find the minimum distance between the two trees
min_distance_ins = component1_tree.query(component2_coords)[0].min()*1000
# min_distance_interested.append(min_distance_ins) # unit: mm
print(f"The gap distance between {component_id1} and {component_id2} is {min_distance_ins:.3f} mm")
gap = 2.0- min_distance_ins
if gap > 0.0 :
    print(f"The gap distance between {component_id1} and {component_id2} is {gap:.3f} mm")
else:
 continue
```

Table 13. Change in Fuel-to-Fuel Gap Distance (Top constrained condition)

Pin ID	Pin ID	distance, mm	Pin ID	Pin ID	distance, mm
pin_1_1	pin_1_2	1.597	pin_2_6	pin_2_7	2.137
pin_1_1	pin_2_1	1.959	pin_2_6	pin_3_8	1.549
pin_1_1	pin_2_2	2.184	pin_2_6	pin_3_9	2.057
pin_1_1	pin_2_12	1.545	pin_2_7	pin_2_8	1.606
pin_1_2	pin_1_3	2.131	pin_2_7	pin_3_9	1.542
pin_1_2	pin_2_2	2.179	pin_2_7	pin_3_10	2.115
pin_1_2	pin_2_3	1.97	pin_2_7	pin_3_11	2.115
pin_1_2	pin_2_4	1.553	pin_2_8	pin_2_9	1.601
pin_1_3	pin_1_4	2.131	pin_2_8	pin_3_11	2.141
pin_1_3	pin_2_4	1.963	pin_2_8	pin_3_12	2.142
pin_1_3	pin_2_5	1.365	pin_2_9	pin_2_10	2.145
pin_1_3	pin_2_6	1.964	pin_2_9	pin_3_12	2.135
pin_1_4	pin_1_5	1.597	pin_2_9	pin_3_13	2.114
pin_1_4	pin_2_6	1.546	pin_2_9	pin_3_14	1.536
pin_1_4	pin_2_7	1.957	pin_2_10	pin_2_11	2.133
pin_1_4	pin_2_8	2.185	pin_2_10	pin_3_14	2.047
pin_1_5	pin_1_6	2.131	pin_2_10	pin_3_15	1.541
pin_1_5	pin_2_8	2.179	pin_2_11	pin_2_12	2.142
pin_1_5	pin_2_9	1.963	pin_2_11	pin_3_15	2.094
pin_1_5	pin_2_10	1.559	pin_2_11	pin_3_16	1.579
pin_1_6	pin_1_1	2.131	pin_2_11	pin_3_17	2.094
pin_1_6	pin_2_10	1.968	pin_2_12	pin_2_1	2.137
pin_1_6	pin_2_11	1.358	pin_2_12	pin_3_17	1.551
pin_1_6	pin_2_12	1.959	pin_2_12	pin_3_18	2.058
pin_2_1	pin_2_2	1.606	pin_3_1	pin_3_2	1.587
pin_2_1	pin_3_1	2.112	pin_3_2	pin_3_3	1.611
pin_2_1	pin_3_2	2.113	pin_3_3	pin_3_4	1.596
pin_2_1	pin_3_18	1.541	pin_3_4	pin_3_5	2.123

pin_2_2	pin_2_3	1.601	pin_3_5	pin_3_6	2.145
pin_2_2	pin_3_2	2.141	pin_3_6	pin_3_7	2.138
pin_2_2	pin_3_3	2.142	pin_3_7	pin_3_8	2.145
pin_2_3	pin_2_4	2.143	pin_3_8	pin_3_9	2.146
pin_2_3	pin_3_3	2.135	pin_3_9	pin_3_10	2.106
pin_2_3	pin_3_4	2.108	pin_3_10	pin_3_11	1.588
pin_2_3	pin_3_5	1.535	pin_3_11	pin_3_12	1.611
pin_2_4	pin_2_5	2.136	pin_3_12	pin_3_13	1.595
pin_2_4	pin_3_5	2.054	pin_3_13	pin_3_14	2.122
pin_2_4	pin_3_6	1.547	pin_3_14	pin_3_15	2.146
pin_2_5	pin_2_6	2.143	pin_3_15	pin_3_16	2.138
pin_2_5	pin_3_6	2.088	pin_3_16	pin_3_17	2.145
pin_2_5	pin_3_7	1.573	pin_3_17	pin_3_18	2.146
pin_2_5	pin_3_8	2.089	pin_3_18	pin_3_1	2.106

Appendix I

Straightness Tolerance of MARVEL Fuel Element

Re: MARVEL: straightness and Mo disc requirements

Adrian R. Wagner <adrian.wagner@inl.gov>
Tue 2/28/2023 10:37 AM

To: Tom M. Pfeiffer <tom.pfeiffer@inl.gov>;Jennifer L. Davlin <Jennifer.Davlin@inl.gov>;Erica M. Moore <Erica.Moore@inl.gov>;Jordan A. Evans <Jordan.Evans@inl.gov>;Carlo Parisi <Carlo.Parisi@inl.gov>;Travis L. Lange <Travis.Lange@inl.gov>;Yasir Arafat <Yasir.Arafat@inl.gov>;Brandon L. Moon <brandon.moon@inl.gov>

Cc: SuJong Yoon <SuJong.Yoon@inl.gov>;Carl E. Baily <carl.baily@inl.gov>

I received the following from TI for their straightness requirement for a loaded element:

> 0.5mm straightness for 587mm length at the final fuel element stage.
>
> You can take into account to add at least 0.1mm/100mm added

Adrian (He/Him)
--
Fuel Fabrication Division
Group Lead for Advanced Manufacturing and Ceramic Fuel Fabrication
Metallurgical Engineer
Idaho National Labs-MFC
(208)533-7273 (Office)
(505)690-2028 (Cell)